

UC Berkeley

UC Berkeley Electronic Theses and Dissertations

Title

The Dynamics of Ecology and Evolution in Simple Experimental Microbial Communities

Permalink

<https://escholarship.org/uc/item/8r62t0fs>

Author

Ascensao, Joao Andre Pereyra

Publication Date

2023

Peer reviewed|Thesis/dissertation

The Dynamics of Ecology and Evolution in Simple Experimental Microbial Communities

by

Joao Ascensao

A dissertation submitted in partial satisfaction of the

requirements for the degree of

Joint Doctor of Philosophy
with University of California, San Francisco

in

Bioengineering

in the

Graduate Division

of the

University of California, Berkeley

Committee in charge:

Professor Oskar Hallatschek, Chair

Professor Adam Arkin

Assistant Professor Jimmie Ye

Fall 2023

The Dynamics of Ecology and Evolution in Simple Experimental Microbial Communities

Copyright 2023
by
Joao Ascensao

Abstract

The Dynamics of Ecology and Evolution in Simple Experimental Microbial Communities

by

Joao Ascensao

Doctor of Philosophy in Bioengineering

University of California, Berkeley

Professor Oskar Hallatschek, Chair

A central problem of evolutionary biology lies in understanding how organisms adapt and evolve in response to environmental and ecological challenges. This thesis delves into the dynamics of evolutionary adaptation and ecology within microbial communities, focusing on *Escherichia coli* as a model organism. Through a series of three interconnected studies, this thesis illuminates the complex interplay between genetic mutations, environmental pressures, and adaptive strategies that govern microbial evolution.

The first chapter sets the foundation by exploring the genetics of adaptation in a simple *E. coli* community. Using controlled experimental settings, it examines how specific genetic variations confer survival advantages under varying environmental conditions. This chapter underscores the significance of genetic diversity as a reservoir for adaptive potential, illustrating how even minor genetic changes can lead to significant evolutionary shifts in microbial populations.

Building on the genetic insights from the first chapter, the second chapter shifts focus to ecological interactions and their impact on evolutionary outcomes. Here, the study investigates how *E. coli* strains can diversify to exploit different ecological niches and the resulting impact on their adaptive trajectories. This chapter reveals the importance of ecological factors in shaping evolutionary pathways, highlighting how microbial communities dynamically respond to ecological constraints and opportunities.

The final chapter extends the discussion to focus on the evolutionary effects of non-adaptive population fluctuations. Using the same *E. coli* communities, it shows how population fluctuations can arise from differences in offspring number correlations between individuals. These fluctuations are distinct from the classical source of population fluctuations, genetic drift, and can have significant impacts on the trajectory of evolution.

Together, these findings emphasize the multifaceted nature of evolutionary adaptation in microbial communities. They highlight the critical role of genetic diversity in providing

the raw material for evolution, the influence of ecological interactions in directing adaptive pathways, and the effect of non-adaptive processes.

Future research can continue to explore the complex dynamics of microbial evolution, particularly focusing on the interplay between genetic and ecological factors over varying temporal scales. This would not only enhance our understanding of microbial adaptation but also provide insights applicable to broader evolutionary contexts, including those of higher organisms.

To Zia

Acknowledgments

No individual exists apart from the tangled bank, and of course, I'm no exception. I owe so much to all the people who have taught me and supported me throughout graduate school, much more than I can hope to express here.

As a green first-year graduate student, the Hallatschek lab was not initially on my radar, but I am truly grateful that I ended up here. I found myself in a lab that prioritized creative, rigorous science, filled with generous and kind people. Here I learned to do and argue science thoughtfully, without losing sight of the humanity behind the process. I have learned an incredible amount from Oskar, as a person and a scientist, and I will forever be grateful. Oskar has largely shaped my trajectory as a scientist, entirely for the best, teaching me how to think carefully and do science that will last.

I am extraordinarily thankful for all the members of the Hallatschek Lab. From late nights in lab, Tahoe trips, and plenty of coffee chats, it was always been a delight to be with everyone. My first mentors in the lab were Jona and Ben, on the experimental and theoretical side, respectively. From Jona, I learned how to be a careful and attentive experimentalist, and to remember to bring joy and camaraderie into science. From Ben, I learned about the remarkable possibilities of rigorous and considered theory, and he constantly pushed me to do the best work I could. Kelly, my collaborator from the Arkin lab, largely taught me bacterial genetics, and has been a constant wellspring of good advice and kindness. QinQin was one of my closest collaborators in the Hallatschek lab. Just one year ahead of me, I always felt that we were learning and growing together on the same path. QinQin always emboldened me to be thoughtful and diligent, and inspired me with her sense of openness and deep well of kindness. Jonas was my other close collaborator in the lab; a theorist by training but experimentally inclined, I had a blast experimenting with him in lab and bouncing ideas off of each other.

I would like to thank my qualifying exam and thesis committee members, for providing essential advice and direction—Oskar Hallatschek, Adam Arkin, Jimmie Ye, Dipti Nayak, Priya Moorjani, and Michi Taga. I would also like to thank all of the teachers, formal and informal, that I've been lucky enough to learn from during my time in Berkeley.

The past few years would have been nothing without all of the friends and family whom I've had the privilege to love. There are too many to fully enumerate, but I will name a few. My parents, João and Vivian, and my brother, Victor, have always supported me in my journeys, cheering me on along the way, and sharing in beautiful memories. My friends, in and out of the Bay Area, have been a constant source of fun and joy. Through countless fun adventures, supporting each other through lockdowns, and laughing together over nothing, I've been so grateful for their friendship. And of course, my fiancée, Zia, has been my rock and the love of my life. The years have contained their share of struggles and joys, and Zia has been there with me through all of it. She inspires me every day, and it has been a joy to go through life by her side.

Chapter 2 appears in its entirety as: Ascensao JA, Wetmore KM, Good BH, Arkin AP, Hallatschek O. Quantifying the local adaptive landscape of a nascent bacterial community. *Nature Communications* 14, 248 (2023).

Chapter 3 appears as an edited version (following one round of peer review) of the preprint: Ascensao JA, Denk J, Lok K, Yu Q, Wetmore KM, Hallatschek O. Rediversification following ecotype isolation reveals hidden adaptive potential. *bioRxiv* (2023).

Chapter 4 was written in collaboration with Kristen Lok and Oskar Hallatschek.

Chapter 1: Introduction

The whole landscape showed design, like man's noblest sculptures. How wonderful the power of its beauty! Gazing awe-stricken, I might have left everything for it. Glad, endless work would then be mine tracing the forces that have brought forth its features, its rocks and plants and animals and glorious weather. Beauty beyond thought everywhere, beneath, above, made and being made forever.

— John Muir, *My First Summer in the Sierra* [1]

The study of evolutionary processes has historically been deeply tied with the mathematical theory of population genetics. Over the past century, population geneticists have developed a successful theoretical framework to predict and model how evolutionary forces, such as natural selection and genetic drift, combine to affect evolutionary outcomes [2]. However, until recently, quantitative tests of these theories have been restricted to retrospective approaches—inferring past evolutionary dynamics by looking at current genetic diversity—which is akin to trying to understand a story by only reading its last chapter. The rise of sequencing technologies and quantitative assays over the past two decades has given us an unprecedented opportunity to precisely test quantitative theories of evolution in real time [3–7].

Microbial populations, with their rapid generation times, have become ideal systems for such studies, enabling observations of evolutionary processes that would span millennia in larger organisms to be condensed into mere days. These evolution experiments have allowed evolutionary biologists to begin to better understand and pull apart the various evolutionary forces acting on a population, such as natural selection, ecological forces, and random population fluctuations (genetic drift). Evolutionary forces often interact in complex ways to determine the fate of a population. For example, natural selection alters the frequency of alleles (gene variants) in a population based on their fitness [8–12]. In contrast, genetic drift randomly changes allele frequencies without a specific trend. Many studies in theoretical population genetics have shown complex interactions between natural selection and genetic drift. For instance, the likelihood of a new mutation becoming dominant in a population largely depends on random drift when the mutation is rare, and on natural selection when it becomes more common [10, 13, 14].

Through an increasingly large body of work, we increasingly see that the framework of theoretical population genetics is unreasonably good at quantitatively predicting, and understanding, aspects of evolutionary dynamics [15–17]. This may come as a surprise because biological systems are often viewed as unmanageably complex, immune to the penetration of the quantitative theories that dominate engineering, physics, and chemistry. But population genetics works so effectively because evolving populations are composed of many individuals, and across nature, we often see that the (probabilistic) dynamics of many-bodied systems are universal across a given class [13]. This allows us to coarse-grain biological idiosyncrasies into effective parameters, which can be measured (at least in principal) by observing the population dynamics, providing the ability to directly compare quantitative theories against experimental data [15, 18]. Even simple, naive initial models can provide a springboard to more correct and realistic theoretical descriptions. The prospect of accurate, quantitative theories of evolution opens the possibility to controlling and designing evolving populations, with potentially significant environmental and health applications.

Perhaps the longest and most significant evolution experiment has been the *Escherichia coli* Long Term Evolution Experiment (LTEE) [19–21]. Started in 1988 by Dr. Richard

Lenski, the LTEE has been continuously running ever since. An initially clonal strain of *E. coli* B was inoculated in twelve identical, independent populations. Every 24 hours, a small portion of the well-mixed, overnight culture is propagated into fresh media. The media and environment has stayed the same for the entire duration of the experiment, and yet the populations have not stopped adapting and evolving [6, 22].

At the outset of the Long-Term Evolution Experiment (LTEE), a notable development was observed in one of the twelve lineages, specifically the ara-2 population. This population spontaneously split into two distinct lineages, known as S and L (reflecting their small and large colony sizes on specific agar plates), as a result of negative frequency dependence [23]. These lineages thrive in the LTEE environment, characterized by serial dilutions in glucose minimal media, by occupying different temporal and metabolic niches. The L lineage shows a faster growth rate on glucose during the exponential phase, whereas the S lineage is better adapted for survival in the stationary phase and efficiently utilizes acetate, a byproduct of overflow metabolism [24, 25]. Over time, these lineages have not only persisted but also continued to evolve and differentiate at the genetic, transcriptional, and metabolic levels [6, 23–28]. Although the ara-2 lineage is the most extensively studied case of diversification within the LTEE, it is not unique in this respect. Recent time-resolved metagenomic sequencing has revealed that, in reality, nine out of the twelve LTEE populations have undergone similar diversification, leading to the evolution of two separate lineages that have coexisted for tens of thousands of generations while continuing to evolve and adapt. This demonstrates that spontaneous diversification followed by coevolution is a significant adaptive strategy in this system. Similar diversification and coevolution events have been observed in many other evolving microbial populations. In both natural systems [29–32] and experimental settings, people have observed rapid ecological diversification, typically propelled by mechanisms such as cross-feeding [24, 33–36], resource partitioning [37–41], spatial niche differentiation [42–45], and potentially other ecological trade-offs [46, 47].

Thus, it has become increasingly apparent that interactions between and within species can dramatically influence evolutionary trajectories, but the precise ways in which this happens remain poorly understood, and an area of active research. Theoretical population genetics has historically paid little attention to explicitly considering ecological interactions between species, although recent efforts have been devoted to bridging the gap with theoretical ecology [48]. Testing and validation of theoretical ideas necessitates gathering high-quality, quantitative data on the evolutionary dynamics of populations.

In this thesis, I use populations from the ara-2 lineage of the LTEE to investigate a suite of related eco-evolutionary questions, centered around uncovering the contribution of species interactions to evolutionary dynamics. The LTEE offers an unparalleled opportunity to observe microbial evolution and diversification over extended periods. The spontaneous diversification observed in the LTEE serves as an ideal model to study the evolutionary dynamics in microbial communities.

This thesis contributes to a deeper understanding of microbial community dynamics by integrating evolutionary biology, ecology, and advanced genetic methodologies. It sheds light on the adaptive potential of microbial communities, the role of ecological interactions in shaping evolutionary pathways, and the emergence of non-adaptive processes. The findings have the potential to inform broader ecological and evolutionary theories, as well as practical applications in environmental management, disease control, and biotechnology.

References

- [1] Muir, J. *My first summer in the Sierra* (Houghton Mifflin company, 1911).
- [2] Ewens, W. J. *Mathematical Population Genetics 1: Theoretical Introduction* (Springer Science & Business Media, 2004).

- [3] Lang, G. I. *et al.* Pervasive genetic hitchhiking and clonal interference in forty evolving yeast populations. *Nature* **500**, 571–574, DOI: [10.1038/nature12344](https://doi.org/10.1038/nature12344) (2013).
- [4] Levy, S. F. *et al.* Quantitative evolutionary dynamics using high-resolution lineage tracking. *Nature* **519**, 181–186, DOI: [10.1038/nature14279](https://doi.org/10.1038/nature14279) (2015).
- [5] Venkataram, S. *et al.* Development of a Comprehensive Genotype-to-Fitness Map of Adaptation-Driving Mutations in Yeast. *Cell* **166**, 1585–1596.e22, DOI: [10.1016/j.cell.2016.08.002](https://doi.org/10.1016/j.cell.2016.08.002) (2016).
- [6] Good, B. H., McDonald, M. J., Barrick, J. E., Lenski, R. E. & Desai, M. M. The dynamics of molecular evolution over 60,000 generations. *Nature* **551**, 45–50, DOI: [10.1038/nature24287](https://doi.org/10.1038/nature24287) (2017).
- [7] Ba, A. N. N. *et al.* High-resolution lineage tracking reveals travelling wave of adaptation in laboratory yeast. *Nature* *2019* 1–11, DOI: [10.1038/s41586-019-1749-3](https://doi.org/10.1038/s41586-019-1749-3) (2019).
- [8] Fisher, R. A. XXI.—On the Dominance Ratio. *Proceedings of the Royal Society of Edinburgh* **42**, 321–341, DOI: [10.1017/S0370164600023993](https://doi.org/10.1017/S0370164600023993) (1923). Publisher: Royal Society of Edinburgh Scotland Foundation.
- [9] Haldane, J. B. S. A Mathematical Theory of Natural and Artificial Selection, Part V: Selection and Mutation. *Mathematical Proceedings of the Cambridge Philosophical Society* **23**, 838–844, DOI: [10.1017/S0305004100015644](https://doi.org/10.1017/S0305004100015644) (1927). Publisher: Cambridge University Press.
- [10] Kimura, M. On the probability of fixation of mutant genes in a population. *Genetics* **47**, 713–719, DOI: [10.1093/genetics/47.6.713](https://doi.org/10.1093/genetics/47.6.713) (1962).
- [11] Uecker, H. & Hermisson, J. On the Fixation Process of a Beneficial Mutation in a Variable Environment. *Genetics* **188**, 915–930, DOI: [10.1534/genetics.110.124297](https://doi.org/10.1534/genetics.110.124297) (2011).
- [12] Barrick, J. E. & Lenski, R. E. Genome dynamics during experimental evolution. *Nature Reviews Genetics* **14**, 827–839, DOI: [10.1038/nrg3564](https://doi.org/10.1038/nrg3564) (2013). Number: 12 Publisher: Nature Publishing Group.
- [13] Kimura, M. Diffusion Models in Population Genetics. *Journal of Applied Probability* **1**, 177–232, DOI: [10.2307/3211856](https://doi.org/10.2307/3211856) (1964). Publisher: Applied Probability Trust.
- [14] Ohta, T. Slightly Deleterious Mutant Substitutions in Evolution. *Nature* **246**, 96–98, DOI: [10.1038/246096a0](https://doi.org/10.1038/246096a0) (1973). Number: 5428 Publisher: Nature Publishing Group.
- [15] Desai, M. M. & Fisher, D. S. Beneficial Mutation–Selection Balance and the Effect of Linkage on Positive Selection. *Genetics* **176**, 1759–1798, DOI: [10.1534/genetics.106.067678](https://doi.org/10.1534/genetics.106.067678) (2007).
- [16] Hallatschek, O., Hersen, P., Ramanathan, S. & Nelson, D. R. Genetic drift at expanding frontiers promotes gene segregation. *Proceedings of the National Academy of Sciences* **104**, 19926–19930, DOI: [10.1073/pnas.0710150104](https://doi.org/10.1073/pnas.0710150104) (2007).
- [17] Hallatschek, O. Selection-Like Biases Emerge in Population Models with Recurrent Jackpot Events. *Genetics* **210**, 1053–1073, DOI: [10.1534/genetics.118.301516](https://doi.org/10.1534/genetics.118.301516) (2018).

- [18] Good, B. H., Rouzine, I. M., Balick, D. J., Hallatschek, O. & Desai, M. M. Distribution of fixed beneficial mutations and the rate of adaptation in asexual populations. *Proceedings of the National Academy of Sciences of the United States of America* **109**, 4950–4955, DOI: [10.1073/pnas.1119910109](https://doi.org/10.1073/pnas.1119910109) (2012).
- [19] Lenski, R. E. Revisiting the Design of the Long-Term Evolution Experiment with *Escherichia coli*. *Journal of Molecular Evolution* DOI: [10.1007/s00239-023-10095-3](https://doi.org/10.1007/s00239-023-10095-3) (2023).
- [20] Lenski, R. E. & Travisano, M. Dynamics of adaptation and diversification: A 10,000-generation experiment with bacterial populations. *Proceedings of the National Academy of Sciences of the United States of America* **91**, 6808–6814, DOI: [10.1073/pnas.91.15.6808](https://doi.org/10.1073/pnas.91.15.6808) (1994).
- [21] Lenski, R. E., Rose, M. R., Simpson, S. C. & Tadler, S. C. Long-Term Experimental Evolution in *Escherichia coli*. I. Adaptation and Divergence During 2,000 Generations. *The American Naturalist* **138**, 1315–1341 (1991). Publisher: [University of Chicago Press, American Society of Naturalists].
- [22] Wisser, M. J., Ribbeck, N. & Lenski, R. E. Long-term dynamics of adaptation in asexual populations. *Science* **342**, 1364–1367, DOI: [10.1126/science.1243357](https://doi.org/10.1126/science.1243357) (2013).
- [23] Rozen, D. E. & Lenski, R. E. Long-Term Experimental Evolution in *Escherichia coli*. VIII. Dynamics of a Balanced Polymorphism. *The American naturalist* **155**, 24–35, DOI: [10.1086/303299](https://doi.org/10.1086/303299) (2000).
- [24] Rozen, D. E., Philippe, N., Arjan de Visser, J., Lenski, R. E. & Schneider, D. Death and cannibalism in a seasonal environment facilitate bacterial coexistence. *Ecology Letters* **12**, 34–44, DOI: [10.1111/j.1461-0248.2008.01257.x](https://doi.org/10.1111/j.1461-0248.2008.01257.x) (2009).
- [25] Großkopf, T. *et al.* Metabolic modelling in a dynamic evolutionary framework predicts adaptive diversification of bacteria in a long-term evolution experiment. *BMC Evolutionary Biology* **16**, 163, DOI: [10.1186/s12862-016-0733-x](https://doi.org/10.1186/s12862-016-0733-x) (2016).
- [26] Rozen, D. E., Schneider, D. & Lenski, R. E. Long-Term Experimental Evolution in *Escherichia coli*. XIII. Phylogenetic History of a Balanced Polymorphism. *Journal of Molecular Evolution* **61**, 171–180, DOI: [10.1007/s00239-004-0322-2](https://doi.org/10.1007/s00239-004-0322-2) (2005).
- [27] Le Gac, M., Plucain, J., Hindré, T., Lenski, R. E. & Schneider, D. Ecological and evolutionary dynamics of coexisting lineages during a long-term experiment with *Escherichia coli*. *Proceedings of the National Academy of Sciences of the United States of America* **96**, 10242–7, DOI: [10.1073/pnas.96.18.10242](https://doi.org/10.1073/pnas.96.18.10242) (2012).
- [28] Plucain, J. *et al.* Epistasis and allele specificity in the emergence of a stable polymorphism in *Escherichia coli*. *Science* **343**, 1366–1369, DOI: [10.1126/science.1248688](https://doi.org/10.1126/science.1248688) (2014).
- [29] Gómez, P. & Buckling, A. Real-time microbial adaptive diversification in soil. *Ecology Letters* **16**, 650–655, DOI: [10.1111/ele.12093](https://doi.org/10.1111/ele.12093) (2013). eprint: <https://onlinelibrary.wiley.com/doi/pdf/10.1111/ele.12093>.
- [30] Folkesson, A. *et al.* Adaptation of *Pseudomonas aeruginosa* to the cystic fibrosis airway: An evolutionary perspective, DOI: [10.1038/nrmicro2907](https://doi.org/10.1038/nrmicro2907) (2012).

- [31] Zhao, S. *et al.* Adaptive Evolution within Gut Microbiomes of Healthy People. *Cell Host and Microbe* **25**, 656–667, DOI: [10.1016/j.chom.2019.03.007](https://doi.org/10.1016/j.chom.2019.03.007) (2019).
- [32] Sousa, A. *et al.* Recurrent Reverse Evolution Maintains Polymorphism after Strong Bottlenecks in Commensal Gut Bacteria. *Molecular Biology and Evolution* **34**, 2879–2892, DOI: [10.1093/MOLBEV/MSX221](https://doi.org/10.1093/MOLBEV/MSX221) (2017).
- [33] M, K. *et al.* Ex uno plures: clonal reinforcement drives evolution of a simple microbial community. *PLoS genetics* **10**, DOI: [10.1371/JOURNAL.PGEN.1004430](https://doi.org/10.1371/JOURNAL.PGEN.1004430) (2014).
- [34] Treves, D. S., Manning, S. & Adams, J. Repeated evolution of an acetate-crossfeeding polymorphism in long-term populations of *Escherichia coli*. *Molecular Biology and Evolution* **15**, 789–797, DOI: [10.1093/oxfordjournals.molbev.a025984](https://doi.org/10.1093/oxfordjournals.molbev.a025984) (1998).
- [35] Rosenzweig, R. F., Sharp, R. R., Treves, D. S. & Adams, J. Microbial evolution in a simple unstructured environment: genetic differentiation in *Escherichia coli*. *Genetics* **137**, 903–917, DOI: [10.1093/genetics/137.4.903](https://doi.org/10.1093/genetics/137.4.903) (1994).
- [36] Kinnersley, M. A., Holben, W. E. & Rosenzweig, F. E Unibus Plurum: Genomic Analysis of an Experimentally Evolved Polymorphism in *Escherichia coli*. *PLOS Genetics* **5**, e1000713, DOI: [10.1371/journal.pgen.1000713](https://doi.org/10.1371/journal.pgen.1000713) (2009). Publisher: Public Library of Science.
- [37] Meyer, J. R. *et al.* Ecological speciation of bacteriophage lambda in allopatry and sympatry. *Science (New York, N.Y.)* **354**, 1301–1304, DOI: [10.1126/science.aai8446](https://doi.org/10.1126/science.aai8446) (2016).
- [38] Herron, M. D. & Doebeli, M. Parallel evolutionary dynamics of adaptive diversification in *Escherichia coli*. *PLoS biology* **11**, e1001490 (2013).
- [39] Friesen, M. L., Saxer, G., Travisano, M. & Doebeli, M. Experimental evidence for sympatric ecological diversification due to frequency-dependent competition in *Escherichia coli*. *Evolution; International Journal of Organic Evolution* **58**, 245–260 (2004).
- [40] Tyerman, J., Havard, N., Saxer, G., Travisano, M. & Doebeli, M. Unparallel diversification in bacterial microcosms. *Proceedings. Biological Sciences* **272**, 1393–1398, DOI: [10.1098/rspb.2005.3068](https://doi.org/10.1098/rspb.2005.3068) (2005).
- [41] Cooper, T. F. & Lenski, R. E. Experimental evolution with *E. coli* in diverse resource environments. I. Fluctuating environments promote divergence of replicate populations. *BMC Evolutionary Biology* **10**, 11, DOI: [10.1186/1471-2148-10-11](https://doi.org/10.1186/1471-2148-10-11) (2010).
- [42] Frenkel, E. M. *et al.* Crowded growth leads to the spontaneous evolution of semistable coexistence in laboratory yeast populations. *Proceedings of the National Academy of Sciences of the United States of America* **112**, 11306–11311, DOI: [10.1073/pnas.1506184112](https://doi.org/10.1073/pnas.1506184112) (2015).
- [43] Rainey, P. B. & Travisano, M. Adaptive radiation in a heterogeneous environment. *Nature* **394**, 69–72 (1998).
- [44] Flohr, R. C. E., Blom, C. J., Rainey, P. B. & Beaumont, H. J. E. Founder niche constrains evolutionary adaptive radiation. *Proceedings of the National Academy of Sciences* **110**, 20663–20668, DOI: [10.1073/pnas.1310310110](https://doi.org/10.1073/pnas.1310310110) (2013). Publisher: Proceedings of the National Academy of Sciences.

- [45] Flynn, K. M. *et al.* Evolution of Ecological Diversity in Biofilms of *Pseudomonas aeruginosa* by Altered Cyclic Diguanylate Signaling. *Journal of Bacteriology* **198**, 2608–2618, DOI: [10.1128/JB.00048-16](https://doi.org/10.1128/JB.00048-16) (2016).
- [46] King, T., Ishihama, A., Kori, A. & Ferenci, T. A regulatory trade-off as a source of strain variation in the species *Escherichia coli*. *Journal of Bacteriology* **186**, 5614–5620, DOI: [10.1128/JB.186.17.5614-5620.2004](https://doi.org/10.1128/JB.186.17.5614-5620.2004) (2004).
- [47] Maharjan, R. P. *et al.* The multiplicity of divergence mechanisms in a single evolving population. *Genome Biology* **13**, R41, DOI: [10.1186/gb-2012-13-6-r41](https://doi.org/10.1186/gb-2012-13-6-r41) (2012).
- [48] Good, B. H., Martis, S. & Hallatschek, O. Adaptation limits ecological diversification and promotes ecological tinkering during the competition for substitutable resources. *Proceedings of the National Academy of Sciences* **115**, DOI: [10.1073/pnas.1807530115](https://doi.org/10.1073/pnas.1807530115) (2018).

Chapter 2: Quantifying the Local Adaptive Landscape of a Nascent Bacterial Community

Abstract

The fitness effects of all possible mutations available to an organism largely shape the dynamics of evolutionary adaptation. Yet, whether and how this adaptive landscape changes over evolutionary times, especially upon ecological diversification and changes in community composition, remains poorly understood. We sought to fill this gap by analyzing a stable community of two closely related ecotypes ("L" and "S") shortly after they emerged within the *E. coli* Long-Term Evolution Experiment (LTEE). We engineered genome-wide barcoded transposon libraries to measure the invasion fitness effects of all possible gene knockouts in the coexisting strains as well as their ancestor, for many different, ecologically relevant conditions. We find consistent statistical patterns of fitness effect variation across both genetic background and community composition, despite the idiosyncratic behavior of individual knockouts. Additionally, fitness effects are correlated with evolutionary outcomes for a number of conditions, possibly revealing shifting patterns of adaptation. Together, our results reveal how ecological and epistatic effects combine to shape the adaptive landscape in a nascent ecological community.

Introduction

Microbial communities are ubiquitous across all environments, and are key players in disease processes, biogeochemical cycling, and ecosystem functioning [1–6]. While most research on natural microbiomes has been fueled by their ecological significance, recent studies have begun to focus on microbial community evolution and uncovered clear signs of adaptation and diversification [7–10]. Thus, microbiome assembly, structure, and function may have to be understood against a backdrop of an ever-churning evolutionary dynamics.

That evolutionary and ecological changes often go together has been most clearly shown in controlled experiments on synthetic microbial communities: evolution can change the way microbes consume resources or otherwise interact with each other [11–15]. This leads to environmental changes that modify selection pressures, forcing lineages into new evolutionary paths [16–21]. Complex adaptive landscapes have been hypothesized to chiefly shape the feedback between ecology and evolution in microbial communities [19, 22], but it is still unclear how diversification and other ecological shifts change those landscapes.

In ecologically simple monoculture populations, population genetic theory has shown that the evolutionary dynamics are largely predictable from knowing local aspects of a static fitness landscape, encoding the fitness effects of all currently available mutations, which is called the "distribution of fitness effects" (DFE) [23–28]. Such work has been successful in rationalizing and predicting outcomes of evolution experiments from DFE measurements [29, 30].

High-quality measurements of the DFE in a given system require sampling and measuring the fitness effects of sufficiently many mutations across the genome. This has only become possible recently, due to the rise of sequencing technologies. DNA barcoding systems have become especially influential to better understand microbial adaptive evolution. By taking advantage of amplicon sequencing methods to measure barcode frequency dynamics, these systems have been used with great success to directly observe evolutionary dynamics [30–33], and identify selected mutations and the statistical patterns that characterize them [34–39].

However, the concept of a *single, static* DFE may not be applicable or useful to describe a diversified population. It is possible that different ecotypes experience different adaptive landscapes, even if they are closely related, which moreover may shift in response to compositional or other ecological changes. Despite the importance of microbial communities, very little is known about how much the local landscape depends on biotic interactions with their coexisting strains versus genetic background alone, and how those patterns shift upon diversification.

Here we aim to elucidate the adaptive landscape of a recently diversified microbial community by measuring how the invasion fitness effects of a large panel of mutations depends on the state of the ecosystem. Invasion fitness refers to the growth rate of a mutant relative to its ancestor when the mutant is rare in the population. To sample from the DFE, we create genome-wide knockout libraries via random-barcoded transposon mutagenesis [40, 41] on the backgrounds of the coexisting ecotypes. While knockout mutations do not represent all possible mutations in the genome, this approach allows us to sample a wide variety of mutations across the genome and to compare the effect of the same mutation across different genetic backgrounds and community compositions. The resulting ecotype-, and composition-dependent DFE statistically characterizes the abundance and specificity of beneficial mutations and, thus, reveals how the rate and pattern of mutation accumulation depends on the state of the ecosystem.

We reasoned that the ecologically-dependent DFEs accessible by our approach are particularly relevant to the fate of a recently diversified ecosystem, consisting of closely related ecotypes with overlapping niches. Additionally, quantifying the DFEs of such a nascent community would shed light on how the discovery and infiltration of a new niche changes the local adaptive landscape, in both focal and “nearby” environments. The composition-dependence of the DFE would also provide information on the types of mutations available to the community—“pure fitness” mutations would show minimal fitness changes in response to composition shifts, whereas frequency-dependent mutations may point to shifts in niche occupation/strategy. Theory suggests that the relative availability of “pure fitness” versus frequency-dependent mutations may strongly influence the resulting evolutionary dynamics, but there have been few empirical measurements of how many mutations show frequency-dependent effects [19].

We therefore chose to focus on a model ecosystem that spontaneously emerged in the course of the *E. coli* Long Term Evolution Experiment (LTEE) – an experiment that has tracked the evolution of several *E. coli* populations over the course of over 70,000 generations (at the time of writing). Early in the LTEE, it was recognized that one of the twelve lineages, the *ara-2* population on which we focus in this study, spontaneously diversified into two lineages that coexist via negative frequency dependence, termed S and L (for their small and large colony sizes on certain agar plates) [42]. S and L coexist by inhabiting different temporal/metabolic niches in the LTEE environment, set up as serial dilutions in glucose minimal media—L grows more quickly on glucose during exponential phase, while S specializes on stationary phase survival and utilizing acetate, a byproduct of overflow metabolism [43, 44]. Following diversification, the lineages have persisted to this day and continued to evolve and adapt, diverging on genetic, transcriptional, and metabolic levels [16, 42–47]. While our focal *ara-2* line is the best studied case of diversification in the LTEE, it is not the only one. Recent time-resolved metagenomic sequencing of the LTEE has shown that, in fact, 9 out of the 12 populations evolved two separate lineages that coexisted with each other for tens of thousands of generations, while continuing to accumulate mutations and adapt [47], demonstrating that spontaneous diversification followed by coevolution is a major adaptive route for this system.

Here we show how the adaptive landscapes change between the ancestor and derived strains of the LTEE, and how they are different between two closely related ecotypes. We found that the invasion fitness effects of many gene knockouts sensitively depends on the genetic background and the ecological conditions, as set by the abiotic environment

and relative frequency of both ecotypes. Despite the idiosyncratic behavior of individual knockouts, we still see consistent statistical patterns of fitness effect variation across both genetic background and community composition. Beneficial knockouts generally show a strong dependence on the community composition, indicating that there are few “pure fitness” mutations. Genes that are in the same operon, or that strongly interact with each other, are more likely to be correlated with each other across backgrounds compared to random pairs of genes. Additionally, fitness effects are correlated with evolutionary outcomes for a number of conditions, possibly revealing shifting patterns of adaptation. Together, our results reveal how ecological and epistatic effects combine to shape the adaptive landscape in a nascent ecological community.

Results

Measuring knockout fitness effects

We sought to measure the knockout fitness effects available to the small LTEE-derived ecosystem of S and L, and how they depend on ecological conditions, specifically, (i) the composition of the community, and (ii) openness of a given metabolic niche. To this end, we created randomly barcoded transposon libraries of three LTEE clones, using previously developed methods (RB-TnSeq) [40, 41]—S and L clones sampled from 6.5k generations, shortly (~500 generations) after diversification [16, 42], and their LTEE ancestor, REL606 (Figure 1A). We used these libraries to measure the knockout fitness effects of nearly all non-essential genes in various environments relevant to the evolution of the population in the LTEE (Table 1), by propagating the libraries in defined conditions (with two biological replicates per experiment) and using Illumina amplicon sequencing to track the frequency trajectories of different barcodes (Figure 1B). By essentially measuring the log-slope of the frequency trajectories, we can estimate the fitness effect, s , of a given mutant (Figure 1C), which we report in units of $1/\text{generation}$. Transposon insertion events were highly redundant, with a median of ~20 insertions per gene, allowing us to combine information from multiple barcode trajectories into one fitness measurement through our statistical fitness inference pipeline and identify significantly non-neutral mutations (FDR correction; $\alpha = 0.05$). We carefully quantified sources of error in barcode frequency measurements and propagated them to our fitness estimates, which was crucial to effective and accurate analysis of the data (see methods section)—for example, we could exclude knockouts with overly noisy fitness measurements, or weight measurements by their error.

Barcoded transposon mutagenesis has been successfully and consistently used to measure knockout fitness effects across many contexts [40, 41], but as the knockouts are not bonafide deletions, it is possible that some genes with transposon insertions retain some activity. However, the fact that we have multiple transposon insertions spread across the length of each gene, along with our outlier barcode detection scheme, allows us to be more confident that our fitness measurements are dominated by the typical effects of an insertion.

After inferring the fitness effect of each gene knockout, we can compare fitness effects across genetic backgrounds and environments. We can first look at knockout fitness effects in the evolutionary condition proxies—the closest approximation to the environment where evolution in the LTEE took place: the REL606 library in monoculture, and S and L libraries together, coexisting at the ecological equilibrium frequency. We chose to highlight the condition where S and L were coexisting at their ecological equilibrium to be able to distinguish environmental versus genetic contributions to fitness effects—the libraries were cocultured together, in the same flasks, thus experiencing the same environment. In coculture experiments, the S/L libraries are mixed in the minority together with wild-type S/L clones at the desired frequency (see methods section). The ecotype frequencies do not change considerably over the time period considered (Figure S3).

If we look at the overall DFE in the evolutionary condition proxies, we see that REL606 has access to beneficial knockouts of much larger effect size than either S or L (Figure 1D),

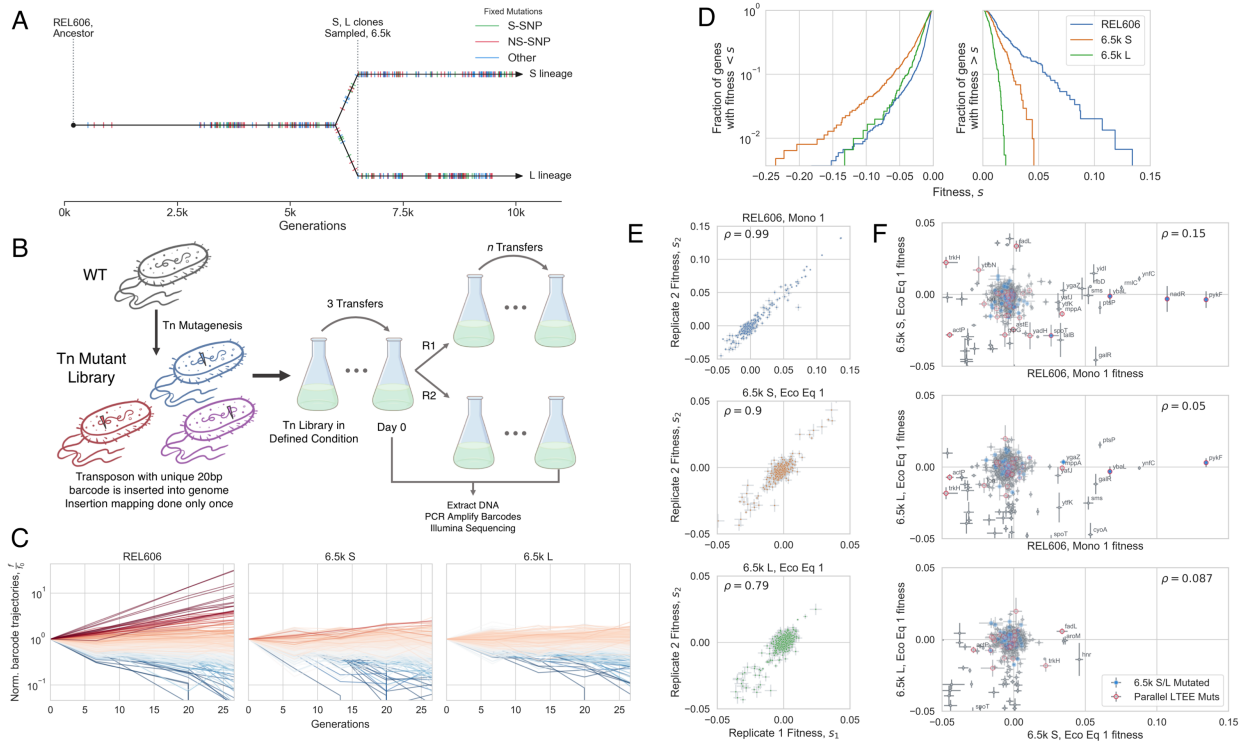


Fig. 1 Measuring mutational fitness effects. (A) Timeline of evolution in the *ara-2* LTEE population, showing mutation accumulation and diversification into S and L around 6k generations, then clone sampling at 6.5k generations; data from [47], jitter added to mutation fixation time for easier visualization. Hypermutator phenotype appeared around 2.5k generations [48]. (B) Schematic of transposon mutagenesis process to generate barcoded libraries of REL606, 6.5k S and L, as well as experimental procedure to observe barcode dynamics. (C) Barcoded knockout mutant frequency trajectories in the evolutionary condition for each genetic background, colored by estimated fitness. All barcodes within a gene were summed together; shown are the trajectories from replicate 1 in the evolutionary condition for each genetic background (monoculture for REL606, together at ecological equilibrium frequency for S and L; representative of both replicates). (D) Overall distributions of fitness effects in the evolutionary condition for each genetic background. The majority of knockouts were neutral, so only genes that were called as significantly non-neutral were included (see supplement section). (E) Replicate-replicate correlation of estimated fitness effects. Error bars represent standard errors. (F) Comparison of knockout fitness effects across genetic backgrounds, which are generally uncorrelated. Points with a blue interior correspond to genes that were mutated (excluding S-SNPs) in 6.5k S/L relative to REL606 (sequencing data from [46]). Points with red outlines correspond to genes that were mutated in parallel in nonmutator LTEE populations (data from [47]). The correlation coefficients decrease slightly if we recompute them, excluding likely neutral genes ($\rho = 0.14, 0.03, 0.03$; top to bottom). In panels E-F, knockouts with high measurement noise ($\sigma_s > 0.3\%$) were excluded (except for labeled genes), and ρ is the weighted Pearson correlation coefficient. Also in panels E-F, the "cloud" of points around 0 mostly represents likely neutral knockouts.

suggesting that REL606 would adapt much quicker than S or L. Additionally, S has a larger beneficial DFE compared to L, which may be because S is starting to exploit an under-utilized niche (acetate specialization), where more significant gains can be made by improving the exploitation of the niche. On the other hand, L has inherited the putative old niche (glucose specialization), which was presumably the primary target of adaptation during the first ~6k generations of evolution. As previously mentioned, the overall shape of the DFE largely controls the instantaneous speed of adaptation [23–28]. The evolutionary tendency towards a “shrinking DFE” is known as global diminishing returns epistasis, which has previously been proposed as a mechanism to explain the decelerating fitness trajectories of the LTEE populations [49, 50]. While diminishing returns epistasis was previously observed to affect the first couple common LTEE mutations [51], global diminishing returns (affecting the whole DFE) after the accumulation of many mutations had not yet been directly observed.

We can also compare the fitness effects of each knockout mutation both between replicates and across genetic backgrounds (Figure 1E-F), to contrast within-sample to between-sample variance. In contrast to a strong replicate-replicate correlation, we see that fitness effects are

Experiment	Libraries	Same flasks?	Description
Mono	R, S, L	N	Library monoculture
1:10 dil	R, S, L	N	Library monoculture, 1:10 daily dilution
Glu exp	R, S, L	N	Library monoculture, kept in glucose exponential phase
Ac exp	R, S, L	N	Library monoculture, kept in acetate exponential phase
Eco Eq 1	S, L	Y	S + L libraries with wt L at ecological equilibrium
Eco Eq 2	S	N	S library with wt S + L at ecological equilibrium
Eco Eq 2	L	N	L library with wt S + L at ecological equilibrium
L in maj	S	N	S library with wt L in majority
S in maj 1	L	N	L library with wt S in majority
S in maj 2	S, L	Y	S + L libraries with wt S in majority
S in maj 3	L	N	L library with wt S in majority

Table 1 Summary of BarSeq experiments reported in this work. Dilution rate was variable in the glucose/acetate exponential phase experiments, to keep the populations in exponential phase (see methods section), but unless otherwise noted, the daily dilution rate was 1:100, consistent with the LTEE condition. All experiments were performed in the LTEE media, DM25, except for the acetate exponential phase experiment. The abbreviations R, S, and L refer to REL606, and 6.5k S/L, respectively. In coculture experiments, (f_S) is the total frequency of S, averaged over all time points and replicates.

largely uncorrelated between genetic backgrounds. It may be unsurprising that mutational effects of S and L are uncorrelated with those of their ancestor, as REL606 may be creating and experiencing a slightly different environment compared to S and L, even though they were all started in the same media. However, as previously mentioned, we measured the fitness effects of S and L while they were coexisting in the same flasks, so the two ecotypes were experiencing the exact same environment. Thus, the lack of correlation between the fitness effects of S and L must be due to epistatic effects. It appears that individual mutations behave idiosyncratically despite statistical patterns of epistasis, in contrast with previous experiments [51, 52] which saw diminishing returns both globally and with individual mutations. Most knockout mutations that were strongly beneficial in REL606 and then acquired a mutation in that gene in the 6.5k S/L background became effectively neutral when knocked out in S/L (*nadR*, *pykF*, *ybaL*, *ygaZ*); it makes sense that mutating a gene that was already mutated (with a fitness effect) wouldn't have an effect, if the mutation was effectively a loss-of-function. One gene, *spoT*, was beneficial in REL606 but deleterious in both S and L when knocked out, indicating that the natural *spoT* SNP may represent a change-of-function rather than a loss-of-function mutation. However, the majority of selected genes in REL606 were not mutated between 0 and 6.5k generations in S/L, so the fact that their fitness effects significantly changed across genetic background implicates the role of widespread, global idiosyncratic epistasis. Furthermore, there are several genes that were mutated in parallel in multiple lines of the LTEE, but are only beneficial on the S background (*trkH*, *ybbN*) or both the S and L backgrounds (*fadL*) when knocked out, while being neutral or deleterious on the REL606 background, suggesting that predictable epistasis could have shaped which mutations became beneficial in the LTEE. 'Coupon collection' is a null model of mutation accumulation/epistasis, where a beneficial DFE is composed of a finite number of mutations, and only changes due to the depletion of those mutations when they fix in a population. While the coupon collecting model is clearly relevant for some mutations, the lack of fitness effect correlation between genetic backgrounds seems to be largely driven by global epistasis.

As a simple check, we compared the fitness effect of one of the largest effect knockouts in our collection, *pykF*, to previously collected data. We reanalyzed data from Peng et al. (2018) Mol Biol Evol [53] (to recalculate fitness using the metric that we use) and found that their *pykF* deletion mutant had a selective coefficient $s \approx 4\%$, compared to our measurement $s \approx 12\%$; the highest fitness effect of a *pykF* nonsynonymous mutation on the ancestral background was $s \approx 9\%$, which is similar to our measurement. Additionally, our measured fitness effect of *pykF* is quite consistent—it is approximately the same across all replicates in the Mono 1 and 2 experiments in REL606 (performed on different days). And all of the individual barcodes that landed in *pykF* appear to have approximately the same slopes. One

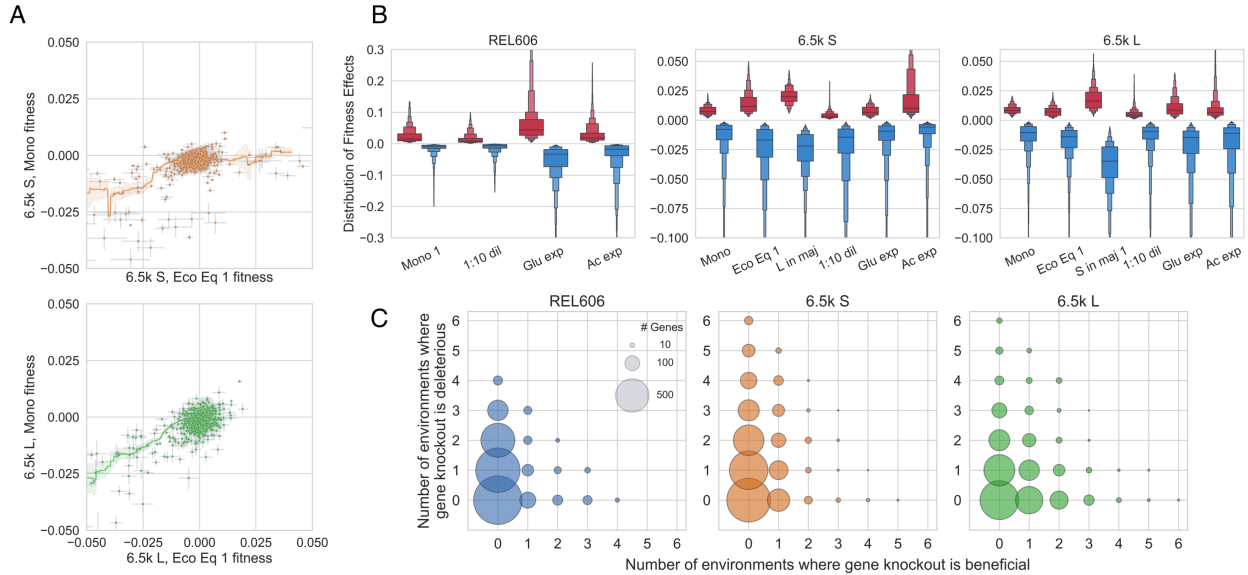


Fig. 2 Statistical properties of DFEs as well as effects of individual mutations sensitively depend on environment. (A) Knockout fitness effects tend to have a larger magnitude when S and L are at ecological equilibrium versus when they are in monoculture. Line shown is a rolling average of fitness effects \pm standard error. (B) Distribution of fitness effects across environments, where we only included knockouts that were called as significantly non-neutral. Please note that the DFEs of REL606 are on a different scale than S and L. (C) Illustration of how the sign of fitness effects changes across environments. Few mutations are unconditionally beneficial or deleterious, many are non-neutral only in one or few environments, and sign-flipping of fitness effects across environments is pervasive. REL606 only has 4 unique environments, compared to 6 for S and L. Size of circle is proportional to number of genes that fall into each class.

possibility to describe the discrepancy could be the presence of frequency dependent fitness effects—the strength of selection may be higher when the mutant is rare (as is the case in our data), compared to when it occupies a sizable portion of the population (as in Peng et al. 2018). Another possibility could be that transposon insertions did not completely eliminate *pykF* activity, as it would in a deletion.

Knockout fitness effects strongly depend on ecological conditions

The ecological interactions between S and L are mediated through the environment, most likely primarily through cross-feeding [43, 44]. Therefore, it's reasonable to think that the environment will change with the ecosystem composition, which could be modified by both ecological and evolutionary processes—indeed, ecotype composition does change significantly and relatively rapidly over evolutionary time ($\sim 1k-10ks$ generations) [42, 47]. Thus, we sought to explore how mutational fitness effects varied with ecosystem composition. Notably, we see a consistent trend where fitness effects generally have a smaller magnitude when S and L are in monoculture compared to when they are in coculture (Figures 2A, S7A). Additionally, we also see that the overall shape of the DFEs change as a function of frequency, with generally larger fitness effects when the ecotype is in the minority, for both beneficial and deleterious knockouts (Figures 2B, S7B). Analogous to the case of global diminishing returns epistasis, this observation holds on a statistical level, but does not explain all of the fitness effect variation between the different conditions, implying that individual mutations are affected by the ecosystem composition in idiosyncratic ways—statistical properties of the DFE seem to be strongly dependent on the ecosystem composition, but the effects of individual mutations may depend on their underlying physiological consequences and how they affect ecological interactions. Thus, it appears that the impact of both ecotypes on the environment is different enough to make selection pressures strongly dependent on the current mixture of ecotypes.

The LTEE environment, while relatively simple, varies quite significantly over the course of a single cycle [43, 54], allowing ecotypes to carve out different temporal ecological niches

during cycles of lag, exponential, and stationary phases. To explore how selection pressures vary in different niches in the growth cycle, we measured fitness in exponential growth on glucose and acetate (which appears in the LTEE environment due to overflow metabolism), and at a reduced dilution rate of 1:10 such that portion of the growth cycle in stationary phase is increased (Table 1). We found that the shape of the DFE changed substantially based on the environment (Figures 2B). For example, while S and L have a similar beneficial DFE shape in monoculture, L has access to stronger beneficial knockout mutations in glucose exponential phase compared to S. As another example, the beneficial DFE in acetate is larger than any other DFE in both S and L, potentially pointing to a substantial, as-of-yet unrealized adaptive potential for adaptation on acetate. Interestingly, despite the environmental variation, REL606 always has a more pronounced beneficial DFE compared to S and L.

It is important to note that measurement noise varied non-negligibly across experiments, primarily because of changes in bottleneck size (and thus in the strength of genetic drift) due to differences in library frequency and other experimental differences (see methods section). Thus, our power to detect selected mutations close to neutrality varied across experiments.

In contrast to previous work [35], it appears that there is no consistent relationship between background fitness and shape of the deleterious DFE, which instead appears to depend more on environment. Possible reasons for the discrepancy include species-dependent differences, and the fact that our set of experiments used backgrounds connected by evolution, while Johnson et al. used evolutionarily unrelated yeast hybrids with varying fitness in the test environment, whose changing DFEs were not controlled by evolution. One possible evolutionary explanation could be second-order selection against mutants with wider deleterious DFEs, because those mutants would be more likely to pick up a deleterious hitchhiker mutation along with any beneficial driver mutation.

In addition to the strong dependence of the macroscopic DFE on environment, it appears that the fitness effects of individual mutations can also change radically by environment. Strikingly, in the set of considered environments, conditional non-neutrality and sign-flipping appear to occur across all three genetic backgrounds (Figure 2C). The majority of knockouts are non-neutral in at least one measured environment; just about ~20% of knockouts are called as neutral across all environments. Very few mutations are unconditionally beneficial or deleterious across all environments, and many more mutations flip signs across environments, suggesting the presence of widespread trade-offs between adapting to different components of an environment. The ubiquitous presence of sign-flipping also suggests that subtle changes to environmental conditions—by changes to community composition or niche openness via adaptation—could meaningfully affect evolutionary outcomes by changing which mutations are likely to establish. The presence of sign-flipping still holds if we reduce the p-value cutoff from 0.05 to 10^{-3} or 10^{-5} to determine non-neutrality (Figure S8), or only consider genes with $|s| > 1\%$ or $|s| > 2\%$ as non-neutral (Figure S9), although more genes are called as neutral, as would be expected. However, it is important to note that we only considered genes to be non-neutral if their fitness was significantly different from 0; thus, it is likely that some knockouts were incorrectly called as neutral, especially if their fitness effect is small. Additionally, we have only measured a relatively small set of closely related environments “nearby” the LTEE environment, so we might expect that if we measure fitness in a sufficiently large number of environments, many more genes would be non-neutral in at least one.

By computing the correlation of mutational fitness effects across environments (weighted by measurement error), we can obtain a measure of the functional similarity of environments, which we can also use to cluster said environments (Figure 3A). As a first observation and check, it is reassuring to see the clustering of quasi-replicate experiments, i.e. experiments with relatively minor differences in the experimental set-up and performed on different days—Eco Eq 1/2, S in maj 1/2/3 (L), and Mono 1/2 (REL606) (see methods section). However,

the correlations between the quasi-replicates are lower than we see for replicate experiments that we did at the same time—this could indicate either that some fitness measurements are sensitive to the small experimental differences (size of flasks, whether libraries are cocultured or not, etc.), or simply performing the experiments on different days with different environmental fluctuations leads to deviations in measured fitness, as is perhaps the case in other systems [37]. The latter hypothesis is further supported by the fact that two experiments were in fact performed at the same time (S in maj 2 and 3), and had among the highest correlation of all quasi-replicates.

Otherwise, there are still some interesting patterns that we can pick out by looking at correlations across environments. For example, it looks like the environments related to the putative ecotype niches—glucose and acetate exponential growth in L and S respectively—cluster with conditions where the ecotype is in the minority. On the other hand, the monoculture experiment in S clusters with glucose exponential phase. Also, in REL606 and L, the acetate experiment is the outgroup compared to all the other environments, and almost completely uncorrelated with fitness in glucose exponential phase, but most correlated with the 1:10 dilution condition. In S, this is not the case, and acetate fitness is *least* correlated with 1:10 dilution fitness. This may indicate that stationary phase in REL606 and L may have much more acetate with which to grow on compared to S, and adaptation to acetate may involve tradeoffs with adaptation to glucose, at least in REL606 and L. We also performed a principal components analysis on our data, using (normalized) fitness effects as features (Figure 3B). We see that L experiments cluster separately from the S and REL606 experiments, with the exception of the acetate exponential phase condition. This may be surprising, given that S was thought to have diversified from an L-like common ancestor [46]. Otherwise, the PCA largely reproduces the insights from the previous correlation clustering analysis.

Correlations between genes across environments

To explore the nature of the strong background dependence that we observed, we sought to understand which genes are correlated with each other across environments, with the intuition that genes that perform the same function should change their fitness effects across environments in similar ways. For example, the *sufABCDSE* operon encodes proteins that help to assemble iron-sulfur clusters [56], and they all have correlated knockout fitness effects across environments in all three genetic backgrounds (Figure S11A)—as they should, if the knockouts all have very similar metabolic/ physiological consequences. However, other gene sets are only correlated in a subset of backgrounds. Most genes in the *fecABCDE* operon are correlated with each other in all backgrounds except for *fecA*, which is well correlated with the others in REL606, less correlated in S, and uncorrelated with the others in L (Figure 4A). Similarly, the genes in the *proVWX* operon are almost perfectly correlated, except one condition where *proV* has a ~7% higher fitness than the other two knockouts (Figure S11B). We can also look at the fitness effects of a subset of knockouts that are beneficial at least once for every genetic background, across environments (Figure S12). We see that subsets of genes that are sometimes beneficial on a background are positively correlated with each other, e.g. *pykF/cyoA* in REL606 and *ptsP/mrcA/gppA* in 6.5k L, perhaps suggesting that the knockouts have common functional effects. These correlations often break when the mutations appear on different genetic backgrounds, e.g. *pykF/cyoA* are no longer correlated on (at least) the 6.5k L background, and *ptsP/mrcA/gppA* are no longer correlated on the 6.5k S background, while *ptsP/mrcA* actually appear *negatively* correlated on the REL606 background. Together, these examples suggest that correlations between knockout fitness effects may change in idiosyncratic ways across genetic backgrounds.

We systematically quantified the pairwise correlation of knockout fitness across environments—termed “cofitness”, previously defined in [41]—where we used the weighted pearson’s correlation coefficient to account for differences in measurement error across environments. We computed the cofitness of all pairs of genes (excluding those called as neutral

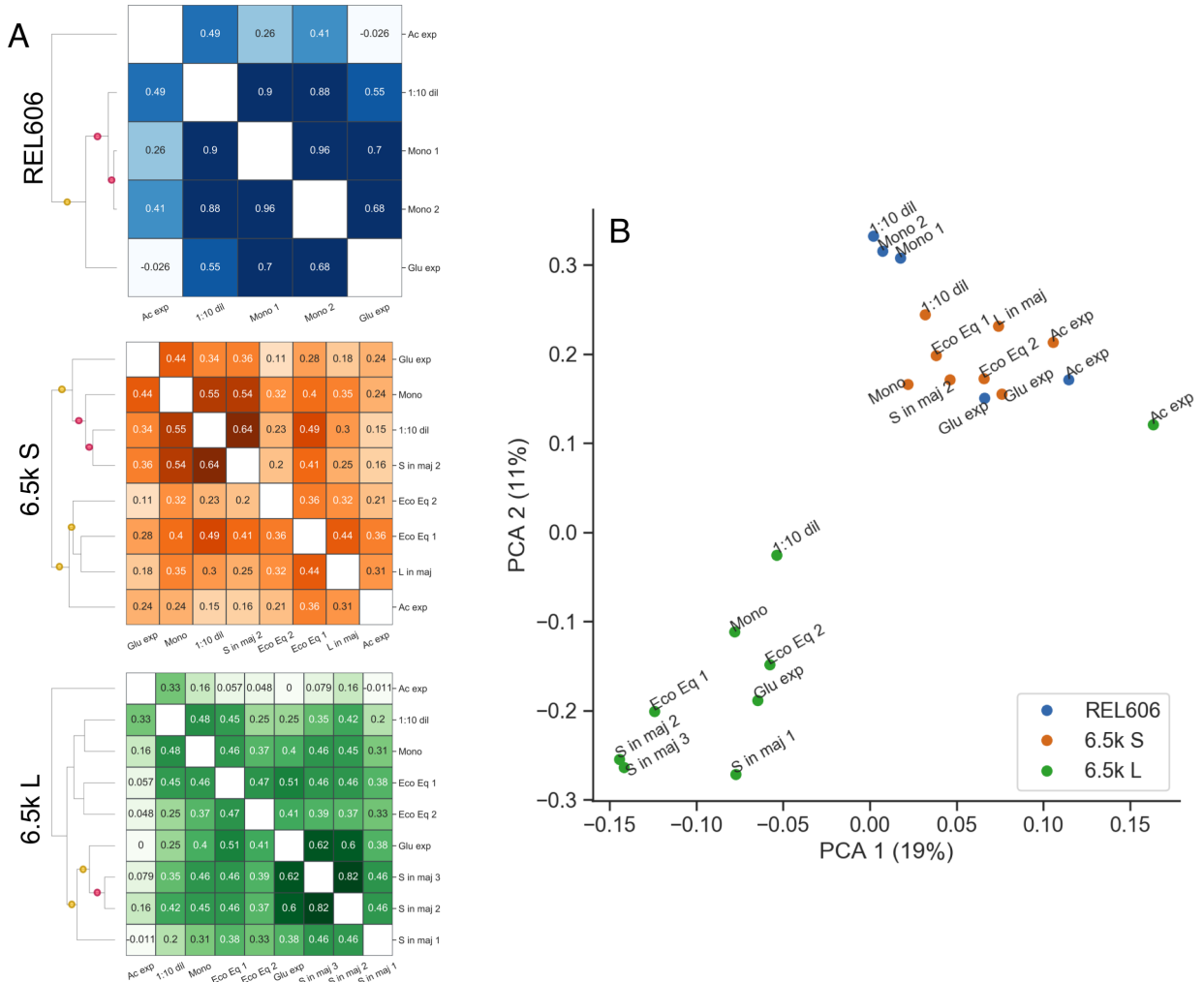


Fig. 3 Similarity of fitness effects between environments. (A) Clustering environments by using fitness effect correlation as a measure of similarity reveals which environments are the most functionally alike. For example, environments related to the putative ecotype niches—exponential acetate growth and glucose growth, for S and L respectively—cluster with conditions where the ecotype is in the minority. The red and yellow dots indicate that the branch has $\geq 90\%$ or $\geq 70\%$ support respectively, computed via bootstrapping. (B) Principal components analysis (PCA) of our data, using (normalized) fitness effects as features (% variance). We see that L experiments cluster separately from the S and REL606 experiments, with the exception of the acetate exponential phase condition.

across all environments) across the REL606, S and L libraries, as well as a null cofitness distribution for each pair to determine if the two genes are significantly correlated; the set of all significant gene-gene correlations determine the edges in the cofitness networks (see methods section). We explored the structure of the resulting cofitness networks via clustering [55] (see methods section), where we found sets of communities for all three libraries with *modularity* > 0 , indicating that there are more edges within each community than between communities (Figure 4B) [57]. We performed a number of controls to ensure that our results weren't driven by measurement noise or technical effects of clustering; see methods section for more information.

The presence of strong communities suggests that most knockouts are significantly correlated with others, potentially pointing to similar functional effects driving changes in fitness. We then wanted to compare how these clusters differ between the different genetic backgrounds, with the idea that how and if clusters change should reveal information on how the effective functions of genes differ across genetic backgrounds. Surprisingly, we find that

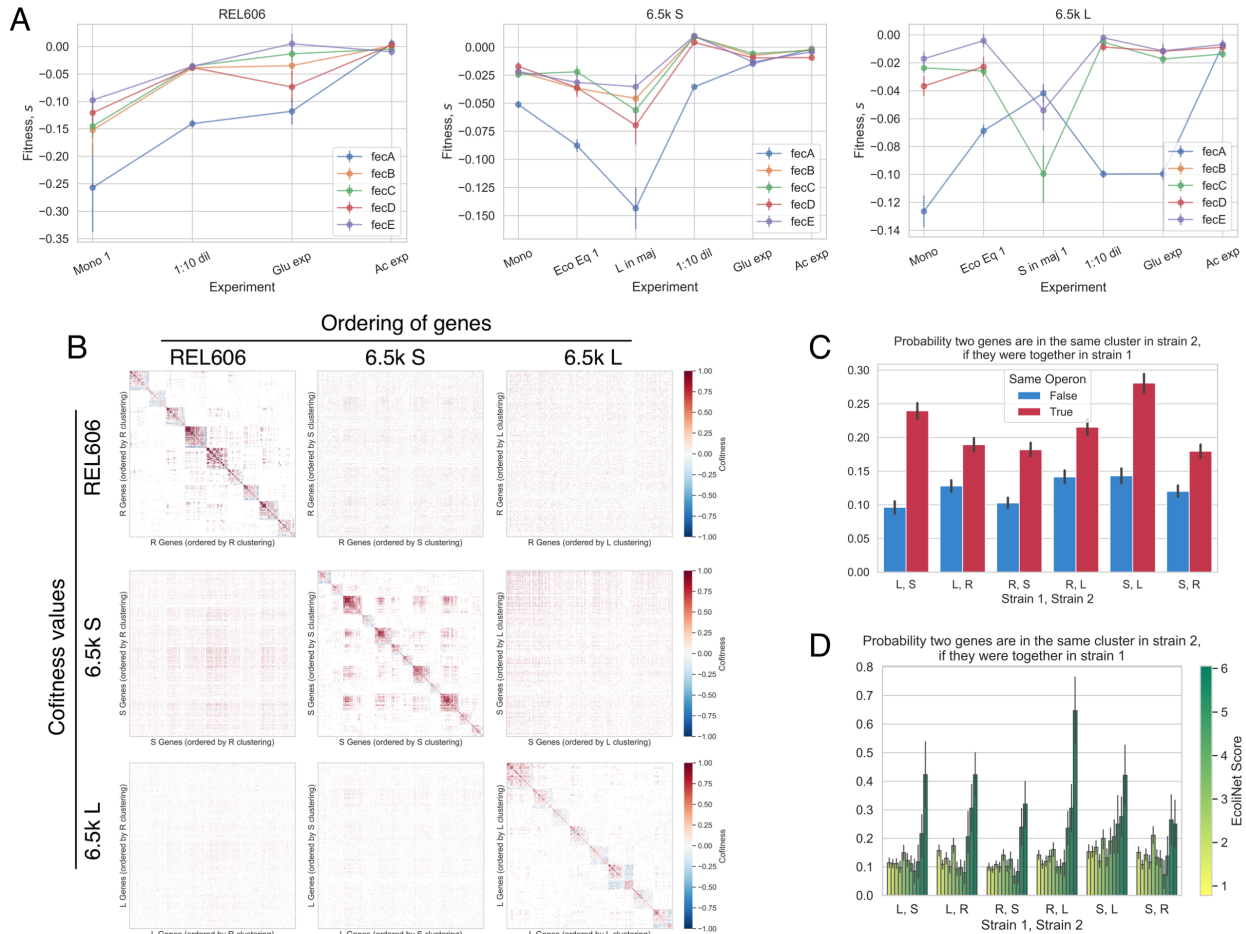


Fig. 4 Correlations between genes across environments. We observed that many pairs of genes have correlated fitness effects across environments, for example (A) most genes of the *fecABCDE* operon. However, *fecA* is correlated with the other genes to varying degrees, depending on the genetic background. (B) We computed the pairwise correlation of fitness effects (cofitness) for all pairs of genes, and then clustered genes with a community detection algorithm [55]. We then rearranged the cofitness matrices by reordering genes based on "optimal" clustering of other genetic backgrounds. For each column, we ordered the genes based on the clustering of a given genetic background. For each row, we used the cofitness matrix for a given background. It is apparent that replotting the cofitness matrix using another strain's clustering does not produce noticeable structure. (C, D) Cluster reassortment is not entirely random—pairs of genes (C) in the same operon and (D) that strongly interact with each other (high EcoliNet score), tend to stay in the same clusters across genetic backgrounds. In contrast, the cofitness of pairs of genes that are not in those categories appear to change in a way that is indistinguishable from random reassortment. In panels C and D, the abbreviations R, S, and L refer to REL606, and 6.5k S/L, respectively. Error bars represent standard errors.

gene clusters are not well preserved across genetic backgrounds, and in fact, genes are typically seemingly randomly reassorted between genetic backgrounds (Figures 4B, S17). In further support of correlations breaking between backgrounds, if we recompute the cofitness networks using only one of the biological replicates per experiment, we see that cofitness networks are more similar within genetic backgrounds compared to between backgrounds (Figure S15). There are a couple clusters that show non-random sampling across genetic background, however, the deviation from random sampling is mostly small, with one noticeable exception—clusters 5, 3, and 1 in REL606, S, and L, respectively, all seem to share a larger than random number of genes with each other ($p < 10^{-4}$ for all clusters). From a Gene Ontology enrichment analysis, genes that are associated with biofilm formation (GO:0043708), adhesion (GO:0022610), and pilus organization (GO:0043711) are over-represented in these clusters, along with genes involved in organonitrogen compound biosynthesis (GO:1901566), although to a weaker extent (Figure S18). This suggests that there is at least one (large)

functionally related group of genes that stay correlated across genetic backgrounds, implying that their fitness-determining effects are mostly the same, regardless of genetic background.

We wanted to know why other functional groups of genes do not stay correlated with each other, and if there was any structure hiding in the seeming randomness of cluster reassortment. A simple first test could ask if genes in the same operon are more likely to stay correlated with each other across backgrounds, which is the case for several of our aforementioned examples. This indeed appears to be the case across all genetic backgrounds (Figure 4C). However, genes often share functions with other genes outside their operons, so we turned to investigating the relationship between the cofitness and genetic networks. We used EcoliNet as a representation of the *E. coli* genetic network, as it attempts to capture all interactions between genes by integrating various data-types, regardless of the mechanism (transcriptional, protein-protein, etc), and assigns a score to each interaction that effectively represents the strength of the interaction [58]. We then computed the probability that two genes are in the same community in one genetic background, given that they're together in another background, as a function of EcoliNet score (Figures 4D). We see that gene pairs that are predicted to strongly interact (high EcoliNet score) are much more likely to be correlated across genetic backgrounds. We can also see these same patterns without referencing any cluster labels—if we look at the correlation between all cofitness pairs across genetic backgrounds, pairs that are in the same operon (Figure S19A) and those with the highest EcoliNet score (Figure S19B) give the highest correlation. It also appears that the shortest distance between two nodes in the EcoliNet network (Figure S21) also predicts if the two genes will stay correlated across genetic background, albeit the effect is weaker. We should note that it is perhaps the case that there are weaker consistencies across backgrounds for non-operon/non-interacting genes pairs that we don't have the statistical power to detect. Still, these analyses suggest that evolution significantly changes which functional effects of genes are important for determining fitness, such that the cofitness of genes pairs is much more preserved across genetic background for the most strongly interacting genes, but not as much for other gene pairs.

Fitness effects are correlated with evolutionary outcomes

We sought to explore if the knockout fitness effects that we measured were correlated with evolutionary outcomes in the LTEE, i.e. establishment of mutations and changes in gene expression. So, we first investigated if genes with non-neutral knockout fitness were more or less likely to be mutated and rise to a sufficiently high frequency in the population. Using the clonal sequencing data from Tenaillon et al. (2016) [59] and Plucain et al. (2014) [46], we identified genes that mutated between selected LTEE time-points, and ran a logistic model with fitness effect as the predictor and mutated status as the response variable (see methods section), separately for beneficial (Figures 5A) and deleterious genes (S22A). We used three sequenced clones (one available for each time point) for both S and L, while we used all clones from all non-mutator populations (at a given time point) for REL606. We used the appearance of a mutation (excluding synonymous SNPs) within a gene as a proxy for establishment.

Fitness of beneficial knockouts in the 1:10 dilution condition and monoculture (LTEE condition) in the REL606 background is strongly correlated with which mutations establish from 0-5k generations, while fitness in acetate exponential phase is only correlated with establishment later in the evolution (difference in slopes between 0-5k and 5-20k is significant at $p < 0.05$ via permutation test for 1:10 dilution and acetate conditions, not for monoculture or glucose conditions). This is potentially a signal that the targets of selection are shifting over time—REL606 may initially adapt via lag phase shortening/stationary phase survival, while only later adapting via increased acetate growth rate. This could happen, for example, by either clonal interference favoring the highest-effect mutations, or due to global epistatic effects [47]. The former hypothesis is supported by the observation that three mutations appear in genes with beneficial acetate knockouts at 2k generations, but they then

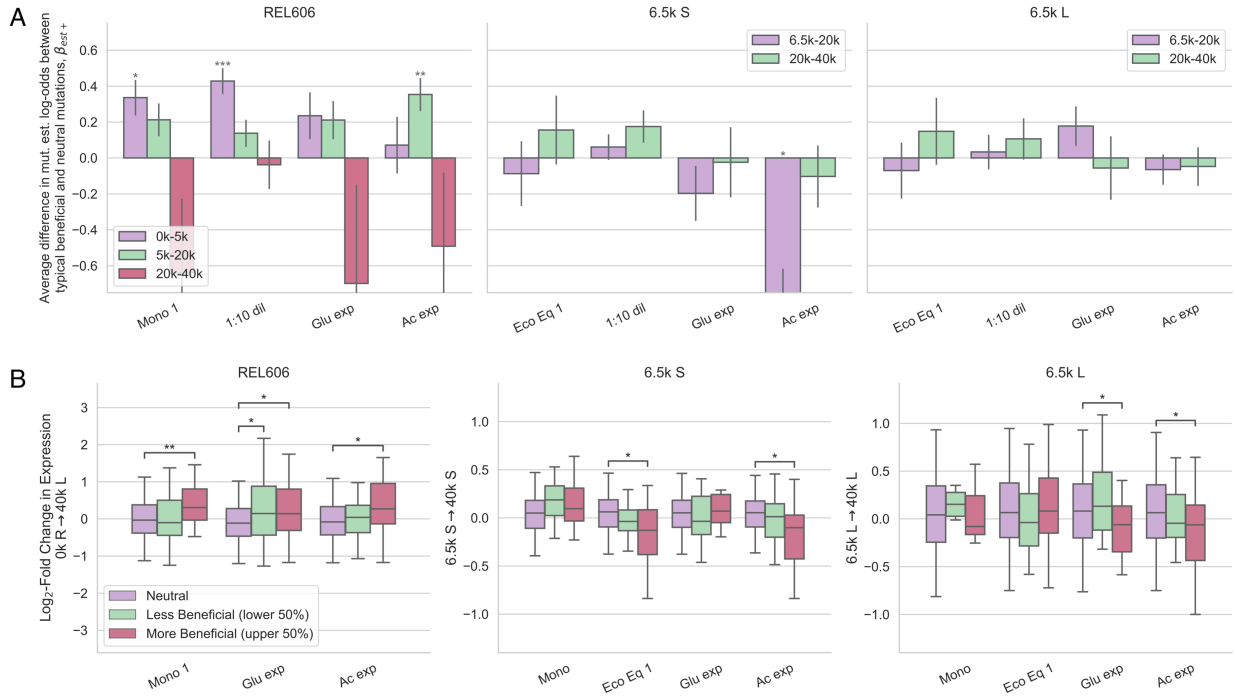


Fig. 5 Fitness effects of beneficial genes are correlated with evolutionary outcomes. We explored if genes with beneficial knockout fitness effects are correlated with (A) establishment of a mutation in a gene, and (B) changes in gene expression over evolutionary time, relative to neutral knockouts. (A) Slopes from logistic models, with presence of a mutation in a gene as the response variable. The fitness effects were normalized by the median beneficial fitness effect, so that coefficients can be interpreted as the average difference in log-odds establishment between neutral knockouts and the 'typical' beneficial knockout. REL606 beneficial knockout fitness is positively correlated with gene establishment probability for most environments, but in different time intervals, potentially pointing to shifting targets of selection. Error bars represent standard errors. (B) We compared the distributions of log-fold change in expression between genes with neutral knockout fitness effects, less beneficial effects (lower 50%), and more beneficial effects (upper 50%). We used the change in expression from 0k genes (REL606) to 40k genes (L), from 6.5k genes (S) to 40k genes (S), and from 6.5k genes (L) to 40k genes (L) for the REL606, 6.5k S, and 6.5k L panels, respectively. The expression change between ancestor and 40k L (left) is nearly identical to the expression change between ancestor and 40k S as well as other timepoints (Figure ??). Beneficial knockout fitness in REL606 is generally positively correlated with increasing gene expression over time. In S and L, fitness in several environments—including the ecological equilibrium and acetate and glucose growth—is correlated with decreasing gene expression. Asterisks denote coefficients/comparisons that are significantly different from 0 (FDR correction; * $p < 0.05$, ** $p < 0.01$, *** $p < 0.001$).

disappeared by 5k generations, potentially indicating that they were out-competed by other beneficial mutations (Figure S24). There is only one S/L condition that shows a significant difference in mutation establishment probability between beneficial and neutral mutations—genes with beneficial fitness in acetate are less likely to mutate compared to neutrals in S. However, changes in gene expression suggest adaptation to acetate may be occurring through indirect routes in S, as detailed below. However, we expect our power to detect correlations between mutational fitness and mutation establishment to be lower for S and L. They have a $\sim 100x$ higher mutation rate than REL606 [48], implying that the ratio of neutral hitchhiking to beneficial driver mutations is higher as well.

We also investigated if fitness effects are correlated with changes in gene expression, using microarray data from Le Gac et al. 2012 [16], which measured gene expression in REL606, and S/L at 6.5k, 17k, and 40k generations. These measurements serve as a distinct readout of evolutionary change compared to genomic mutational dynamics, because even if a gene is not directly mutated, gene expression can still change through indirect genetic interactions. Thus, gene expression measurements allow us to probe the effects of the cumulative mutations fixed by evolution. We compared the distribution of log-fold expression changes over approximately 40k generations for genes with neutral and non-neutral knockout fitness effects, separately for beneficial (Figure 5B) and deleterious genes (Figure S22B). We see that the median

change in gene expression is significantly different between neutral and beneficial genes across several conditions, but generally only for the upper 50% of beneficial genes. This indicates that the magnitude of the knockout fitness effect is important for determining how much the median gene changes in expression. We can get more power to detect relationships between the magnitude of the knockout fitness effect and log-fold change in gene expression by fitting linear models to the data (Figure S25). The same patterns hold if we restrict our analysis to highly expressed genes (Figure S26).

In REL606, genes with beneficial knockout fitness effects tend to increase in expression (relative to neutral genes) over evolutionary time; this is perhaps surprising, because we would expect selection to decrease gene expression if knocking out that gene is beneficial. We saw the same pattern with deleterious genes (Figure S22B). One possibility to explain every, the expression of growth-relevant genes is increased by some mutation with a highly pleiotropic effect (e.g. in a master regulator), whose overall benefits outweigh the costs of raising the expression of beneficial knockout genes.

In contrast, in S and L, there are a couple of environments where gene expression significantly decreases over evolutionary time for genes with beneficial knockout fitness effects (compared to neutrals). These conditions include environments related to the putative ecotype niches—acetate and glucose exponential growth in S and L respectively. On the other hand, while fitness in the ecological equilibrium is associated with decreased gene expression, this is not the case for fitness in monoculture and the 1:10 dilution environments, indicating again that the latter environments are less relevant for evolution in the LTEE environment. Despite the fact that acetate-adapting mutations are not establishing on the S background (at least initially), gene expression still decreases by 40k generations, perhaps indicating that adaptation to acetate is occurring through routes other than directly mutating genes with beneficial knockout effects.

We also saw that S and L beneficial knockout fitness in glucose exponential phase is *positively* correlated with an increase in gene expression from 0-6.5k (Figure S25). On average, those same genes decrease in relative gene expression when evolving on the L background, whereas they do not change on the S background. This set of data could indicate that from 0-6.5k many genes increased in gene expression via adaptive evolution that were actively unhelpful for glucose growth, either because of transcriptomic misallocation or other types of antagonistic pleiotropy, such that knocking them out conferred a benefit. Upon diversification of S and L, the direction of gene expression change appears to switch for L, perhaps suggesting that L is evolving towards a more glucose growth-optimized transcriptome, while S is not. This set of observations provides a possible example of how diversification changes the selection pressures acting on organisms.

Interestingly, deleterious knockout fitness effects across all environments in S/L tend to be associated with an increase in gene expression between 0 and 6.5k generations (Figure S22B). This observation may provide a partial explanation for why some knockouts become deleterious in S/L when they were neutral in REL606—6.5k generations of evolution caused the genes to suddenly become important, so they became more costly to knock out. Another, unrelated observation could help us to understand why some genes have deleterious knockout fitness effects—it appears that deleterious genes are more highly connected in the *E. coli* gene interaction network (EcoliNet) compared to neutrals (on average), indicating that some genes may be deleterious because when they're knocked out, they also affect the functioning of many other genes (Figure S27).

Discussion

In order to be able to predict how evolution will proceed in community contexts, we need to know the distribution of mutational fitness effects, along with how it depends on genetic background and ecological conditions. To that end, we measured the genome-wide knockout fitness effects of a recently diversified ecosystem, S and L, and their ancestor, REL606. Despite the fact that the fitness effects of individual mutations appear to be highly dependent

on both genetic background and environment (strong $(G \times) G \times E$ effects), we saw consistent statistical patterns of variation across both axes, namely global diminishing returns epistasis and a negative frequency-fitness correlation (in S and L). In contrast, previous studies that observed diminishing returns epistasis saw both the mean of the DFE as well as the fitness effects of individual mutations decrease as a function of background fitness [51, 52]; this discrepancy may indicate that uniform negative epistasis of individual mutations may only be relevant for the first handful of mutational steps, before yielding to more complex and idiosyncratic forms of epistasis. While the underlying mechanism that generates this form of global epistasis is still unclear, our observations are consistent with recent theoretical [60] and experimental work [61] that suggest that global diminishing returns epistasis may arise as a general consequence of idiosyncratic epistasis.

Even though S and L only diverged ~500 generations ago, the mixing ratio of the two ecotypes strongly affects the DFEs, suggesting that strong eco-evolutionary coupling is possible even in closely related strains. This would imply that selective pressures depend strongly on the community mixture, which changes significantly and relatively rapidly due to evolution [42, 47]. The sensitivity of knockout fitness effects to relatively minor variations on the LTEE environment, such as changing niche availability or ecosystem composition, may be evolutionarily significant—we know that the growth traits of S and L also change quite drastically during their coevolution [16, 44], which along with changes to ecosystem composition, will change the environment, and thus change which mutations are favored by selection. One specific hypothesis that emerges from our data is that selective forces may be more similar to environments related to the putative ecotype niches when the ecotype is rare, for both S and L. This is supported by both clustering environments by fitness effect correlations, and which environments were correlated with changes in gene expression. It would follow that selection could favor different degrees of specialization within the current niche as the ecotype frequencies and growth traits change due to evolution. Regardless of the specific implementation, the process where (i) mutations change growth traits and ecosystem composition, which (ii) change ecological conditions, which in turn (iii) change the mutational fitness effects of both ecotypes, could represent an important and pervasive type of eco-evolutionary feedback.

We aimed to better understand the background and environment dependence of mutational fitness effects by systematically studying fitness correlations across environments. Our intuition was that knocking out genes with similar functions should have similar effects across environments. We saw that, by and large, different sets of genes were correlated with each other across genetic backgrounds; only strongly interacting pairs of genes were likely to be correlated across all backgrounds. These widespread changes could be caused by a number of different evolutionary phenomena—for example, evolution could have induced widespread changes in the functional effects of genes or which functional effects matter for fitness. Additionally, inasmuch as fitness in an environment is a reflection of phenotype—e.g. fitness in exponential phase is likely a simple function of exponential growth rate—the extensive changes in fitness across environments could be interpreted as support for ubiquitous pleiotropic effects of knockout mutations.

We investigated if our measured knockout fitness effects were correlated with evolutionary outcomes, i.e. mutation establishment and gene expression changes. We found significant correlations across several, but not all environments, leading to hypotheses on how selection has acted on LTEE populations. From correlations of knockout fitness effects with mutation establishment, we found potential signals of shifting selection over time in REL606. Changes in gene expression provide a distinct window into evolutionary change, as expression can change through genetic interactions, even if a gene is not directly mutated. Among other patterns, the fitness correlations with gene expression changes potentially reveal how the traits under selection changed from pre- to post-diversification, and how they are different between S and L. Pinpointing the precise causes of these patterns could be a fruitful avenue for future work. Overall, the connections between evolutionary changes and knockout fitness

effects demonstrates the utility of our approach to understand how adaptation happens in the “natural” evolutionary context.

Ultimately, we would like to predict the outcomes of evolution in community contexts. By showing how the distribution of invasion fitness effects changes as a result of genetic background and ecological conditions, our dataset represents a major step forward in that direction. The invasion fitness effects directly impact the establishment probability of a beneficial mutation, as well as the mutant dynamics until it reaches a substantial proportion of the population. The distribution of deleterious invasion fitness effects also controls other relevant evolutionary phenomena, including the equilibrium reached by mutation-selection balance, and the probability that a deleterious mutation will hitchhike on a beneficial mutant (“genetic draft”). However, in principal, the fitness effect of a mutation could change as it approaches fixation (within the ecotype) due to frequency-dependent effects. We are not able to measure these effects with our experimental set-up, as our ability to measure fitness effects in high-throughput requires that mutants remain rare. However, frequency-dependent mutations could significantly alter expected evolutionary dynamics, so as such, measuring such effects are a major direction for future work.

As previously mentioned, we only surveyed the fitness effects of knockout mutations, which represent a subset of all mutations available to an organism. While it is possible that other types of mutations could display different patterns, knockout mutations appear to be prevalent and important for adaptation in the LTEE [47, 62], and our measured knockout fitness effects are correlated with evolutionary outcomes. Additionally, we studied a relatively simple ecosystem, consisting of just two recently diverged ecotypes; measuring the mutational effects in more complicated ecosystems and how they change as a result of longer periods of evolution is likely a fruitful future avenue of investigation. Overall, the methods and results presented here pave the way for future studies investigating how mutational fitness effects depend on eco-evolutionary processes, and how eco-evolutionary feedback arises from changing fitness effects.

Methods

Barcoded transposon library construction

To construct the barcoded transposon libraries, we isolated subclones of REL606, REL11555 (6.5k S), and REL11556 (6.5k L), all gifts of Richard Lenski (Michigan State University). Transposon mutagenesis was performed as previously described [40, 41] by mating each LTEE clone with an *E. coli* WM3064 donor (Diaminopimelic acid [DAP] auxotroph and *pir*⁺) containing previously described [40] randomly barcoded Tn5 plasmids with a kanamycin cassette and an R6K origin of replication. The LTEE clones were grown in DM2000 (Davis Minimal Media with 2000mg/L D-glucose), and the donor was grown in LB/Kan, all to mid-log phase. After washing the cultures, each LTEE culture was then mixed with the donor in a 1:1 ratio, then placed on 0.45 μ M nitrocellulose filters (Millipore cat. no. HAWP04700) on top of a 1% agar plate with EZ-MOPS rich, defined media (Teknova cat. no. M2105) + 20mM sodium pyruvate (‘EZ-py’) + 0.3mM DAP. The rich media was chosen because it had a number of different carbon sources (glucose, amino acids, pyruvate) and sufficient amounts of all other required macro/micronutrients, lessening the chances of substantial negative selection in the growth media. After conjugation, the filters were picked up and placed in rich media; subsequently, the resuspended cells were plated on EZ-py agar plates supplemented with 50 μ g/mL kanamycin. After approximately 24hrs of growth at 37C, colonies were scraped up and grown in EZ-py liquid media with 50 μ g/mL kanamycin until OD~1; we then saved the cultures in several 10% glycerol stocks. Transposon insertion mapping (Tn-Seq) libraries were prepared as previously described [40]; libraries were then sequenced on the Illumina HiSeq 4000 (150PE) at the Vincent J. Coates Genomics Sequencing Laboratory at UC Berkeley. The resulting sequencing data was used to create a table relating each barcode to a genomic insertion location, using a previously developed script (MapTnSeq.pl) [40].

BarSeq experiments

Set-up of experiments

To start a BarSeq experiment, we first unfroze 1mL glycerol stock of the REL606, 6.5k S and/or 6.5k L transposon libraries and transferred the entirety to 10mL EZ-py media (media used for library construction) in 50mL glass erlenmeyer flasks, which were grown for 16-24hrs at 37C, shaken at 120rpm. All cultures for all experiments were grown with the same shaker, in the same 37C warm room. In several experiments where we measured fitness effects of 6.5k S/L barcoded libraries at various ecotype frequencies, we also grew the wild type S/L with the same media, under the same conditions. The next day, we washed the cultures by pelleting via centrifugation for 3 minutes at 2500 xg, aspirating the supernatant, and resuspending in DM0 (Davis Minimal Media without a carbon source) three times. After thoroughly vortexing the cultures, we transferred them 1:1000 to the appropriate media in n flasks (see below)—depending on the experiment, we used different numbers of flasks and different sizes, either 10mL media in 50mL glass flasks or 200mL media in 1L glass flasks (same ratios, scaled up). We used multiple flasks and larger flasks to increase the total population size, decreasing fluctuations due to genetic drift. We then performed two more transfers in the appropriate conditions for the experiment to help physiologically adapt the cultures to the conditions. If we were doing a coculture experiment, we would mix the cultures at the appropriate frequencies during the second transfer. If we used multiple flasks in an experiment, we would sample an equal amount of culture from each flask into a microcentrifuge or Falcon tube, thoroughly mix the cultures, and redistribute among the same number of flasks with new media—thus, the cultures distributed in multiple flasks were effectively all part of the same population. After the third transfer, we would collect cells for day 0 of the experiment, and use that culture to start two biological replicates that are independently propagated for the remainder of the experiment. All cultures were grown at 37C, shaken at 120rpm. Cells were harvested at defined time points by centrifugation at approximately 20,000xg for 10min of ~60mL culture for all experiments except Ac Exp (10mL) and Mono 2 (30mL), pooling culture from all flasks in an experiment/replicate at equal ratios. Subsequently, the pellets were stored at -80C until the experiment was finished.

The number of generations does not depend on the growth rate, only on the initial and final abundance of the cultures, $\# \text{ generations} = \log_2(n_f/n_0)$. If the final density of the culture is approximately the same across transfers, as is the case in all our experiments except the “exponential phase” experiments, then the number of generations only depends on the dilution rate, $\# \text{ generations} = \log_2(\text{dilution rate})$.

Conditions for each experiment

Monoculture

For the Mono (1) experiments, we propagated the libraries alone in DM25 (Davis Minimal Media with 25mg/L D-glucose) in 5x 50mL flasks over the course of 4 days. For the REL606 Mono 2 experiment, we used 3x 50mL flasks over the course of 8 days, with four biological replicates in DM25. We transferred cultures 1:100 every 24hrs, and took the number of generations per transfer as $\log_2 100$.

Coculture experiments

As mentioned above, we started wildtype cultures of 6.5k S and/or L clones (same clones used to make the RB-Tn libraries) at the same time and with the same procedure as the library cultures (Table 1), and mixing the cultures at the appropriate frequencies at the second “adaptation” serial transfer. We measured the ecological equilibrium frequency to be approximately 15 – 20% S (Figure S4), so we ensured that the S frequency was started in that range for the “ecological equilibrium” experiments. We started the “S/L in majority” experiments such that the minority ecotype was $> 10\%$ of the total population (Figure S3).

We used DM25 media and propagated the cultures for 4 days, except for S in maj 2/3 where we used 6 days, transferring 1:100 every 24hrs ($\log_2 100$ generations) for all coculture experiments. For the Eco Eq 1 experiment, we mixed both S and L libraries in the same cultures along with wildtype L, using 4x 1L flasks. For the Eco Eq 2 experiments, S and L libraries were in separate cultures, both with wildtype S and L set at the appropriate frequency, with RB-Tn library frequency around 5–10% (Figure S3); cultures were propagated in 10x 50mL flasks. For the L in Maj and S in Maj 1 experiments, we mixed wt L + S library and wt S + L library, respectively; cultures were propagated in 10x 50mL flasks. For the S in maj 2/3 experiments, we mixed wt S with S+L and L libraries respectively; cultures were propagated in 4x 1L flasks.

We measured the frequency of S/L in the population by plating and counting colonies at the end of a transfer on TM plates (tetrazolium maltose; 10g/L tryptone [Sigma T7293], 1g/L yeast extract [Sigma Y1625], 5g/L NaCl, 16g/L agar, 10g/L maltose, 1mL/L 5% TTC [Sigma T8877]), where S appears as red colonies and L appears as white colonies, previously used in [46]. We could also measure the frequency of cells from RB-Tn libraries by plating the cultures on LB/Kanamycin plates, as the transposon has a kanamycin resistance cassette (Figure S3). We diluted all cultures (at the end of a cycle) in DM0. Dilution rates varied over experiments: in Eco Eq 1, we diluted cultures by a factor of $2 * 10^{-5} \text{ mL}^{-1}$ to plate on both TM and LB/Kan plates, in Eco Eq 2 we used dilution rates of 10^{-5} mL^{-1} and 10^{-4} mL^{-1} to plate on TM and LB/Kan plates respectively, in the L in Maj and S in Maj 1 experiments we used a $2 * 10^{-5} \text{ mL}^{-1}$ dilution rate to plate on just TM plates, and in the S in maj 2/3 experiments we used dilution rates of $2 * 10^{-5} \text{ mL}^{-1}$ and $2 * 10^{-4} \text{ mL}^{-1}$ to plate on TM and LB/Kan plates respectively.

1:10 dilution

We propagated cultures with a 1:10 dilution, instead of the standard LTEE dilution rate of 1:100, to investigate the effect of a lengthened stationary phase relative to exponential phase. We used DM27.8 media (Davis Minimal Media with 27.8mg/L D-glucose), because the concentration of glucose would fall to 25mg/L after dilution. We used 1x 1L flask for each library culture (180mL media + 20mL culture), propagating the cultures for 8 days every 24hrs with $\log_2 10$ generations per day. We pelleted and saved cultures every other day (0,2,4,6,8).

Acetate exponential phase

We sought to measure knockout fitness effects when the RB-Tn libraries were kept in acetate exponential phase, where we used DM2000-acetate (Davis Minimal Media with 2000mg/L Sodium Acetate) and grew the cultures in 1x 50mL flask. We first measured exponential growth rates for wt REL606, L, and S clones in DM2000-acetate, which were approximately 0.08/hr, 0.12/hr, and 0.18/hr respectively. We also observed that all cultures were still in mid-exponential phase at $OD \sim 0.6$. So, if we started at initial OD_0 of 0.09, 0.03, 0.008 for REL606, L, and S respectively, the cultures would end up at $OD \sim 0.6$ after 24 hours. Thus, for each transfer, we would measure the actual OD for each culture (after 24hrs of growth) and transfer the appropriate volume of old culture to new 10mL DM2000-acetate such that the final concentration was the appropriate OD_0 . We recorded the number of generations for each cycle as $\log_2 OD_f / OD_0$. Due to the variable number of generations per transfer for each genetic background (owing to different growth rates), we collected samples at days 0,2,4,6,8 for REL606; 0,1,2,4,5,6 for L; 0,1,2,3,4,5 for S.

Glucose exponential phase

We measured knockout fitness effects in glucose exponential phase with DM25 media in 1x 1L flask. We measured the length of DM25 exponential phase to be about 8.25 hrs for REL606, and 5.25 hrs for both S and L after a 1:100 dilution into new media. For the adaptation phase, we did two full 24hr cycles of growth in DM25, followed by one cycle of growth for ~ 8 hrs and

~5hrs for REL606 and S/L, respectively. After the adaptation phase, we transferred cultures 1:100 into new DM25 media (warmed to 37C) four times, after 7.5-8hrs for REL606 and 4.5-5hrs for S and L. As DM25 media is quite dilute and thus OD measurements are relatively inaccurate, we estimated the number of cells that were transferred by plating the cultures on LB plates at a $2 * 10^{-5} mL^{-1}$ dilution rate and counting colonies, calculating the number of generations for that transfer as $\log_2 100 CFU_f / CFU_0$. We only ended up including the first two transfers of the REL606 library experiment (time points 0,1,2), as it was apparent from CFUs that the third transfer resulted in a large bottleneck owing to a smaller than expected population size before the transfer, likely because of slower than expected growth.

DNA extraction, PCR, Sequencing

After the experiment was finished, pellets were pulled from the -80C freezer and genomic DNA was extracted with the Qiagen DNeasy tissue and blood extraction kit (cat no. 69504), eluted in double distilled water with typical yields around 50ng/ μ L. DNA barcodes were amplified from gDNA samples via PCR with Q5 Hot Start Polymerase (NEB, cat. no. M0493S); 50ul reactions were composed of 5 μ L PCR primers, 5 μ L gDNA, 10 μ L 5x buffer, 10 μ L GC enhancer, 1 μ L dNTPs, 0.5 μ L Q5 polymerase, 18.5 μ L water. We used custom dual-indexed primers that contained binding sites up- and down-stream of the barcode region, along with the necessary Illumina read/index binding sites; fwd primer (AATGAT ACGGCG ACCACC GAGATC TACACT CTTTCC CTACAC GACGCT CTTCCG ATCT N_nXXXXXX GTCGAC CTGCAG CGTACG) where X stands for the custom forward 6bp index, and N_n is 1-4 random nucleotides, varying with the primer pair; rev primer (CAAGCA GAAGAC GGCATA CGAGAT XXXXXX GTGACT GGAGTT CAGACG TGTGCT CTTCCG ATCTGA TGTCCA CGAGGT CTCT) where X stands for standard Illumina 6bp IT index. We used a different primer pair for each gDNA sample from a different experiment/replicate/time point, so that we could demultiplex the samples after sequencing. The PCR program was 4min at 95C, [30sec at 95C, 30sec at 55C, 30sec at 72C] x25 cycles, 5min at 72C. We verified that we had the correct PCR products via agarose gel electrophoresis. All PCR reactions were then pooled and cleaned with the Zymo DNA Clean and Concentrator kit (cat. no. D4013), and eluted in double distilled water. The final pooled sample was then sequenced on an Illumina HiSeq 4000 (50SR) at the Vincent J. Coates Genomics Sequencing Laboratory at UC Berkeley.

Fitness inference pipeline

Read counting and error correction

We first processed the raw (demultiplexed) sequencing reads using a previously developed Perl script [40, 41] that pulls out the barcode sequence by trimming regions corresponding to the sequencing primers and regions up/downstream of the barcode, as well as discarding reads that do not match the secondary sequencing index or have insufficiently high quality scores (MultiCodes.pl). Then, counts of unique barcodes are tabulated to get a table corresponding barcode sequence to counts.

However, due to errors that arise during PCR and sequencing, some of the barcode reads acquire mutations that would prevent them from directly mapping to a transposon insertion location. Thus, we must correct for these sequencing errors by matching mutated barcodes to their parent, and merging the read counts together. The aforementioned Perl script identifies off-by-one barcode pairs; if the minority barcode (the one with fewer counts) unambiguously maps to a single majority barcode, the barcode counts are merged. To detect larger mutational distances between the derived and parent barcodes, we computed the Levenshtein (edit) distance between pairs of barcodes (as implemented in the Python C package `Levenshtein` [63]). Barcode read counts were merged if the edit distance was 4 or less, and if the minority barcode only mapped to one majority barcode at the minimum edit distance.

We then used previously acquired TnSeq data that maps the barcode identity to its transposon insertion location in order to identify which gene (if any) the barcoded transposon disrupted. Transposons that hit the first or last 5% of the gene sequence were excluded, as it is possible that these insertions do not result in disruption of production of the gene product.

To ensure that barcodes at least begin their trajectories at a sufficiently high read count, if there were barcodes within a gene with low initial counts, $r_{0,i} < 80$, we summed the lowest (initial) count barcode into the next-lowest count barcode until $\min_i r_{0,i} \geq 80$. We restricted our analysis to genes that had ≥ 4 barcodes, allowing us to gain confidence that the measured knockout fitness is not dependent on rare fluctuations or secondary mutations. Additionally, some barcodes went extinct during the course of the experiment, either due to genetic drift or selection; if a barcode went extinct, i.e. has 0 counts from t_{ext} to T , we would trim all time points after, but not including, t_{ext} . We eliminated barcodes that go extinct after just one time point. Statistics of the final constructed RB-TnSeq libraries are summarized in Table 2.

Library	# genes hit ≥ 3 times	# barcodes	% bc reads mapped
REL606	3,401	609,854	84%
6.5k S	3,382	522,253	84%
6.5k L	2,877	157,260	89%

Table 2 Summary of statistics of constructed RB-TnSeq libraries.

Probabilistic model of read count trajectories and fitness inference

To infer the fitness of individual genotypes from BarSeq count data, we must first understand what frequency trajectories we would expect for a given fitness, and how technical noise (e.g. from sample preparation and sequencing) and genetic drift affect those trajectories. Consistent with previous work [30, 31, 35], we construct a maximum-likelihood estimator to infer fitness from trajectories of barcode read counts, using a deterministic approximation of frequency dynamics.

On average, when the frequency of a lineage is sufficiently small $f_{t,i} \ll 1$, the frequency dynamics will exponentially grow/decay according to the genotype fitness, s , as well as the mean fitness of the population, \bar{x}_t (see section),

$$\langle f_{t,i} \rangle = f_{0,i} e^{(s - \bar{x}_t)t}$$

We measured the time in *generations*, which we measured for each time point in each experiment (see section). The reason we used a timescale of $1/\text{generation}$ instead of e.g. $1/\text{cycle}$ was to be able to better compare the magnitude of effects across experiments—e.g. the two exponential phase experiments had varying numbers of generations from cycle-to-cycle and between strains (due to differences in exponential growth rates). However, the fitness effects can be scaled by a factor of approximately 6.64 to get per-cycle fitness effects, at least in the 1:100 serial dilution experiments. The number of generations does not depend on the growth rate, only on the initial and final abundance of the cultures, # generations = $\log_2(n_f/n_0)$. If the final density of the culture is approximately the same across transfers, as is the case in our experiments, then the number of generations only depends on the dilution rate, # generations = $\log_2(\text{dilution rate})$. This is the typical manner in which the number of generations is calculated in both the LTEE and other serial transfer-based evolution experiments.

The two sources of noise—genetic drift and measurement noise—both arise from counting processes, so the combined noise will follow $\text{var}(f_{t,i}) \propto \langle f_{t,i} \rangle$ (see section). To account for the inherent discreteness of counting sequencing reads—especially important to accurately model deleterious genotypes that quickly drop to low frequencies—we modeled the observed

counts at time t (always measured in generations) of barcode i inserted in a given gene, $r_{t,i}$, as a negative binomial random variable,

$$r_{t,i} \mid s, f_{0,i} \sim \text{NB}(\mu_{t,i}, c_t) \quad (1)$$

$$\langle r_{t,i} \rangle = \mu_{t,i} \quad (2)$$

$$\text{var}(r_{t,i}) = c_t \langle r_{t,i} \rangle \quad (3)$$

$$\mu_{t,i} = R_t f_{0,i} e^{(s - \bar{x}_t)t} \quad (4)$$

Where R_t is the total number of counts, and c_t is the measured variance parameter. The final likelihood for the fitness, s , of a given gene knockout is obtained by numerically integrating over $f_{0,i}$ ('integrated likelihood' with a flat prior)—incorporating the uncertainty in the intercept nuisance parameters into the fitness estimate and turning the problem into a one-dimensional maximum likelihood—and then combining the likelihoods of all barcodes inserted into the gene,

$$P(\mathbf{r}_i \mid s, f_{0,i}) = \prod_t \frac{\Gamma\left(r_{t,i} + \frac{\mu_{t,i}}{c_t - 1}\right)}{\Gamma\left(\frac{\mu_{t,i}}{c_t - 1}\right) \Gamma(r_{t,i} + 1)} \frac{(c_t - 1)^{r_{t,i}}}{c_t^{r_{t,i} + \frac{\mu_{t,i}}{c_t - 1}}} \quad (5)$$

$$\mathcal{L}(s \mid \mathbf{r}) = \prod_i \int df_{0,i} P(\mathbf{r}_i \mid s, f_{0,i}) \quad (6)$$

The point estimate of the knockout fitness, \hat{s} , is then numerically computed as the maximum likelihood, and the standard error is approximated as the inverse, square-root observed information,

$$\hat{s} = \underset{s}{\text{argmax}} \log \mathcal{L}(s \mid \mathbf{r}) \quad (7)$$

$$\text{std } \hat{s} = 1 / \sqrt{-\partial_s^2 \log \mathcal{L}(s \mid \mathbf{r}) \big|_{\hat{s}}} \quad (8)$$

We ran biological replicates for all experiments reported here; to obtain combined genotype fitness estimates across replicates we simply multiplied the likelihoods together, repeating the maximum likelihood procedure.

As the majority of barcoded knockouts are neutral or nearly so ($s \approx 0$), we must have a method to distinguish between likely neutral and selected knockout mutations; this can be accomplished by computing a p-value under the null hypothesis $s = 0$. For ease of computation and generality we compute the p-value as the posterior probability that the likelihood ratio between null and alternative hypotheses is greater than 1, i.e. the probability that the data more strongly support the null hypothesis over the alternative,

$$p = P_{s|\mathbf{r}} \left(\frac{\mathcal{L}(0 \mid \mathbf{r})}{\mathcal{L}(s \mid \mathbf{r})} > 1 \right)$$

$$P(s \mid \mathbf{r}) \propto \mathcal{L}(s \mid \mathbf{r})$$

This convenient definition has been shown to be equivalent to the frequentist definition of the p-value using a likelihood ratio test statistic (if the distribution is invariant under transformation) [64, 65], and does not require asymptotic approximations.

In practice, this p-value can be calculated by first, finely discretizing the likelihood curve along s and normalizing it to get the posterior,

$$P_j(s_j | \mathbf{r}) = \frac{\mathcal{L}(s_j | \mathbf{r})}{\sum_j \mathcal{L}(s_j | \mathbf{r})} \quad (9)$$

Then, calculating the log-likelihood ratio along all discretized s values,

$$\text{LLR}_j = \log \mathcal{L}(0 | \mathbf{r}) - \log \mathcal{L}(s_j | \mathbf{r}) \quad (10)$$

And finally, summing to get the posterior probability that the data supports the null hypothesis more than the alternative, where $I[\cdot]$ is the indicator function,

$$p = \sum_j I[\text{LLR}_j > 0] P_j(s_j | \mathbf{r})$$

We used the standard method of Benjamini & Hochberg to control for the false discovery rate at $\alpha = 0.05$.

Estimation of error parameters

In order to estimate fitness of individual genotypes from BarSeq data, we must first obtain an estimate of the error parameters for each time point in the experiments. There are two distinct sources of noise in our BarSeq measurements—measurement (technical) noise, arising from library preparation and sequencing error, which is uncorrelated in time, and variance due to genetic drift, which accumulates over time. Both sources of noise are count processes, where the variance of barcode population frequencies will be proportional to the mean,

$$\langle f_{t,i} \rangle = \frac{\langle r_{t,i} \rangle}{R_t} \propto \text{var}(f_{t,i})$$

In order to eliminate the dependence of the variance on the mean, we apply a variance-stabilizing transformation,

$$\phi_{t,i} \equiv \sqrt{f_{t,i}}$$

The variance of barcode frequencies of neutral lineages over two time points will then depend on the variance that has accumulated due to genetic drift, as well as the technical noise at the sampled time points. If there are sufficiently many read counts/individuals such that the central limit theorem applies, the variances will simply be additive,

$$\kappa_{j,k} \equiv \text{var}(\phi_{i,j} - \phi_{i,k}) = \zeta_j + \zeta_k + \frac{|j - k|}{4N_e} \quad (11)$$

Where ζ_t is the technical noise at time point t , N_e is the effective population size, and $|j - k|$ is the number of transfers performed between times j and k . The above equation defines a set of linear equations, with ζ_t and N_e as unknown parameters.

We can measure $\kappa_{j,k}$ for all possible combinations of t_j and t_k given large enough set of neutral barcodes. Our RB-TnSeq libraries have a large number of transposons that were inserted into intergenic regions, the vast majority of which presumably have no fitness effect; thus, we use these intergenic barcodes as our set of putatively neutral barcodes. We confirmed that our measured $\kappa_{j,k}$ did not systematically vary as a function of r_j (Figure S28), indicating that the expected mean-variance relationship, $\text{var}(f_{t,i}) \propto \langle f_{t,i} \rangle$, is consistent with our data.

We only included intergenic barcodes that satisfy $50 < r_{t,i} < 500$, as our computation depends on having sufficiently many counts such that the central limit theorem applies, and barcodes at a higher frequency are more likely to have acquired secondary mutations and be impacted by selection. In order to further guard against the effects of potential 'outlier' barcodes (those with non-neutral fitnesses), we compute variance estimates, $\hat{\kappa}_{j,k}$, with a more robust measurement of variability, the median absolute deviation (MAD),

$$\psi_{i,j,k} \equiv \phi_{i,j} - \phi_{i,k} \quad (12)$$

$$\text{MAD}_{j,k} = \text{med}_i |\psi_{i,j,k} - \text{med}_i \psi_{i,j,k}| \quad (13)$$

$$\hat{\kappa}_{j,k} = \left(\frac{\text{MAD}_{j,k}}{0.67449} \right)^2 \quad (14)$$

We resampled barcodes with replacement (standard bootstrapping) 500 times to compute the relative errors on the $\hat{\kappa}_{j,k}$ measurements. To decompose variability into the correlated ($1/N_e$) and uncorrelated (ζ_t) components, we numerically minimized squared error of the expected relationship (eq. 11) between the noise parameters and the measured $\hat{\kappa}_{j,k}$, with inverse variance weighting,

$$\zeta, N_e = \underset{\zeta, N_e}{\text{argmin}} \sum_{j,k} \frac{\left(\zeta_j + \zeta_k + \frac{|j-k|}{4N_e} - \hat{\kappa}_{j,k} \right)^2}{\text{var}(\hat{\kappa}_{j,k})}$$

We subjected the minimization to the constraint that $\zeta_t \geq \frac{1}{4R_t}$, i.e. technical noise must be at least as large as variance due to sampling. After converting the variance parameters from frequencies back to read counts, the total marginal variance parameter at a single time point is,

$$\hat{c}_t = (4\zeta_t + 1/N_e)R_t$$

The number of intergenic barcodes included varies across RB-TnSeq libraries, experiments, and time points, but approximately on the order of $\sim 10^4$ intergenic barcodes are used to estimate the variance parameters. The errors on the estimated \hat{c}_t are generally small ($\lesssim 1\%$), so the point estimate \hat{c}_t was directly used for all downstream inferences.

Estimation of mean fitness dynamics

As beneficial mutations increase in frequency, and deleterious mutations decrease, the mean fitness of the population changes over time, impacting the rate of frequency change of all genotypes in the population. To estimate the mean fitness dynamics for each experiment, we can track the dynamics of neutral genotypes, again using the large set of intergenic barcodes. We obtain an estimate of the mean fitness between times 0 and t by simply taking the negative log slope over many barcodes,

$$\hat{x}_{t,i} = -\frac{1}{t} \left[\log \left(\frac{r_{t,i}}{R_t} \right) - \log \left(\frac{r_{0,i}}{R_0} \right) \right]$$

As detailed in the previous section, it is advantageous to use robust forms of estimation to guard against the presence of outliers. Groups of ~ 100 randomly selected intergenic barcodes with $r_{t,i} < 500$ were summed together to create "super-barcodes", in order to improve individual estimates. The mean fitness $\hat{x}_{t,i}$ was estimated for each super-barcode separately, and then the final estimate $\hat{\hat{x}}_t$ was obtained by taking the median over all super-barcodes. The standard error was estimated via the median absolute deviation between all

super-barcodes, analogous to equations 13-14. Again, the point estimate \hat{x}_t is used for all downstream analyses, as mean fitness error was consistently small.

Identification of putative outlier barcodes

We observed that some barcodes had trajectories that noticeably differed from the rest of the barcodes within the genotype, likely caused by the presence of secondary (selected) mutations that arose elsewhere in the genome or rare frequency fluctuations. We observed outlier barcodes with both beneficial and deleterious trajectories relative to the rest of the barcodes within the genotype. Problematically, some of these outlier barcodes were at high abundance relative to the other barcodes in the genotype, thus dominating the genotype fitness estimate. This necessitated a need to either accommodate outliers in our fitness estimation procedure or detect and reject outliers. We found that a number of robust estimators that we explored (e.g. maximum median/trimmed likelihood) had unreasonably high variance in fitness given our data ($\text{std } \hat{s} \gtrsim \hat{s}$). Thus, we opted to use a method to detect and reject outlier barcodes within genotypes. We based our outlier detection method on the resistant diagnostic RD_i introduced by Rousseeuw and Leroy (1987) [66], a high-breakdown measure of statistical deviation.

For every genotype with at $n_{bc} \geq 4$ unique barcodes, we computed a fitness estimate for each barcode, \hat{s}_i , via maximum likelihood (eqs. 5-8). We then used a resampling approach to randomly sample 200 different combinations of $n_r = \lceil n_{bc}/2 \rceil$ barcodes, where samples are labeled J . To get an estimate of the 'typical' fitness, $\hat{s}_{J,typ}$, of the barcodes within a gene, we either take the weighted median ($n_r < 10$) or weighted trimmed mean ($n_r \geq 10$, trim 30% off each tail) of the resampled barcode fitnesses, where in both cases, samples are weighted by their inverse variance, $w_i = 1/(\text{var } \hat{s}_i)$. The weighted median is used for low number of samples, while the trimmed weighted mean is used for high number of samples, because the trimmed weighted mean generally has lower sampling variance when the number of samples remaining after trimming is sufficiently large. To compare the strength of evidence for a fitness of \hat{s}_i or $\hat{s}_{J,typ}$ for barcode i , we compute the likelihood ratio,

$$\text{LR}_{J,i} = \log \frac{\mathcal{L}_i(\hat{s}_i | \mathbf{r}_i)}{\mathcal{L}_i(\hat{s}_{J,typ} | \mathbf{r}_i)}$$

The deviation of barcode i from the rest of the barcodes in the genotype is then,

$$u_i = \max_J \frac{\text{LR}_{J,i}}{\text{med}_i \text{LR}_{J,i}}$$

The final resistant diagnostic is finally calculated as a standardized version of u_i ,

$$RD_i = \frac{u_i}{\text{med}_i u_i}$$

If $RD_i > \text{cutoff}$, then barcode i is considered an outlier and thrown away.

Simulations

To determine an appropriate cutoff value, we performed simulations of the data generating process, and calculated the RD for each barcode within a simulated gene using the above method. Specifically, we simulated trajectories of lineage frequencies with $s \in \{-0.02, 0, 0.02\}$ gen^{-1} with the standard diffusion approximation, assuming $f \ll 1$,

$$\partial_t f = sf + \sqrt{\frac{f}{N_e}} \eta(t)$$

$$\begin{aligned}\langle \eta(t) \rangle &= 0 \\ \langle \eta(t)\eta(t') \rangle &= \delta(t - t')\end{aligned}$$

We ‘observed’ trajectories at the end of each ‘day’ (≈ 6.64 gen) for 4 days, and added measurement noise,

$$\begin{aligned}\phi_t &\equiv \sqrt{f_t} \\ \phi_t^{obs} \mid \phi_t &\sim \mathcal{N}(\phi_t, \zeta)\end{aligned}$$

We used $N_e = 10^8$ *day* and $\zeta = 2 * 10^{-8}$. We then grouped 20 simulated lineages together into a ‘gene’ (approximate median number of barcodes per gene in our libraries), with $n \in \{1, 2, 3\}$ selected lineages (of the same sign), and the rest as neutral lineages. After calculating the *RD* for each simulated gene, we calculated the true positive/negative rate for calling a lineage as an outlier for a given threshold (Figure S29).

We can see that the method can sensitively detect relatively small, $\sim 2\%$, differences in fitness, while minimizing the number of neutral barcodes that are incorrectly thrown away. True positive rate decreases somewhat if there are multiple outlier barcodes within a gene, but the difference appears to be minimal, as expected from the construction of the *RD* as a high-breakdown deviance statistic. From the simulations, we chose a cutoff of 6, which only falsely throws out $\sim 5\%$ of neutral lineages, while detecting $\sim 85 - 95\%$ of outliers. This threshold also seems to empirically work with our data, detecting at least the most obvious outliers (see e.g. Figure S30).

Consequences of potential barcode frequency biases

One major assumption of the above analyses is that the frequency of barcodes from BarSeq data represents an *unbiased* estimate of the actual frequency of barcoded cells in the population. While we expect this assumption to generally hold, there are two major ways that this assumption could be violated: (1) if barcodes are differentially amplified due to e.g. differences in GC content, and (2) if genomic regions near the chromosomal origin of replication are present at a higher copy number due to fast growth. Both types of biases have been observed in some previous RB-TnSeq experiments [40, 41]. We can check for the presence of frequency biases by comparing the inferred value of the error parameter κ_t (see section) for barcodes with different GC contents and across genomic positions, as biases in frequency measurements will change the apparent strength of genetic drift. We see that κ_t generally does not change across these conditions (Figure S31), and thus the aforementioned sources of frequency biases do not seem to be particularly prevalent or strong in our system.

Of course, other unknown sources of frequency bias could be present, or too weak to detect; but, under our inference pipeline, biases in frequency would only affect the variance of inferred s , not its expected value, as long as the bias across time points remains constant. We can see this by considering the deterministic (mean) dynamics of mutant frequencies f in a population with m genotypes,

$$f_i(t) = \frac{f_{0,i}e^{s_i t}}{\sum_j^m f_{0,j}e^{s_j t}}$$

We could then include a strain-specific, constant multiplicative bias parameter, γ_i . The observed frequencies would then follow,

$$f_i(t) = \frac{\gamma_i f_{0,i} e^{s_i t}}{\sum_j^m \gamma_j f_{0,j} e^{s_j t}}$$

By observing these biased frequencies instead of the actual frequencies, we would infer s_i and $\gamma_i f_{0,i}$, therefore only biasing the nuisance intercept parameter.

As expected from the above analysis, there was no consistent, detectable correlation between genomic position and inferred fitness (Figure S2). However, there is one exception: in a couple of the L experiments, it looks like there is a dip in median fitness around ~ 2.7 Mb, seemingly caused by a lack of neutral/beneficial variants. This position is about ~ 1 Mb downstream from the origin of replication (3.8Mb), and ~ 1 Mb upstream of the termination of replication and Dif site (~ 1.5 Mb). So it appears to be unlikely an artifact of uneven copy numbers or a DNA extraction bias. The origin of this signal is unclear, but seems to indicate that there is a region of the L genome that is more likely to have deleterious effects from knockout mutations. However, in any case, the dip seems to be isolated to a seemingly unremarkable portion of the genome, and thus does not call into question the general validity and assumptions of our model.

Analysis

Similarity of fitness effects across environments

To compute the correlation of knockout fitness effects across environments for a given genetic background (main text Figure 3), we first removed genes with noisy fitness effects ($\sigma_s > 1\%$), then calculated the weighted pearson correlation coefficient, where genes are labeled k and environments are labeled i, j ,

$$w_k = 1/(\text{var } \hat{s}_{i,k} + \text{var } \hat{s}_{j,k}) \quad (15)$$

$$\mu(x) = \frac{\sum_k w_k x_k}{\sum_k w_k} \quad (16)$$

$$\text{wcov}(x, y; w) = \frac{\sum_k w_k (x_k - \mu(x))(y_k - \mu(y))}{\sum_k w_k} \quad (17)$$

$$\rho_{i,j} = \frac{\text{wcov}(\hat{s}_i, \hat{s}_j; w)}{\sqrt{\text{wcov}(\hat{s}_i, \hat{s}_i; w)\text{wcov}(\hat{s}_j, \hat{s}_j; w)}} \quad (18)$$

We then performed hierarchical clustering using Ward’s method across environments for each genetic background, with $1 - \rho_{i,j}$ as the distance metric. Environment pairs with $\rho_{i,j} < 0$ are set to 0 for the purposes of clustering, as there were few negative correlations, and all were small.

We used a bootstrapping procedure to estimate the statistical support for each cluster of environments. Using only the intersection of genes that passed across all environments, we performed standard resampling of genes with replacement, and then repeated the correlation measurement of knockout fitness values for each pair of environments. Then we repeated the hierarchical clustering and compared each branching of the original tree to the bootstrapped tree using the method of [67]. We repeated the resampling procedure 5000 times for each genetic background and reported the average support for each clade.

We performed a principal components analysis on our data, using normalized fitness effects as the features. We only included genes that had measured fitness effects across all experiments. We normalized the fitness data separately for each experiment so that the scale of fitness effects was comparable across conditions. We first performed a quantile transform (to a gaussian distribution) on the fitness effects using `sklearn.preprocessing.quantile_transform`, and then subsequently centered and scaled the data to turn it into a standard normal. We performed the PCA with `sklearn.decomposition.PCA`.

Network of gene-by-gene correlations

To investigate potential relationships between genes in the different strain investigated in our work, we sought to quantify the degree of correlation of fitness measurements across all environments between every pair of genes, a quantity that has been referred to as cofitness [41]. Highly correlated fitness measurements may indicate that genes are connected via gene regulation. In order to account for the fact that the measurement error in fitness measurements varies between genes and environments, we computed the cofitness of every pair of genes i, j as the weighted pearson correlation coefficient, where environments are labeled k , analogous to equations 15-18. We excluded genes that were not called as significantly non-neutral in at least one experiment, and genes with successful fitness measurements in < 4 experiments.

The vast majority of non-zero correlations are likely generated by chance, due to the relatively small number of environments where fitness is measured. Therefore, for each pair of genes, we generated a null cofitness distribution through a resampling procedure performed 300 times, by (1) randomly permuting the fitness assignments for both genes, (2) resampling each fitness value such that $\hat{s}_{boot} \sim \mathcal{N}(\hat{s}, \text{std } \hat{s})$ (“parametric bootstrapping”), and (3) recalculating cofitness via equations 15-18. We then compared the measured cofitness to the null distribution to generate a 1-sided p-value. After correcting the set of p-values with a Benjamini-Hochberg FDR correction, we considered gene pairs to be significantly correlated at $\alpha = 0.05$, effectively drawing an edge between the two genes in the cofitness network.

After identifying statistically significant correlations between genes across environments, we sought to cluster genes into communities, without considering the magnitude or sign of the cofitness values. We used the ‘Fluid Communities’ algorithm [55], as implemented in the `networkx` python package [68], because of the flexibility of the algorithm, and the resulting communities had the highest modularity of all community-finding algorithms we explored. As the fluid communities algorithm is initialized stochastically, and requires pre-specifying k communities, we ran the algorithm on our data across varying community sizes, $k \in [4, 20]$, with 200 replicates for each k (Figure S13). We then picked the communities with the highest modularity for each genetic background. For the purposes of community finding, we treated all significant edges as the same, without considering the actual cofitness value of the edge. All community sets found had *modularity* > 0 , indicating that genes were more tightly connected within their community compared to between communities.

Standard gene ontology enrichment analysis was performed on each community in each genetic background with the `goatools` python package [69], using Fisher’s exact test to find significantly over-represented annotations in a gene set, with an FDR correction and $\alpha = 0.05$.

We sought to check if variance in fitness across environments for any given knockout could predict if two genes would stay in the same cluster across genetic backgrounds, as a control for the observed correlation with EcoliNet score. We average fitness variance across environments over the two knockouts of interest, referring to the quantity as $\langle \text{var}(s) \rangle$. We fit a logistic model with normalized EcoliNet score of the gene pair, $n\text{score} \equiv \text{score}/\text{std score}$ and $n\text{var} \equiv \langle \text{var}(s) \rangle/\text{std}\langle \text{var}(s) \rangle$ as the predictors (standard deviation is taken over all knockout pairs), and the probability that the two genes are together in strain 2, if they were together in strain 1 as the response variable, $\log p_i/(1-p_i) = n\text{score}e\beta_{\text{score}} + n\text{var}\beta_{\text{var}} + \beta_0 + \epsilon_i$. The results are shown in Figure S20.

It is known that community detection algorithms can have potential surfaces with large plateaus without a clear maximum, i.e. can give many solutions with similar modularity but different groupings [70]. We wanted to see if the observed (mostly) “random reassortment” of genes among clusters between genetic backgrounds could be explained by this effect. Thus, we compared the optimal partition of each background to the 100 next-best partitions across all backgrounds (Figure S14). For each suboptimal partition, we asked if two genes were in the same cluster in the optimal partition, what is the probability that they are also in the same cluster in the suboptimal partition. We see that if we compare partitions in the same genetic background, this probability is around 40%, while it is around 10% when comparing

partitions across background. This suggests that different reasonable partitions of the cofitness networks are much more similar within genetic backgrounds than between backgrounds. We also re-ordered the genes of the cofitness network such that they followed the ordering of another genetic background’s optimal partition (Figure 4B). It is apparent that replotting the cofitness matrix using another genetic background’s clustering does not produce noticeable structure. Together, these results suggest that while different reasonable partitions can give slightly different clusters, the observed reassortment of knockout fitness correlations among backgrounds cannot just be explained by failures of the community detection algorithm. We also investigated the extent to which the structure of our cofitness networks was driven by measurement noise (Figure S15, S16). We leveraged the fact that we had at least two biological replicates per experiment, and computed new cofitness networks (in the same manner as described above), only using either biological replicate “1” or “2”. We can see that even when the data is independently split, the cofitness networks within a genetic background are more similar than between backgrounds.

Genome evolution

We sought to understand if knockout fitness measurements could predict the probability that a gene would mutate in the LTEE. To that end, we downloaded clonal sequencing data from Tenaillon et al. (2016) [59], where the authors isolated and sequenced clones from a number of time points across all 12 lines of the LTEE, and identified mutations relative to the REL606 ancestor. We excluded synonymous SNPs from our analysis. A representation of the raw data can be found in Figure S24.

We then sought to understand if knockout fitness effects can predict if a mutation will appear in a gene in the Tenaillon et al. dataset, as a proxy for establishment. For REL606, classified a gene as mutated if a mutation appeared in one of the 12 LTEE lines (excluding mutator populations). For S and L, we classified genes as mutated only if they were present in the appropriate sublineage, i.e. in REL11830, REL11036 or REL11831, REL11035 for S and L respectively. We also excluded mutations that were already present in our S and L clones, which we determined from clonal sequencing data from Plucain et al. (2014) [46]. We then fit a logistic model with knockout fitness effect as the predictor variable and gene mutated status (between time points) as the response variable,

$$\log p_{est,i}/(1 - p_{est,i}) = \pm \tilde{s}_i \beta_{est\pm} + \beta_0 + \epsilon_i$$

We fit two different coefficients for beneficial and deleterious mutations in each environment, β_{est+} and β_{est-} respectively. We only include genes that are putatively neutral, i.e. $|s| < 0.005$ and not called as significantly non-neutral, along with genes that are either significantly beneficial or deleterious, all at significance level $\alpha = 0.05$. We normalized the fitness values by the median value of the non-neutral genes, i.e.

$$\tilde{s}_i = \frac{s_i}{\text{med}_{i \notin \text{neutral}} s_i} \quad (19)$$

We use the logistic model implementation in the `statsmodels` python package [71]. We used the standard method of Benjamini & Hochberg to control for the false discovery rate, pooling all tests across beneficial and deleterious coefficients. To test if there is a significant difference between REL606 logit slopes at 0-5k and 5-20k, we employed a permutation test. To construct a null distribution of the difference in slopes, for each gene we shuffled whether it ‘established’ (0 or 1) between 0-5k and 5-20k and recomputed the regression coefficients 1000 times, recording the difference. We then compared the actual difference in coefficients to the null distribution to get p-values.

Changes in gene expression

We used a microarray gene expression dataset reported by Le Gac et al. (2012) [16] to compare to our knockout fitness measurements, downloaded from the NCBI Gene Expression Omnibus [72], importing data with GEOquery [73]. We primarily used the GEO2R tool to process the raw microarray data along with the R package `limma` [74, 75]. After applying a \log_2 transform to the data, we ensured that all collected samples had approximately the same intensity distributions by performing a quantile normalization. Then, pooling all replicates within a strain, we fit a linear model to our data to determine the relative log-fold change in expression between different strains, taking into account the measured mean-variance relationship. A representation of the raw data can be found in Figure S23. We also compared the distribution of log-fold fitness effects between neutral and non-neutral genes (Figure 5B). We computed p-values to compare the distributions with standard Mann-Whitney U tests.

We then fit a linear model to investigate if there was a correlation between fitness measured in a given environment, s_i , and log-change in gene expression between evolutionary time points ΔE_i , such that

$$\Delta E_i = \pm \tilde{s}_i \beta_{exp\pm} + \beta_0 + \epsilon_i$$

Similar to the gene establishment model, we fit two different coefficients for beneficial and deleterious mutations in each environment, β_{exp+} and β_{exp-} respectively (Figure S25). We only include genes that are putatively neutral, i.e. $|s| < 0.005$ and not called as significantly non-neutral, along with genes that are either significantly beneficial or deleterious, all at significance level $\alpha = 0.05$. We normalized the fitness values by the median value of the non-neutral genes, in the same manner as equation 19. We fit the model with weighted least squares, as implemented in the `statsmodels` python package [71], with weights $w_i \propto 1/\text{var } \Delta E_i$, to incorporate the fact that there are different levels of measurement error in the log-fold change expression for each gene. We used the standard method of Benjamini & Hochberg to control for the false discovery rate, pooling all tests across beneficial and deleterious coefficients.

As a control, we also investigated if our results would change if we excluded poorly expressed genes. It is perhaps the case that neutral knockouts are potentially a bad comparison class, because many of them may be poorly expressed at all times, and thus ineligible to undergo large changes in expression. We can test for this alternative hypothesis by focusing our analysis on solely initially highly expressed (50th percentile) genes, excluding poorly expressed genes. The results are shown in figure S26. The regression coefficients change somewhat, but not qualitatively, showing that the aforementioned hypothesis is not likely the driver of the signals we observed.

Data Availability

Glycerol stock copies of the REL606, 6.5k S, and 6.5k L Tn5 barcoded libraries are available upon request. Raw sequencing reads have been deposited in the NCBI BioProject database under accession number PRJNA900607 [<https://www.ncbi.nlm.nih.gov/bioproject/PRJNA900607>]. All processed data are available on GitHub,

<https://github.com/joaoascensao/S-L-REL606-BarSeq>

Other datasets referenced may be accessed online: the LTEE time-resolved clonal sequencing data (<https://barricklab.org/shiny/LTEE-Ecoli/>) [59]; the LTEE time-resolved metagenomic sequencing data (<https://github.com/benjaminhgood/LTEE-metagenomic>) [47]; S and L clonal sequencing data (Plucain et al. (2014) SI) [46]; EcoliNet (<https://www.inetbio.org/ecolinet/>) [58]; transcriptomic measurements of LTEE strains (BioProject PRJNA144635) [16].

Code Availability

All code used to process the data and perform the analyses are available on GitHub, <https://github.com/joaoascensao/S-L-REL606-BarSeq>

References

- [1] Freya Harrison. Microbial ecology of the cystic fibrosis lung. *Microbiology (Reading, England)*, 153(Pt 4):917–923, 4 2007. ISSN 1350-0872. doi: 10.1099/MIC.0.2006/004077-0.
- [2] Susannah Selber-Hnativ, Belise Rukundo, Masoumeh Ahmadi, Hayfa Akoubi, Hend Al-Bizri, Adelekan F. Aliu, Tanyi U. Ambeaghen, Lilit Avetisyan, Irmak Bahar, Alexandra Baird, Fatema Begum, H el ene Ben Soussan, Virginie Blondeau- ethier, Roxane Bordaries, Helene Bramwell, Alicia Briggs, Richard Bui, Matthew Carnevale, Marisa Chancharoen, Talia Chevassus, Jin H. Choi, Karyne Coulombe, Florence Couvrette, Samantha D’Abreau, Meghan Davies, Marie Pier Desbiens, Tamara Di Maulo, Sean Anthony Di Paolo, Sabrina Do Ponte, Priscyla dos Santos Ribeiro, Laure Anne Dubuc-Kanary, Paola K. Duncan, Fr ed erique Dupuis, Sara El-Nounou, Christina N. Eyangos, Natasha K. Ferguson, Nancy R. Flores-Chinchilla, Tanya Fotakis, H. D.Mariam Gado Oumarou, Metodi Georgiev, Seyedehnazanin Ghiassy, Natalija Glibetic, Julien Gr egoire Bouchard, Tazkia Hassan, Iman Huseen, Marlon Francis Ibuna Quilatan, Tania Iozzo, Safina Islam, Dilan B. Jaunky, Aniththa Jeyasegaram, Marc Andr e Johnston, Matthew R. Kahler, Kiranpreet Kaler, Cedric Kamani, Hessem Karimian Rad, Elisavet Konidis, Filip Konieczny, Sandra Kurianowicz, Philippe Lamothe, Karina Legros, Sebastien Leroux, Jun Li, Monica E. Lozano Rodriguez, Sean Luponio-Yoffe, Yara Maalouf, Jessica Mantha, Melissa McCormick, Pamela Mondragon, Thivaedee Narayana, Elizaveta Neretin, Thi T.T. Nguyen, Ian Niu, Romeo B. Nkemazem, Martin O’Donovan, Matthew Oueis, Stevens Paquette, Nehal Patel, Emily Pecs i, Jackie Peters, Annie Petteorelli, Cassandra Poirier, Victoria R. Pompa, Harshvardhan Rajen, Reginald Olivier Ralph, Josu e Rosales-Vasquez, Daria Rubinshtein, Surya Sakr, Mohammad S. Sebai, Lisa Serravalle, Fily Sidibe, Ahnjana Sinnathurai, Dominique Soho, Adithi Sundarakrishnan, Veronika Svistkova, Tsolaye E. Ugbeye, Megan S. Vasconcelos, Michael Vincelli, Olga Voitovich, Pamela Vrabel, Lu Wang, Maryse Wasfi, Cong Y. Zha, and Chiara Gamberi. Human gut microbiota: Toward an ecology of disease. *Frontiers in Microbiology*, 8(JUL):1265, 7 2017. ISSN 1664302X. doi: 10.3389/FMICB.2017.01265/BIBTEX.
- [3] Paul G. Falkowski, Tom Fenchel, and Edward F. Delong. The microbial engines that drive Earth’s biogeochemical cycles. *Science (New York, N.Y.)*, 320(5879):1034–1039, 5 2008. ISSN 1095-9203. doi: 10.1126/SCIENCE.1153213.
- [4] Steven J. Biller, Paul M. Berube, Debbie Lindell, and Sallie W. Chisholm. Prochlorococcus: the structure and function of collective diversity. *Nature Reviews Microbiology* 2014 13:1, 13(1):13–27, 12 2014. ISSN 1740-1534. doi: 10.1038/nrmicro3378.
- [5] Cameron Wagg, Yann Hautier, Sarah Pellkofer, Samiran Banerjee, Bernhard Schmid, and Marcel G.A. van der Heijden. Diversity and asynchrony in soil microbial communities stabilizes ecosystem functioning. *eLife*, 10, 3 2021. ISSN 2050084X. doi: 10.7554/ELIFE.62813.
- [6] Emily B. Graham, Joseph E. Knelman, Andreas Schindlbacher, Steven Siciliano, Marc Breulmann, Anthony Yannarell, J. M. Beman, Guy Abell, Laurent Philippot, James Prosser, Arnaud Foulquier, Jorge C. Yuste, Helen C. Glanville, Davey L. Jones, Roey

- Angel, Janne Salminen, Ryan J. Newton, Helmut Bürgmann, Lachlan J. Ingram, Ute Hamer, Henri M.P. Siljanen, Krista Peltoniemi, Karin Potthast, Lluís Bañeras, Martin Hartmann, Samiran Banerjee, Ri Qing Yu, Geraldine Nogaró, Andreas Richter, Marianne Koranda, Sarah C. Castle, Marta Goberna, Bongkeun Song, Amitava Chatterjee, Olga C. Nunes, Ana R. Lopes, Yiping Cao, Aurore Kaisermann, Sara Hallin, Michael S. Strickland, Jordi Garcia-Pausas, Josep Barba, Hojeong Kang, Kazuo Isobe, Sokratis Papaspyrou, Roberta Pastorelli, Alessandra Lagomarsino, Eva S. Lindström, Nathan Basiliko, and Diana R. Nemergut. Microbes as engines of ecosystem function: When does community structure enhance predictions of ecosystem processes? *Frontiers in Microbiology*, 7(FEB):214, 2 2016. ISSN 1664302X. doi: 10.3389/FMICB.2016.00214/BIBTEX.
- [7] Shijie Zhao, Tami D. Lieberman, Mathilde Poyet, Kathryn M. Kauffman, Sean M. Gibbons, Mathieu Groussin, Ramnik J. Xavier, and Eric J. Alm. Adaptive Evolution within Gut Microbiomes of Healthy People. *Cell Host and Microbe*, 25(5):656–667, 2019. ISSN 19346069. doi: 10.1016/j.chom.2019.03.007.
- [8] Anders Folkesson, Lars Jelsbak, Lei Yang, Helle Krogh Johansen, Oana Ciofu, Niels Hoiby, and Soren Molin. Adaptation of *Pseudomonas aeruginosa* to the cystic fibrosis airway: An evolutionary perspective, 12 2012. ISSN 17401526.
- [9] Ana Sousa, Ricardo S. Ramiro, João Barroso-Batista, Daniela Güleresi, Marta Lourenço, and Isabel Gordo. Recurrent Reverse Evolution Maintains Polymorphism after Strong Bottlenecks in Commensal Gut Bacteria. *Molecular Biology and Evolution*, 34(11): 2879–2892, 11 2017. ISSN 0737-4038. doi: 10.1093/MOLBEV/MSX221.
- [10] Nandita R Garud, Benjamin H Good, Oskar Hallatschek, and Katherine S Pollard. Evolutionary dynamics of bacteria in the gut microbiome within and across hosts. *bioRxiv*, pages 1–38, 2017.
- [11] Evgeni M. Frenkel, Michael J. McDonald, J. David Van Dyken, Katya Kosheleva, Gregory I. Lang, and Michael M. Desai. Crowded growth leads to the spontaneous evolution of semistable coexistence in laboratory yeast populations. *Proceedings of the National Academy of Sciences of the United States of America*, 112(36):11306–11311, 2015. ISSN 10916490. doi: 10.1073/pnas.1506184112.
- [12] Z. D. Blount, C. Z. Borland, and R. E. Lenski. Historical contingency and the evolution of a key innovation in an experimental population of *Escherichia coli*. *Proceedings of the National Academy of Sciences*, 105(23):7899–7906, 6 2008. ISSN 0027-8424. doi: 10.1073/pnas.0803151105.
- [13] Helling RB, Vargas CN, and Adams J. Evolution of *Escherichia coli* during growth in a constant environment. *Genetics*, 116(3):349–358, 7 1987. ISSN 0016-6731. doi: 10.1093/GENETICS/116.3.349.
- [14] Kinnersley M, Wenger J, Kroll E, Adams J, Sherlock G, and Rosenzweig F. Ex uno plures: clonal reinforcement drives evolution of a simple microbial community. *PLoS genetics*, 10(6), 2014. ISSN 1553-7404. doi: 10.1371/JOURNAL.PGEN.1004430.
- [15] Matthew D. Herron and Michael Doebeli. Parallel Evolutionary Dynamics of Adaptive Diversification in *Escherichia coli*. *PLoS Biology*, 11(2):e1001490, 2 2013. ISSN 1545-7885. doi: 10.1371/journal.pbio.1001490.

- [16] Mickaël Le Gac, Jessica Plucain, Thomas Hindré, Richard E. Lenski, and Dominique Schneider. Ecological and evolutionary dynamics of coexisting lineages during a long-term experiment with *Escherichia coli*. *Proceedings of the National Academy of Sciences of the United States of America*, 96(18):10242–7, 8 2012. ISSN 0027-8424. doi: 10.1073/pnas.96.18.10242.
- [17] David M Post and Eric P Palkovacs. Eco-evolutionary feedbacks in community and ecosystem ecology: interactions between the ecological theatre and the evolutionary play. *Philosophical transactions of the Royal Society of London. Series B, Biological sciences*, 364(1523):1629–40, 6 2009. ISSN 1471-2970. doi: 10.1098/rstb.2009.0012.
- [18] K. N. Laland, F. J. Odling-Smee, and M. W. Feldman. Evolutionary consequences of niche construction and their implications for ecology. *Proceedings of the National Academy of Sciences*, 96(18):10242–10247, 1999. ISSN 0027-8424. doi: 10.1073/pnas.96.18.10242.
- [19] Benjamin H Good, Stephen Martis, and Oskar Hallatschek. Adaptation limits ecological diversification and promotes ecological tinkering during the competition for substitutable resources. *Proceedings of the National Academy of Sciences of the United States of America*, 115(44):E10407–E10416, 10 2018. ISSN 1091-6490. doi: 10.1073/pnas.1807530115.
- [20] Kyle I Harrington and Alvaro Sanchez. Eco-evolutionary dynamics of complex social strategies in microbial communities. *Communicative & Integrative Biology*, 7(1):e28230, 1 2014. ISSN 1942-0889. doi: 10.4161/cib.28230.
- [21] Sandeep Venkataram, Huan-Yu Kuo, Erik F. Y. Hom, and Sergey Kryazhimskiy. Mutualism-enhancing mutations dominate early adaptation in a microbial community. *bioRxiv*, page 2021.07.07.451547, 7 2022. doi: 10.1101/2021.07.07.451547.
- [22] Massimo Amicone and Isabel Gordo. Molecular signatures of resource competition: Clonal interference favors ecological diversification and can lead to incipient speciation. *Evolution*, 2021. ISSN 1558-5646. doi: 10.1111/EVO.14315.
- [23] John H. Gillespie. Molecular Evolution Over the Mutational Landscape. *Evolution*, 38(5):1116, 9 1984. doi: 10.2307/2408444.
- [24] H. Allen Orr. The Population Genetics of Adaptation: The Distribution of Factors Fixed during Adaptive Evolution. *Evolution*, 52(4):935, 8 1998. doi: 10.2307/2411226.
- [25] H Allen Orr. The distribution of fitness effects among beneficial mutations. *Genetics*, 163(4):1519, 4 2003.
- [26] Benjamin H. Good, Igor M. Rouzine, Daniel J. Balick, Oskar Hallatschek, and Michael M. Desai. Distribution of fixed beneficial mutations and the rate of adaptation in asexual populations. *Proceedings of the National Academy of Sciences of the United States of America*, 109(13):4950–4955, 2012. ISSN 00278424. doi: 10.1073/pnas.1119910109.
- [27] Daniel P Rice, Benjamin H Good, Michael M Desai, and R. Korona. The evolutionarily stable distribution of fitness effects. *Genetics*, 200(1):321–9, 5 2015. ISSN 1943-2631. doi: 10.1534/genetics.114.173815.

- [28] Michael M Desai and Daniel S Fisher. Beneficial mutation selection balance and the effect of linkage on positive selection. *Genetics*, 176(3):1759–98, 7 2007. ISSN 0016-6731. doi: 10.1534/genetics.106.067678.
- [29] Michael M. Desai, Daniel S. Fisher, and Andrew W. Murray. The Speed of Evolution and Maintenance of Variation in Asexual Populations. *Current Biology*, 17(5):385–394, 2007. ISSN 09609822. doi: 10.1016/j.cub.2007.01.072.
- [30] Alex N. Nguyen Ba, Ivana Cvijović, José I. Rojas Echenique, Katherine R. Lawrence, Artur Rego-Costa, Xianan Liu, Sasha F. Levy, and Michael M. Desai. High-resolution lineage tracking reveals travelling wave of adaptation in laboratory yeast. *Nature* 2019, pages 1–11, 2019. ISSN 0028-0836. doi: 10.1038/s41586-019-1749-3.
- [31] Sasha F. Levy, Jamie R. Blundell, Sandeep Venkataram, Dmitri A. Petrov, Daniel S. Fisher, and Gavin Sherlock. Quantitative evolutionary dynamics using high-resolution lineage tracking. *Nature*, 519(7542):181–186, 3 2015. ISSN 0028-0836. doi: 10.1038/nature14279.
- [32] Kimberly S. Vasquez, Lisa Willis, Nate J. Cira, Katharine M. Ng, Miguel F. Pedro, Andrés Aranda-Díaz, Manohary Rajendram, Feiqiao Brian Yu, Steven K. Higginbottom, Norma Neff, Gavin Sherlock, Karina B. Xavier, Stephen R. Quake, Justin L. Sonnenburg, Benjamin H. Good, and Kerwyn Casey Huang. Quantifying rapid bacterial evolution and transmission within the mouse intestine. *Cell Host & Microbe*, 29(9):1454–1468, 9 2021. ISSN 1931-3128. doi: 10.1016/J.CHOM.2021.08.003.
- [33] Jamie R. Blundell, Katja Schwartz, Danielle Francois, Daniel S. Fisher, Gavin Sherlock, and Sasha F. Levy. The dynamics of adaptive genetic diversity during the early stages of clonal evolution. *Nature Ecology & Evolution*, 3(2):293–301, 2 2019. ISSN 2397-334X. doi: 10.1038/s41559-018-0758-1.
- [34] Sandeep Venkataram, Barbara Dunn, Yuping Li, Atish Agarwala, Jessica Chang, Emily R Ebel, Kerry Geiler-Samerotte, Lucas Hérisant, Jamie R Blundell, Sasha F Levy, Daniel S Fisher, Gavin Sherlock, and Dmitri A Petrov. Development of a Comprehensive Genotype-to-Fitness Map of Adaptation-Driving Mutations in Yeast. *Cell*, 166(6):1585–1596, 9 2016. ISSN 1097-4172. doi: 10.1016/j.cell.2016.08.002.
- [35] Milo S. Johnson, Alena Martsul, Sergey Kryazhimskiy, and Michael M. Desai. Higher-fitness yeast genotypes are less robust to deleterious mutations. *Science*, 366(6464):490–493, 10 2019. ISSN 10959203. doi: 10.1126/science.aay4199.
- [36] Celia Payen, Anna B. Sunshine, Giang T. Ong, Jamie L. Pogachar, Wei Zhao, and Maitreya J. Dunham. High-Throughput Identification of Adaptive Mutations in Experimentally Evolved Yeast Populations. *PLOS Genetics*, 12(10):e1006339, 10 2016. ISSN 1553-7404. doi: 10.1371/JOURNAL.PGEN.1006339.
- [37] Grant Kinsler, Kerry Geiler-Samerotte, and Dmitri Petrov. Fitness variation across subtle environmental perturbations reveals local modularity and global pleiotropy of adaptation. *eLife*, 9:1–52, 12 2020. doi: 10.7554/ELIFE.61271.
- [38] Yuping Li, Sandeep Venkataram, Atish Agarwala, Barbara Dunn, Dmitri A. Petrov, Gavin Sherlock, and Daniel S. Fisher. Hidden Complexity of Yeast Adaptation under Simple Evolutionary Conditions. *Current Biology*, 28(4):515–525, 2 2018. ISSN 09609822. doi: 10.1016/j.cub.2018.01.009.

- [39] Yuping Li, Dmitri A. Petrov, and Gavin Sherlock. Single nucleotide mapping of trait space reveals Pareto fronts that constrain adaptation. *Nature Ecology and Evolution*, 3(11):1539–1551, 2019. ISSN 2397334X. doi: 10.1038/s41559-019-0993-0.
- [40] Kelly M Wetmore, Morgan N Price, Robert J Waters, Jacob S Lamson, Jennifer He, Cindi A Hoover, Matthew J Blow, James Bristow, Gareth Butland, Adam P Arkin, and Adam Deutschbauer. Rapid quantification of mutant fitness in diverse bacteria by sequencing randomly bar-coded transposons. *mBio*, 6(3):00306–15, 5 2015. ISSN 2150-7511. doi: 10.1128/mBio.00306-15.
- [41] Morgan N. Price, Kelly M. Wetmore, R. Jordan Waters, Mark Callaghan, Jayashree Ray, Hualan Liu, Jennifer V. Kuehl, Ryan A. Melnyk, Jacob S. Lamson, Yumi Suh, Hans K. Carlson, Zuelma Esquivel, Harini Sadeeshkumar, Romy Chakraborty, Grant M. Zane, Benjamin E. Rubin, Judy D. Wall, Axel Visel, James Bristow, Matthew J. Blow, Adam P. Arkin, and Adam M. Deutschbauer. Mutant phenotypes for thousands of bacterial genes of unknown function. *Nature*, page 1, 5 2018. ISSN 0028-0836. doi: 10.1038/s41586-018-0124-0.
- [42] Daniel E Rozen and Richard E Lenski. Long-Term Experimental Evolution in *Escherichia coli*. VIII. Dynamics of a Balanced Polymorphism. *The American naturalist*, 155(1):24–35, 1 2000. ISSN 1537-5323. doi: 10.1086/303299.
- [43] Daniel E. Rozen, Nadège Philippe, J. Arjan de Visser, Richard E. Lenski, and Dominique Schneider. Death and cannibalism in a seasonal environment facilitate bacterial coexistence. *Ecology Letters*, 12(1):34–44, 1 2009. ISSN 1461023X. doi: 10.1111/j.1461-0248.2008.01257.x.
- [44] Tobias Großkopf, Jessika Consuegra, Joël Gaffé, John C. Willison, Richard E. Lenski, Orkun S. Soyer, and Dominique Schneider. Metabolic modelling in a dynamic evolutionary framework predicts adaptive diversification of bacteria in a long-term evolution experiment. *BMC Evolutionary Biology*, 16(1):163, 12 2016. ISSN 1471-2148. doi: 10.1186/s12862-016-0733-x.
- [45] Daniel E. Rozen, Dominique Schneider, and Richard E. Lenski. Long-Term Experimental Evolution in *Escherichia coli*. XIII. Phylogenetic History of a Balanced Polymorphism. *Journal of Molecular Evolution*, 61(2):171–180, 8 2005. ISSN 0022-2844. doi: 10.1007/s00239-004-0322-2.
- [46] Jessica Plucain, Thomas Hindré, Mickaël Le Gac, Olivier Tenaillon, Stéphane Cruveiller, Claudine Médigue, Nicholas Leiby, William R. Harcombe, Christopher J. Marx, Richard E. Lenski, and Dominique Schneider. Epistasis and allele specificity in the emergence of a stable polymorphism in *Escherichia coli*. *Science*, 343(6177):1366–1369, 2014. ISSN 10959203. doi: 10.1126/science.1248688.
- [47] Benjamin H. Good, Michael J. McDonald, Jeffrey E. Barrick, Richard E. Lenski, and Michael M. Desai. The dynamics of molecular evolution over 60,000 generations. *Nature*, 551(7678):45–50, 10 2017. ISSN 0028-0836. doi: 10.1038/nature24287.
- [48] Paul D. Sniegowski, Philip J. Gerrish, and Richard E. Lenski. Evolution of high mutation rates in experimental populations of *E. coli*. *Nature*, 387(6634):703–705, 1997. ISSN 00280836. doi: 10.1038/42701.
- [49] Benjamin H. Good and Michael M. Desai. The Impact of Macroscopic Epistasis on Long-Term Evolutionary Dynamics. *Genetics*, 199(1):177–190, 1 2015. ISSN 0016-6731.

doi: 10.1534/genetics.114.172460.

- [50] Michael J. Wiser, Noah Ribeck, and Richard E. Lenski. Long-term dynamics of adaptation in asexual populations. *Science*, 342(6164):1364–1367, 2013. ISSN 10959203. doi: 10.1126/science.1243357.
- [51] A. I. Khan, D. M. Dinh, D. Schneider, R. E. Lenski, and T. F. Cooper. Negative Epistasis Between Beneficial Mutations in an Evolving Bacterial Population. *Science*, 332(6034):1193–1196, 6 2011. ISSN 0036-8075. doi: 10.1126/science.1203801.
- [52] Sergey Kryazhimskiy, Daniel P Rice, Elizabeth R Jerison, and Michael M Desai. Global epistasis makes adaptation predictable despite sequence-level stochasticity. *Science (New York, N.Y.)*, 344(6191):1519–1522, 6 2014. ISSN 1095-9203. doi: 10.1126/science.1250939.
- [53] Peng F, Widmann S, Wünsche A, Duan K, Donovan KA, Dobson RCJ, Lenski RE, and Cooper TF. Effects of Beneficial Mutations in pykF Gene Vary over Time and across Replicate Populations in a Long-Term Experiment with Bacteria. *Molecular biology and evolution*, 35(1):202–210, 1 2018. ISSN 1537-1719. doi: 10.1093/MOLBEV/MSX279.
- [54] Farida Vasi, Michael Travisano, and Richard E. Lenski. Long-Term Experimental Evolution in *Escherichia coli*. II. Changes in Life-History Traits During Adaptation to a Seasonal Environment. <https://doi.org/10.1086/285685>, 144(3):432–456, 10 1994. doi: 10.1086/285685.
- [55] Ferran Parés, Dario Garcia-Gasulla, Armand Vilalta, Jonatan Moreno, Eduard Ayguadé, Jesús Labarta, Ulises Cortés, and Toyotaro Suzumura. Fluid Communities: A Competitive, Scalable and Diverse Community Detection Algorithm. *Studies in Computational Intelligence*, 689:229–240, 3 2017.
- [56] Yasuhiro Takahashi and Umechiyo Tokumoto. A Third Bacterial System for the Assembly of Iron-Sulfur Clusters with Homologs in Archaea and Plastids. *Journal of Biological Chemistry*, 277(32):28380–28383, 8 2002. ISSN 0021-9258. doi: 10.1074/JBC.C200365200.
- [57] Ulrik Brandes, Daniel Delling, Marco Gaertler, Robert Görke, Martin Hofer, Zoran Nikoloski, and Dorothea Wagner. On Modularity Clustering. *IEEE Transactions on Knowledge and Data Engineering*, 20(2):172–188, 2 2008. ISSN 10414347. doi: 10.1109/TKDE.2007.190689.
- [58] Kim H, Shim JE, Shin J, and Lee I. EcoliNet: a database of cofunctional gene network for *Escherichia coli*. *Database : the journal of biological databases and curation*, 2015, 2015. ISSN 1758-0463. doi: 10.1093/DATABASE/BAV001.
- [59] Olivier Tenaillon, Jeffrey E. Barrick, Noah Ribeck, Daniel E. Deatherage, Jeffrey L. Blanchard, Aurko Dasgupta, Gabriel C. Wu, Sébastien Wielgoss, Stéphane Cruveiller, Claudine Médigue, Dominique Schneider, and Richard E. Lenski. Tempo and mode of genome evolution in a 50,000-generation experiment. *Nature*, 536(7615):165–170, 8 2016. ISSN 14764687. doi: 10.1038/nature18959.
- [60] Gautam Reddy and Michael M. Desai. Global epistasis emerges from a generic model of a complex trait. *bioRxiv*, page 2020.06.14.150946, 6 2020. doi: 10.1101/2020.06.14.150946.

- [61] Christopher W. Bakerlee, Alex N. Nguyen Ba, Yekaterina Shulgina, Jose I. Rojas Echenique, and Michael M. Desai. Idiosyncratic epistasis leads to global fitness-correlated trends. *Science*, 376(6593):630–635, 5 2022. ISSN 0036-8075. doi: 10.1126/SCIENCE.ABM4774.
- [62] Rohan Maddamsetti, Philip J. Hatcher, Anna G. Green, Barry L. Williams, Debora S. Marks, and Richard E. Lenski. Core Genes Evolve Rapidly in the Long-Term Evolution Experiment with *Escherichia coli*. *Genome Biology and Evolution*, 9(4):1072, 4 2017. doi: 10.1093/GBE/EVX064.
- [63] Antti Haapala, Esa Määttä, Mikko Ohtamaa, and David Necas. python-Levenshtein.
- [64] Murray Aitkin, Richard J. Boys, and Tom Chadwick. Bayesian point null hypothesis testing via the posterior likelihood ratio. *Statistics and Computing*, 15(3):217–230, 2005. ISSN 09603174. doi: 10.1007/s11222-005-1310-0.
- [65] Isabelle Smith and André Ferrari. Equivalence between the posterior distribution of the likelihood ratio and a p-value in an invariant frame. *Bayesian Analysis*, 9(4):939–962, 2014. ISSN 19316690. doi: 10.1214/14-BA877.
- [66] Peter J. Rousseeuw and Annick M. Leroy. *Robust Regression and Outlier Detection*. Wiley Series in Probability and Statistics. John Wiley & Sons, Inc., Hoboken, NJ, USA, 10 1987. ISBN 9780471852339. doi: 10.1002/0471725382.
- [67] F. Lemoine, J.-B. Domelevo Entfellner, E. Wilkinson, D. Correia, M. Dávila Felipe, T. De Oliveira, and O. Gascuel. Renewing Felsenstein’s phylogenetic bootstrap in the era of big data. *Nature 2018 556:7702*, 556(7702):452–456, 4 2018. ISSN 1476-4687. doi: 10.1038/s41586-018-0043-0.
- [68] Aric A Hagberg, Daniel A Schult, and Pieter J Swart. Exploring Network Structure, Dynamics, and Function using NetworkX. In Gaël Varoquaux, Travis Vaught, and Jarrod Millman, editors, *Proceedings of the 7th Python in Science Conference*, pages 11–15, Pasadena, CA USA, 2008.
- [69] D. V. Klopfenstein, Liangsheng Zhang, Brent S. Pedersen, Fidel Ramírez, Alex Warwick Vesztrocy, Aurélien Naldi, Christopher J. Mungall, Jeffrey M. Yunes, Olga Botvinnik, Mark Weigel, Will Dampier, Christophe Dessimoz, Patrick Flick, and Haibao Tang. GOATOOLS: A Python library for Gene Ontology analyses. *Scientific Reports*, 8(1):10872, 12 2018. ISSN 2045-2322. doi: 10.1038/s41598-018-28948-z.
- [70] Benjamin H. Good, Yves Alexandre De Montjoye, and Aaron Clauset. Performance of modularity maximization in practical contexts. *Physical Review E - Statistical, Nonlinear, and Soft Matter Physics*, 81(4):046106, 4 2010. ISSN 15393755. doi: 10.1103/PHYSREVE.81.046106/FIGURES/14/MEDIUM.
- [71] Skipper Seabold and Josef Perktold. statsmodels: Econometric and statistical modeling with python. In *9th Python in Science Conference*, 2010.
- [72] NCBI GEO. Evolution of gene expression during long term coexistence in a bacterial evolution experiment, <https://www.ncbi.nlm.nih.gov/geo/query/acc.cgi?acc=GSE30639>.
- [73] Davis S and Meltzer PS. GEOquery: a bridge between the Gene Expression Omnibus (GEO) and BioConductor. *Bioinformatics (Oxford, England)*, 23(14):1846–1847, 7 2007.

ISSN 1367-4811. doi: 10.1093/BIOINFORMATICS/BTM254.

- [74] G. K. Smyth. limma: Linear Models for Microarray Data. *Bioinformatics and Computational Biology Solutions Using R and Bioconductor*, pages 397–420, 12 2005. doi: 10.1007/0-387-29362-0{_}23.
- [75] Smyth GK. Linear models and empirical bayes methods for assessing differential expression in microarray experiments. *Statistical applications in genetics and molecular biology*, 3(1), 2004. ISSN 1544-6115. doi: 10.2202/1544-6115.1027.

Acknowledgements

We thank Matti Gralka and QinQin Yu for early-phase experimental assistance. We thank current and former members of the Hallatschek and Arkin labs for productive discussions and feedback regarding this project, especially Morgan Price, Jonas Denk, and QinQin Yu. We thank Richard Lenski for sending us the REL606, 6.5k S and L clones, along with experimental advice and feedback. Research reported in this publication was supported by a National Science Foundation CAREER Award (1555330) and by the Miller Institute for Basic Research in Science, University of California, Berkeley. Some elements of this project were funded by ENIGMA-Ecosystems and Networks Integrated with Genes and Molecular Assemblies (<http://enigma.lbl.gov>), a Science Focus Area Program at Lawrence Berkeley National Laboratory, and is based upon work supported by the U.S. Department of Energy, Office of Science, Office of Biological & Environmental Research under contract number DE-AC02-05CH11231. JAA acknowledges support from an NSF graduate research fellowship, a Berkeley fellowship (from UC Berkeley), and Lloyd and Brodie scholarships (from UC Berkeley Dept of Bioengineering). BHG acknowledges support from an award from the Alfred P. Sloan Foundation (FG-2021-15708). This research used resources of the National Energy Research Scientific Computing Center (NERSC), a U.S. Department of Energy Office of Science User Facility located at Lawrence Berkeley National Laboratory, operated under Contract No. DE-AC02-05CH11231 using NERSC award ERCAP0021398. This work used the Vincent J. Coates Genomics Sequencing Laboratory at UC Berkeley, supported by NIH S10 OD018174 Instrumentation Grant.

Author Contributions Statement

J.A.A., K.M.W., B.H.G., A.P.A., and O.H. designed the project; J.A.A. and K.M.W. constructed the transposon libraries and performed the TnSeq mapping; J.A.A. conducted the experiments and generated the sequence data; J.A.A. designed and conducted the bioinformatic and computational analyses; J.A.A., K.M.W., B.H.G., A.P.A., and O.H. analyzed the data and wrote the paper.

Competing Interests Statement

The authors declare no competing interests.

Chapter 3: Rediversification following ecotype isolation reveals hidden adaptive potential

Abstract

Microbial communities play a critical role in ecological processes, and their diversity is key to their functioning. However, little is known about if communities can regenerate ecological diversity following ecotype removal or extinction, and how the rediversified communities would compare to the original ones. Here we show that simple two-ecotype communities from the *E. coli* Long Term Evolution Experiment (LTEE) consistently rediversified into two ecotypes following the isolation of one of the ecotypes, coexisting via negative frequency-dependent selection. Communities separated by more than 30,000 generations of evolutionary time rediversify in similar ways. The rediversified ecotype appears to share a number of growth traits with the ecotype it replaces. However, the rediversified community is also different compared to the original community in ways relevant to the mechanism of ecotype coexistence, for example in stationary phase response and survival. We found substantial variation in the transcriptional states between the two original ecotypes, whereas the differences within the rediversified community were comparatively smaller, but with unique patterns of differential expression. Our results suggest that evolution may leave room for alternative diversification processes even in a maximally reduced community of only two strains. We hypothesize that the presence of alternative evolutionary pathways may be even more pronounced in communities of many species, where there are even more potential niches, highlighting an important role for perturbations, such as species removal, in evolving ecological communities.

Introduction

Ecological diversification refers to the evolution of a population or community of organisms to occupy distinct ecological niches or habitats within an ecosystem [1]. Such diversification can manifest through various mechanisms, including the evolution of unique physical or behavioral traits that enable individuals to utilize diverse resources or withstand varied environmental conditions [2–4]. The propensity for ecological diversification in a community is influenced by factors like environmental conditions, prevailing biodiversity, and the interactions among the species present [4–7]. The potential for diversification can be modulated by the presence of unoccupied niches, or “ecological opportunities” [5, 8]. These opportunities may diminish as diversity increases and niches become occupied. However, existing communities can also generate new niches, facilitating the introduction of novel ecotypes. An example is cross-feeding, where species produce metabolites that pave the way for the rise of new ecotypes by forming exploitable niches [9–13].

Microbial communities offer a valuable model for investigating the intertwined evolutionary and ecological processes driving diversification due to their rapid reproductive and evolutionary rates [11, 13–20]. In both natural settings [21–24] and experimental systems, swift ecological diversification in microbial communities has been documented, typically propelled by mechanisms such as cross-feeding [25–29], resource partitioning [11, 30–33], spatial niche differentiation [15, 34–36], and potentially other ecological trade-offs [37, 38]. Interactions within microbial communities can either inhibit [17, 18], promote [11, 13], or have mixed impacts [39] on diversification. The enduring coexistence of a new ecotype with its immediate ancestor is not assured and may hinge on community characteristics, such as metabolic

trade-offs [12, 40]. In experimental contexts, ecological differentiation of a diversified ecotype is often indicated when an ecotype’s fitness inversely correlates with its frequency, i.e. displaying negative frequency-dependent fitness effects. Stable coexistence between the diversified ecotype and its ancestor is implied if the former can invade when rare but not when abundant.

Even when ecotypes can stably coexist, it does not guarantee that they will coexist indefinitely or at all locations. Ecotypes can migrate to new territories, potentially without other community members, or some ecotypes within the community may spontaneously go extinct (e.g. due to demographic stochasticity or environmental fluctuations). In either case, the community becomes perturbed, losing one or more members and potentially leaving ecological niches unfilled. Environmental disturbances that cause ecotype loss are prevalent across diverse types of microbial ecosystems, including aquatic, soil, and human-associated environments [41–47]. Oftentimes, local ecotype/species extinction is not benign—loss of microbial taxa has been associated with deterioration of ecosystem functioning in natural systems [48, 49]. It has long been noted among biologists that newly isolated species, and species extinctions, can open up ecological opportunities and lead to rapid diversification events [50–53].

Theoretical models suggest that perturbed communities may respond with a combination of ecological and evolutionary changes [54–57]. These evolutionary changes may include both directional and diversifying selection [57], with newly evolved variants either replacing existing community members or coexisting alongside them. However, it remains unclear which communities have the potential to rediversify. When rediversification does occur after ecotype removal, there are two possible scenarios: (i) the perturbed community rediversifies and eventually returns to a state similar to the original community before the disturbance, or (ii) the perturbed community rediversifies and forms a community that is qualitatively different from the original one.

Here, we investigate the aforementioned questions surrounding rediversification using a minimal microbial model community of only two, naturally diversified *E. coli* strains. Specifically, we employ two strains derived from the *E. coli* Long-Term Evolution Experiment (LTEE), which was started by Dr. Richard Lenski and has been running for over 30 years or more than 70,000 generations [58]. An initially isogenic strain of *E. coli* was split into 12 replicate populations and propagated through daily dilutions in glucose minimal media (DM25). At the outset of the LTEE around 6.5k generations, it was found that one lineage, *ara-2*, spontaneously diversified into two lineages—*S* and *L*—that coexist via negative frequency dependence [59]. The ecotypes were named for the sizes of their colonies on certain agar plates, either small (*S*) or large (*L*). The *S* and *L* lineages inhabit distinct temporal and metabolic niches in the LTEE environment. During exponential phase, *L* grows more quickly on glucose, while *S* specializes in stationary phase survival and utilizes acetate, a byproduct of overflow metabolism [26, 60]. Since their diversification, the lineages have persisted and evolved over time, exhibiting genetic, transcriptional, and metabolic divergence [26, 59–65]. The LTEE-derived communities are ideal for our plan to investigate the possibility and potential patterns of rediversification over evolutionary time. We can revive the *S-L* community at 6.5k generations to probe rediversification right after emergence of the community, and compare with rediversification at later stages of the evolution experiment.

We found that when we isolated the *S* ecotype under certain conditions, it would spontaneously rediversify, giving rise to a new big colony ecotype S_B , even if we used *S* clones separated by more than 30,000 generations of evolutionary time. The new ecotype, S_B , displays hallmarks of ecological differentiation, including negative frequency-dependent fitness effects when in coculture with its ancestral *S* clone. We dissected the new, rediversified community, and found that while S_B shares a number of traits with both *L* and *S*, it also behaves in entirely new ways. Our findings suggest that even in a maximally reduced community of only two strains, evolution may leave room for alternative diversification processes,

suggesting a hidden adaptive potential only revealed by ecotype removal. This raises the possibility that perturbations, such as ecotype removal, could play an important role in evolving ecological communities by creating opportunities for alternative evolutionary pathways.

Results

S can quickly diversify into a new ecotype

The ability of the *S* ecotype to emerge and coexist with the *L* ecotype in the LTEE has been attributed to its proficiency in scavenging acetate released from overflow metabolism during glycolysis, as well as its ability to survive and thrive during stationary phase [26, 60]. It has been proposed that the *L-S* and similar polymorphisms may arise because of a fundamental, hard-to-break trade-off between glucose and acetate growth rates in *E. coli* [12, 66]. Based on these explanations, one may suspect, that after removing either *L* or *S* in the two-ecotype community, the community may eventually rediversify and will eventually approach a two-ecotype community similar to the original *L-S* community.

We performed a simple experiment where we cultured an *S* clone isolated around 6.5k generations, immediately after the *ara-2* lineage diversified into *S* and *L*, in glucose minimal media (DM25) for approximately 60 generations (9 days), with 12 biological replicates. To visualize colony morphologies of the resulting cultures, we plated the cultures on tetrazolium arabinose (TA) agar plates. Surprisingly, 2 of the independent cultures displayed a mixture of large and small colonies (Figure 1A).

After eliminating contamination possibilities by sequencing several diagnostic genetic loci, we examined whether the large colony phenotype was heritable. We isolated several large and small colonies and propagated them in DM25 for around 30 generations (5 days). The phenotype appeared to be stably heritable for all selected colonies. To avoid prematurely associating the larger colony phenotype with the *L* type, we referred to the emerging type in our experiments as *S_B*, due to its large (big) colonies and its ancestor *S*.

To gain insights into the robustness of the observed rediversification after isolation of *S* over evolutionary timescales, we isolated *S* from later generations, spanning more than 30,000 generations of evolution. We repeated the same experiment with *S* clones from 17k and 40k generations with 24 independent cultures each; however, we did not see any noticeable emergence of big colonies after 60 generations (screened about 200 colonies per plate). It is unclear why we did not see any big colonies; one possible explanation may be that the rate at which *S* morphs transition to *S_B* morphs may be low enough that we would need to have many more replicate cultures to observe rediversification (as in the 6.5k *S* clones). We previously noticed that 6.5k *S_B* clones (labeled 1 and 6) grew much better in LB liquid media compared to *S* clones (potentially accounting for their bigger colonies sizes on similar agar plates). Thus, we sought to see if we could enrich for the appearance of *S_B* by growing 6.5k, 17k, and 40k *S* clones in LB liquid culture. Under these growing conditions, we indeed saw that *S_B* colonies appeared rapidly, within 1-3 days, in nearly all of the independent *S* cultures across the three LTEE timepoints (Figure S6). We attributed this to the higher fitness of *S_B* in LB, relative to *S* (Figure S7). The new *S_B* clones were again stably heritable for at least 30 generations.

The big colony phenotype *S_B* bears at least a superficial resemblance to *L*, which begs the question: do *S_B* and *S* represent genuinely different ecotypes, occupying different ecological niches, with the potential to coexist with each other? To answer this question, we performed reciprocal invasion experiments, where we mixed *S* and *S_B* clones at high and low frequencies, and tracked how their frequencies change via flow cytometry over the course of three growth cycles (see Methods), to estimate their relative, frequency-dependent fitness effects (Figure 1B). While relative frequencies of LTEE strains are typically measured by colony counting, we found significant bias (Figure S2) in frequency measurements of *S/L* when measured via colony forming units (CFUs). In contrast, we see that flow cytometry provides unbiased frequency measurements (Figure S1). We thus chose to use flow cytometry for all further

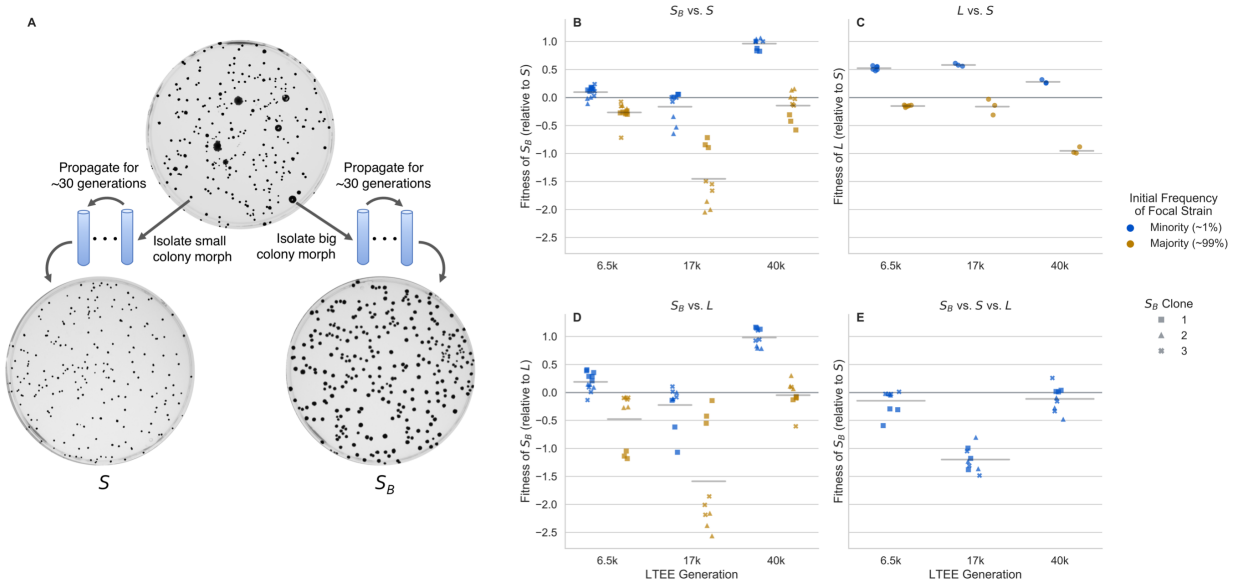


Fig. 1 Emergence of the stably heritable S_B morph and frequency-dependent fitness effects. **(A)** Big colony morphs can arise in S cultures derived from 3 different LTEE timepoints, separated by more than 30,000 generations of evolution (6.5k clones are shown here as an example). When both small and big colonies are isolated and propagated in liquid DM25 culture for about 30 generations, then plated on TA agar plates, we see that the colony size is heritable. **(B-D)** Reciprocal invasion experiments, measuring relative fitness of clones when they are in the minority (approximately 1%) or in the majority (approximately 99%). Each point represents a biological replicate, horizontal lines represent mean across all points. Competitions between **(B)** S_B clones and S , **(C)** S and L , and **(D)** S_B and L . We generally see negative frequency dependent fitness effects across all strains and competitions. **(E)** Triple competition between S_B , S , and L , where L and S_B are near their equilibrium frequencies and S_B in the minority (around 1%).

measurements instead of CFUs, owing to its minimal bias and reduced measurement noise (Figures S1 and S2B). The introduction of genomically-integrated fluorescent proteins does not have a measurable impact on fitness (Figure S5).

We found that most S_B clones had significant negative frequency-dependent fitness differences when in competition with their parental S clone, a hallmark of ecological differentiation ($p < 0.05$ for all clones except 6.5k S_B 3). These data suggest that many of the S_B clones can coexist with S , because relative fitness is greater than 0 at low frequencies and less than 0 at high frequencies. However, it is not clear if this is the case for all of the isolated S_B clones, as some have a relative fitness near or less than 0 at low frequencies. This may be because the aforementioned S_B clones either genuinely do not coexist with S , or perhaps they coexist at a frequency around or lower than the one where we took the measurements.

The frequency-dependent fitness differences between S_B and S were similar in magnitude to the fitness differences between L and S (Figure 1C), which were all significant at $p < 0.01$. We also competed S_B against L (Figure 1D), and again found significant frequency-dependent fitness differences for most clones ($p < 0.01$ for all clones except 6.5k S_B 3 and 17k S_B 1). However, if at least some S_B clones can invade both S and L when rare, why has the S_B morph not appeared in the *ara-2* population of the LTEE, where L and S have been coexisting and coevolving for tens of thousands of generations? We hypothesized that S_B could not invade an already "full" community, and could only have the chance to invade when one of the ecotypes is removed. We performed a triple competition experiment, with L and S near their equilibrium frequency and S_B in the minority (Figure 1E). We found that most S_B clones had a significantly lower fitness compared to when it was in the minority with either S or L alone ($p < 0.05$ except for 6.5k S_B clones 2 and 3 compared to when competed against S alone, and 17k S_B 1 6.5k S_B 3 when competed against L alone).

While we have shown that S_B spontaneously emerges from a monoclonal population of S and occupies a distinct ecological niche, it is not yet clear how S_B compares to S and L .

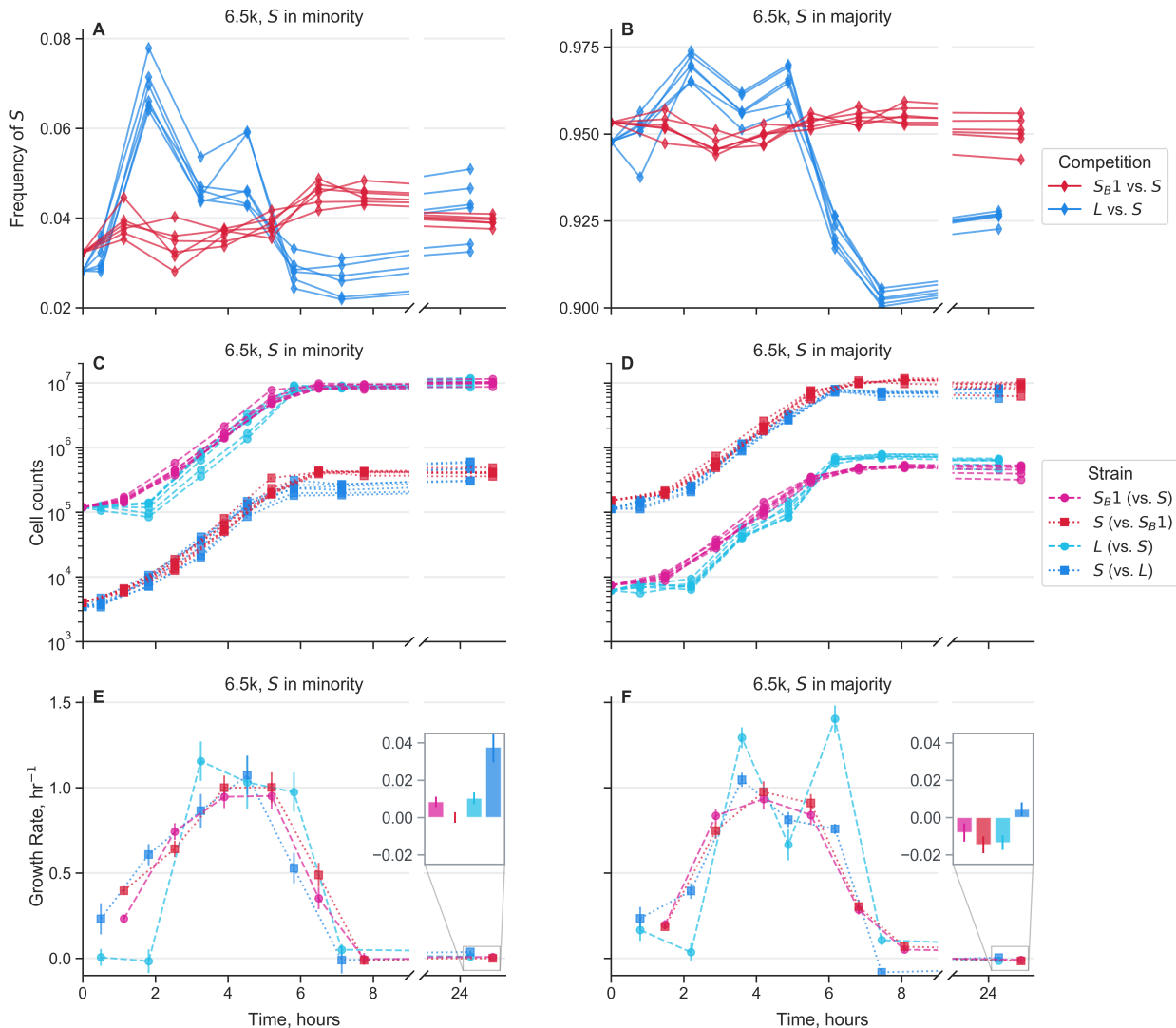


Fig. 2 Growth dynamics of cocultures over the course of one twenty-four hour growth cycle. Measurements were taken approximately every hour via flow cytometry for the first eight hours after transfer into new media. An additional measurement was taken approximately 24 hours after the start of the cycle. Mixed S_B 1 with S along with L with S , all from 6.5k generations, where ecotypes were mixed both in the majority and minority of the population. Different lines represent biological replicates. (A–B) Frequency dynamics of S against S_B and against L . (C–D) Total cell count dynamics, separated by each strain in the cocultures. (E–F) Empirically measured growth rates over time for each strain in the cocultures, calculated as the slope of log-transformed abundance between adjacent timepoints, using the second timepoint as the x-axis location. Insets show growth rates during stationary phase, from around 8 to 24 hours, on the y-axis—presented to provide a more fine-grained view of the slow changes in abundance during stationary phase. Error bars represent standard errors.

In particular, we want to understand if S_B simply fills the same niche that L had occupied before removal, making it somewhat functionally equivalent to L . The negative frequency-dependent selection between L and S_B suggests that they must be different to some degree, but it is still unclear if S_B represents a sort of intermediate between S and L , or if it shows novel traits. In the following, we will show that while S_B resembles L in some of its growth properties, it also shows clear differences that are critical for its coexistence with S .

Within-cycle growth dynamics of cocultures

To better understand how ecological differentiation arises in the S_B - S and L - S systems, we measured the within-cycle growth dynamics of S_B , L , and S in coculture with each other via

flow cytometry. The LTEE environment is a seasonal one [26, 67]—every 24 hours, cultures are transferred 1:100 into fresh glucose minimal media. The populations spend the first part of the day in exponential phase; the remaining time, more than 2/3 of the day, is spent transitioning out of exponential phase and in stationary phase. It has been previously shown that L and S occupy different temporal niches from one another, where L specializes on exponential growth on glucose, and S specializes on stationary phase survival and growth on acetate. Thus, it is natural to ask how temporal variations in growth are similar or different in the S_B - S system.

To perform the experiments, we propagated S , S_B , and L separately in monocultures for two days, before mixing S with S_B and S with L , both at high and low frequencies. We mixed strains with their partners from the same LTEE generation. For simplicity, we only used S_B clone 1 for all experiments and LTEE generations. We propagated the cocultures for one more cycle to allow the populations to physiologically adapt to the new environment. At the end of the 24 hour cycle, we took a flow cytometry measurement of the culture, then split the cultures into biological replicates and diluted the cocultures 1:100 into fresh media. Afterwards, we took flow cytometry measurements from the cocultures approximately every hour for about eight hours, then we took one last measurement at the end of the 24 hour cycle (Figures 2, S10). We chose this design because the fastest dynamics occur during and right after exponential phase—the first 8 hours—while dynamics in stationary phase are much slower. The cultures were grown in a 37°C shaking water bath. We corrected the cell counts measured in flow cytometry by the total dilution rate.

We initially focus on the dynamics of strains from 6.5k generations (Figure 2). Overall, it is immediately clear that there are larger differences in dynamics in the L - S cocultures compared to the S_B - S cocultures. When S is in both the majority and minority, L has a long, two hour lag time, while S starts growing much more quickly (Figure 2C-D), causing a large upward spike in S frequency. We fit a generalized logistic model to the growth curves to more precisely extract the lag times (Figure S11), and we see that 6.5k L has a longer lag time than S ($p < 0.01$, in both cases). When S is cocultured with S_B , we do not see any noticeable lag time; however, when S is in the minority, S “wakes up” more quickly than S_B ($p = 7 \cdot 10^{-8}$), leading to a small spike in S frequency at the beginning of the time course. We see similar patterns in the cocultures from 17k and 40k generations—both L and S_B appear to have growth rates very close to 0 at the beginning of the timecourse, but S consistently has a larger initial growth rate (Figure S10). The initially faster growth of S only occurs when S is in the minority for both L and S_B strains ($p < 0.02$, across all comparisons); there is no longer a noticeable difference when S is in the majority ($p > 0.1$, across all comparisons).

When 6.5k L starts growing, it has a significantly larger growth rate than S , pushing the frequency of S back down. The magnitude of this growth rate difference is similar regardless of the relative frequency of the ecotypes (Figure 2E-F). In contrast, the differences between S_B and S are much smaller. At both starting frequencies, S_B may have a small growth rate advantage compared to S early in exponential phase, then S appears to grow faster in late exponential phase.

In contrast to the dynamics in lag and exponential phase, the later “stationary phase” dynamics are highly dependent on which ecotype is in the majority. While most conditions show non-zero growth rates after about eight hours of growth, we still refer to this period as stationary phase, because the growth rates are small. When S is cocultured with L , S grows better than L under both conditions, but the absolute growth rates differ between the conditions (insets in Figure 2E-F). When S is in the minority with L , both S and L have net positive growth in stationary phase, although it is higher for S ($p = 9 \cdot 10^{-4}$), potentially pointing to the favorable conditions of L -dominated stationary phase and the putatively large amount of excreted acetate available for exploitation. In contrast, when S is in the majority with L , S has a smaller, albeit still positive, net growth rate, while L has a net negative growth rate in stationary phase ($p = 5 \cdot 10^{-4}$). Concordantly, these patterns suggest that S -dominated stationary phase is much less hospitable to both S and L .

We see different stationary phase patterns when S_B and S are in coculture, where S_B now performs consistently better than S (insets in Figure 2E-F). The ecotype growth rates are significantly different ($p = 0.016$) when S_B is in the majority with S — S_B has a moderately positive net growth rate, while S has essentially a net 0 growth rate in stationary phase. Then when S_B is in the minority, both S_B and S have net negative growth rates, but S declines more than S_B , although the difference is non-significant ($p = 0.16$). If S_B were more similar to L , i.e. an exponential phase specialist that secretes a substantial amount of acetate, we would have expected that S_B - S and L - S cocultures would have similar behavior in stationary phase. Instead, S_B appears to have enhanced survival in stationary phase, and decreases the survival prospects of S , perhaps because of the reduced availability of acetate. Thus, while S_B does not have a significant advantage over S in exponential phase, like L has, it compensates with a clear advantage over S in stationary phase, essential for coexistence of S_B with S .

The results show differences in stationary phase behavior across generations, as well as several conserved features (Figure S10). Similar to the 6.5k strains, when 17k S are in the minority with L , S has a large positive growth rate during stationary phase, while L does not grow. However, when S is in the majority with L , its growth rate is comparable to that of L . The 40k S and L strains show different patterns, where L generally has a higher stationary phase growth rate. However, this appears to be offset by a large growth advantage of S right at the end of exponential phase/beginning of stationary phase; this growth advantage is much larger when S is in the minority compared to when it is in the majority. This indicates that the growth advantage of 40k S has shifted earlier, potentially because it has adapted to consumed the acetate secreted by L much more quickly.

Again, the stationary phase behavior when 17k and 40k S and S_B are grown in coculture is noticeably distinct from the behavior of L - S coculture. Similarly, 17k S also does not grow well in S_B -dominated stationary phase. And 17k S_B actually has a large positive stationary phase growth rate when S is setting the environment, suggesting that S_B has more to gain from stationary phase when it is in the minority compared to vice versa. The picture shifts again with the 40k strains— S_B benefits very little from being in stationary phase, but in contrast, S grows well in stationary phase, especially when dominated by S_B . This is quite different from the behavior of 40k S - L cocultures, albeit in a different direction than the strains from the earlier generations. Thus, in 40k cultures, it appears that S_B - S cocultures act more like L - S cocultures from earlier generations, where S_B is the clear exponential phase specialist and S is the stationary phase specialist.

Together, these results show that growth traits of L - S cocultures change over evolutionary time, and S_B - S cocultures are similar in important ways (e.g. initial growth rates), but also show departures from the original community (e.g. stationary phase behavior) that reveal how the ecological dynamics have shifted with the new, rediversified ecotype.

Growth traits in novel environments

While we have shown that S_B has distinct growth traits when in coculture with S in the evolutionary condition, does S_B also behave differently compared to S in novel environments that neither have been in contact with before? If S and S_B mostly behave similarly in novel environments, then perhaps the underlying change between the two morphs is targeted only towards traits relevant to the mechanism of ecological differentiation. Other newly diversifed ecotypes have previously shown targeted changes to niche adaptation, such as acetate-specialist *E. coli* ecotypes that evolve due to specific mutations in the main acetate-scavenging gene, *acs* [28, 29]. On the other hand, if pleiotropic effects are widespread, then the underlying metabolic/physiological shift in S_B may involve global, rather than targeted changes.

To this end, we competed S_B clones against S clones for each LTEE timepoint in the same minimal media base as the evolutionary condition (DM), supplemented with different carbon sources (Figure 3). For comparison, we also competed S against L clones for each LTEE

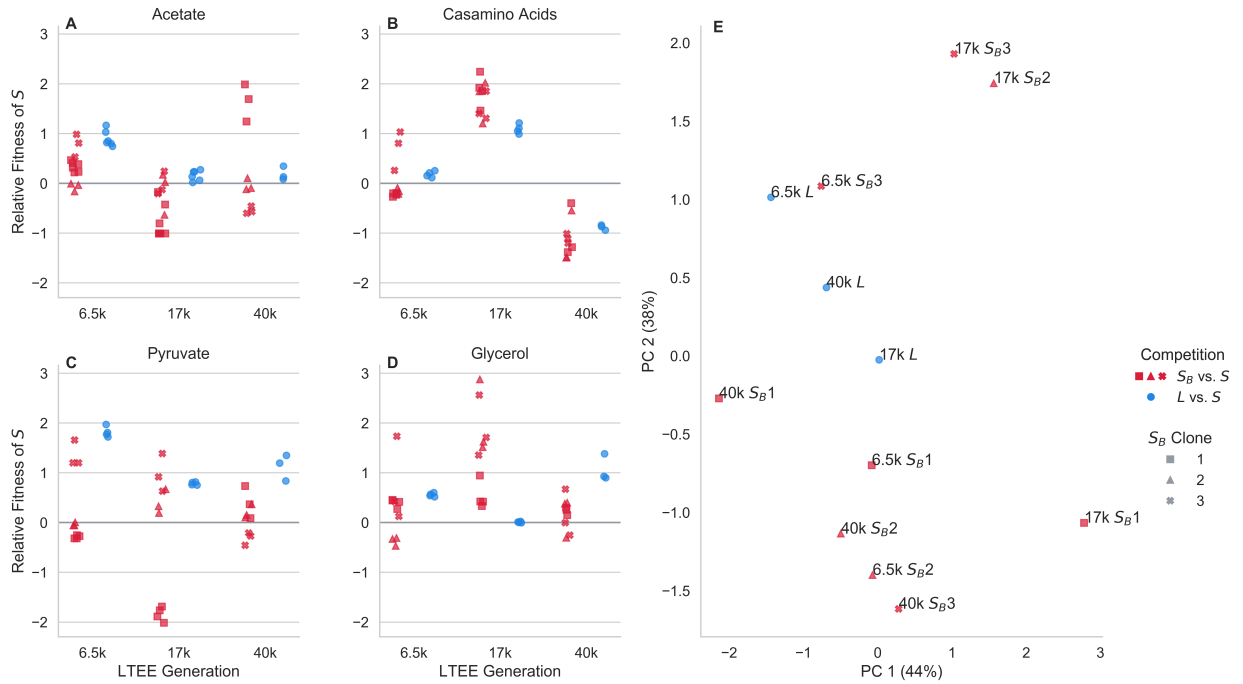


Fig. 3 Competition of S_B and L against S in novel environments. (A-D) Red and blue points represent the relative fitness of S in competition with S_B and L clones from the same LTEE timepoint, respectively, where different symbols represent different clones. Competitions performed in exponential phase in the same media base (DM) supplemented with different carbon sources: (A) 200mg/L acetate, (B) 1mg/mL casamino acids, (C) 20mM pyruvate, (D) 20mM glycerol. (E) Principal components analysis, using relative fitness in each environment as features. Percentages in parentheses represent percent variance explained by each principal component.

timepoint in each of the conditions. We chose four different carbon sources that support growth of S , S_B , and L clones from all timepoints and that enter into central metabolism at different points [68], potentially allowing us to gain insight into global changes in physiology and metabolism. After growing cocultures together for two days in DM25, we diluted them 1:100 in each different media. We kept the cultures in exponential phase, and took two ecotype frequency measurements via flow cytometry: one right before transfer into the new media, and one at the end of exponential phase. As usual, relative fitness was computed as the change in logit frequency.

We see that for most S_B clones, across most conditions, S_B is noticeably non-neutral relative to S (FDR-corrected two-sided t -tests; SI section 5). Consistent with previous experiments [62], we see that L is also usually non-neutral relative to S across the different carbon sources. The relative fitness of S_B and L clones varies considerably across timepoints and carbon sources. There is not a clear relationship between the fitness of S_B (relative to S) and the fitness of L (relative to S) from the same timepoint, also visible in the PCA representation of the data (Figure 3E). In the PCA, it appears that S_B clones within timepoints generally cluster together (but not completely), not with the L clones from their timepoint; however, leveraging a modified permutational multivariate analysis of variance (PERMANOVA) test (see Methods), we could not reject the null hypothesis that S_B clones within a timepoint cluster together more than the L clone within the timepoint ($p > 0.15$ for all timepoints).

Again, there is some variation between different S_B clones. For example, the 17k S_B 1 clone behaves noticeably differently compared to the 17k S_B 2 and S_B 3 clones especially in the pyruvate ($p < 0.001$, both clones) and glycerol ($p < 0.02$, both clones) conditions, while the three clones cluster together in the acetate condition. The 17k S_B 2 and S_B 3 clones also appear to cluster together, away from the 17k S_B 1 clone in the PCA plot (Figure 3E). The

17k S_B 1 clone also behaved differently compared to the other two in the reciprocal invasion experiment against 17k L , where 17k S_B 1 did not show noticeable frequency-dependence (Figure 1D). The 6.5k S_B 3 and 40k S_B 1 clones also cluster away from the other two clones within their timepoint. The conditions where these "outlier" clones diverge from the other clones varies between timepoints—6.5k S_B 3 is different when grown in pyruvate and casamino acids ($p < 0.03$, all comparisons), and 40k S_B 1 is primarily different in the acetate condition ($p < 0.03$, all comparisons).

Across all three timepoints, we see that S is better at growth in acetate compared with L . The evidence for this is stronger for strains from 6.5k generations ($p = 5 \cdot 10^{-4}$) and 17k generations ($p = 0.017$), compared to those from 40k generations ($p = 0.093$). This is consistent with prior findings[60], and the notion that S represents a consistent acetate-scavenging specialist over evolutionary time. In contrast, the behavior of S_B in acetate is more variable, both across time points and between different S_B clones. Two of three 6.5k S_B clones have a fitness disadvantage in acetate ($p < 0.03$, in both cases) relative to S (albeit less pronounced compared to L), whereas at least one S_B clone from both 17k and 40k generations have a fitness *advantage* in acetate ($p < 0.02$, in both cases).

We found the fitness disadvantage of 6.5k S_B in acetate puzzling, because it appears to generally perform better in stationary phase compared to S (Figure 2). At least in the S - L community, the advantage of S in stationary phase appears to be mostly driven by decreased lag time to acetate growth [69], increased acetate growth rate [60], and increased ability to scavenge dead cells [26]. We began by testing if S_B has a smaller glucose-to-acetate lag time compared to S , which could explain its stationary phase advantage. By growing S_B , S , and L strains on media containing both glucose and acetate, we could observe how they transition from glucose to acetate growth (Figure S8). Contrary to expectations, S_B actually has a longer lag time than S , more similar to that of L , which should give it a disadvantage in stationary phase. So we moved on to testing if S_B could scavenge cell debris more efficiently than S . To do so, we competed mixtures of S_B and S , and L and S , together in heat-killed cultures, resuspended in blank media to eliminate the presence of extracellular metabolites (Figure S9). Consistent with prior data [26], we see that S is generally more efficient than L at growing and surviving in an environment of dead cells, albeit with a frequency-dependent effect. In contrast, S_B is able to scavenge dead cells better than S , which may explain its ability to perform better in stationary phase.

Together, this is another sign that S_B is occupying a genuinely different ecological niche compared to L , which may be shifting over evolutionary time.

Transcriptional differences between ecotypes

Given the strong heritability of the S_B phenotype, and multiple traits that differ with respect to S , we reasoned that the S_B phenotype may have an underlying genetic cause. Thus, we performed whole-genome shotgun sequencing of several S and S_B clones with both short-read sequencing (Illumina) and long-read sequencing (Nanopore) (see Methods). After reference-based assembly, we saw that all S_B clones had several mutations relative to their ancestor, and all S clones from the same LTEE generation also has several mutations relative to each other. The mutations were a mix of synonymous and non-synonymous point mutations, insertions and deletions, and several large genomic rearrangements (see SI section 4). However, none of the mutations differentiated S and S_B —there were no consistent mutations in specific genes or operons. The large number of mutations separating S_B clones from their S ancestor is not surprising; the *ara-2* lineage fixed a hypermutator allele before the S and L lineages split, such that the germline mutation rate is about 100x higher than that of the LTEE ancestor [70]. This makes it likely that many of the mutations are likely (nearly) neutral hitchhikers, or otherwise were not affected by selection. We attempted to determine if there was any parallelism on the level of KEGG annotations instead of genes, but again, we did not detect anything. Thus, because of the combination of the high mutational background and lack of detectable genetic parallelism, we cannot determine if the S_B phenotype

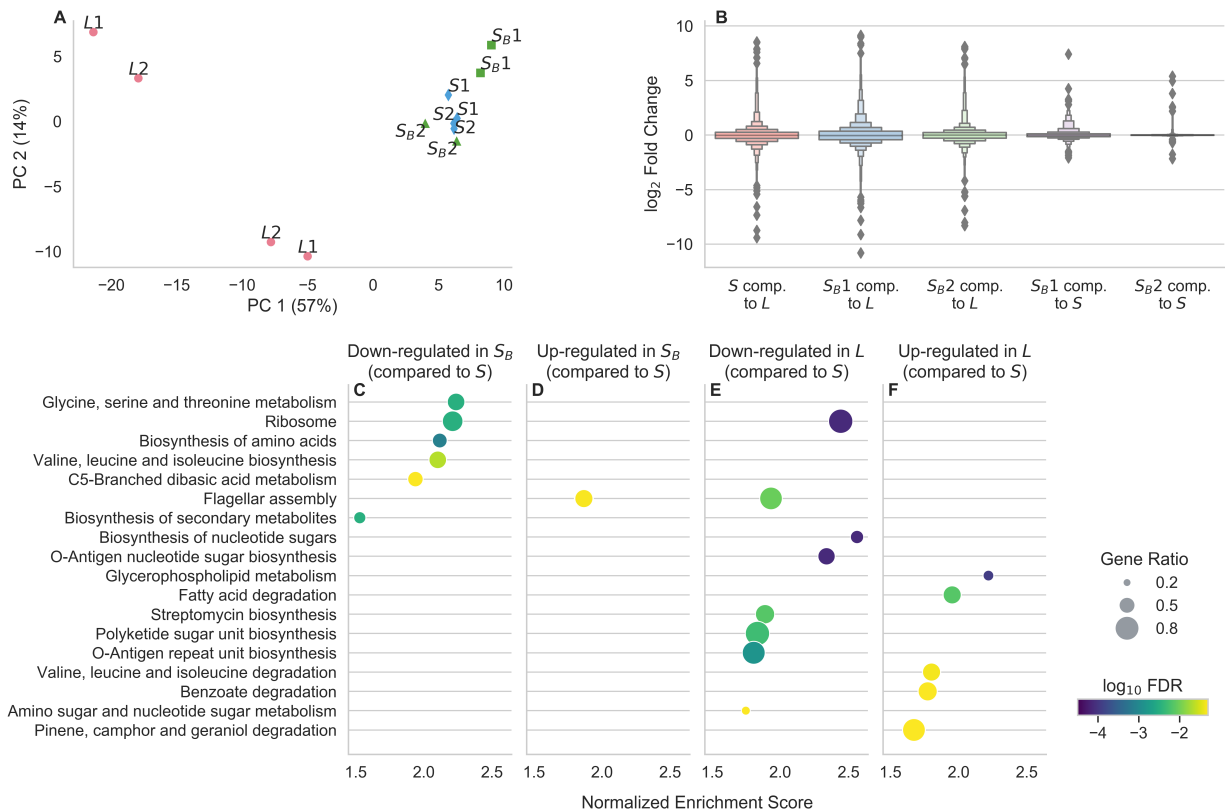


Fig. 4 Results from RNA-Seq of *L*, *S*, and *S_B* clones from 6.5k generations. (A) Principal components analysis of RNA-Seq data, after processing. Samples with the same name represent biological replicates of the same clone; the 1 and 2 labels are to indicate which clone the samples come from. (B) Distributions of log₂ fold changes in gene expression across all genes, comparing different strains to each other. (C-F) Results of a KEGG gene set enrichment analysis to identify pathways with coordinated changes in gene expression between ecotypes, where (C-D) is comparing *S_B* to *S* and (E-F) is comparing *L* to *S*. Only pathways that are called as significant at $p < 0.05$ after an FDR correction are included; points are colored by FDR-corrected log₁₀ p-value. Pathways are ordered by normalized enrichment score, which is roughly a measure of the extent to which pathway-associated genes are overrepresented at the top or bottom of the entire list of genes, ranked by fold expression change. The size of the points is proportional to the "gene ratio", which is the ratio of core enrichment genes to the total number of genes in the pathway, i.e. the fraction of genes in the pathway that show differential expression.

has a genetic cause, or what the causative mutation(s) would be. If the *S_B* phenotype is caused by some genetic change, it is likely that many different mutations are able to cause a similar phenotype.

To further understand the underlying causes of the *S_B* phenotype, we turned to measuring transcriptional differences between *L*, *S*, and *S_B* from 6.5k generations using RNA-Seq. We chose to focus on 6.5k strains because this is the LTEE timepoint immediately after the *S* and *L* lineages diversified, allowing us to focus on the "minimal" differences between *S* and *L*, rather than after extensive evolution and divergence. We cultured two biological replicates of two independent clones of each *L*, *S*, and *S_B* from 6.5k generations in glucose minimal media, and collected samples in mid-exponential phase (see Methods), in line with previous, similar transcriptomic measurements [62, 71]. For a broad overview of the data, we first performed a principal components analysis, using (normalized, transformed) expression for each gene as the features (Figure 4A). We see that the first principal component already captures more than half of the variance between samples, which primarily serves to separate the *L* clones from the *S* and *S_B* clones. The *S* clones appear to cluster together strongly, with the *S_B* clones flanking them. Hierarchical clustering also reveals that the *S* clones cluster together, with the *S_B* 2 clone as the next most similar, and the *S_B* 1 clone as the outer-most member of the cluster (Figure S12). This suggests that there are more differences between *S* and *S_B*

than there are between the two S clones, but there are stronger differences comparing both S and S_B with the L clones. The same picture emerges if we look at the distribution of \log_2 fold expression changes between different ecotypes (Figures 4B, S13). Comparing S and S_B with L , there are many genes with a large range of expression changes, both increasing and decreasing in expression. In contrast, there are generally smaller differences between the two S_B clones and S . Again, there are larger and more differences between S_B 1 and S , compared with S_B 2 and S , suggesting variability between the two S_B clones.

Given that there are noticeable differences between S_B and S , we next sought to understand what those differences represent. Are there identifiable pathways with coordinated expression changes? How do they compare with the differences between L and S ? To this end, we performed gene set enrichment analyses to identify differentially expressed KEGG (Kyoto Encyclopedia of Genes and Genomes) pathways [72]. We first compared S_B to S and L to S , and only look at pathways that are significantly enriched at $p < 0.05$ after a multiple-testing correction (Figure 4C-F). We see that there are a number of pathways significantly down-regulated in S_B compared to S , and only one pathway significantly up-regulated (Figure 4C-D). Most of the down-regulated pathways are related to different aspects of amino acid metabolism. We also separately compared S_B 1 and S_B 2 against S to better understand the variability between the two clones (Figure S14). As expected, most of the terms identified in the pooled analysis (e.g. ribosomal proteins, amino acid metabolism terms) appeared as the top terms when we analyzed the clones separately, albeit at a lower significance level than when the data from the two clones are pooled together. There are potentially a handful of differences in enriched pathways between the two clones. For example, terms related with O-antigen biosynthesis (e.g. Biosynthesis of nucleotide sugars, O-Antigen nucleotide sugar biosynthesis) may be upregulated in S_B 1, but not S_B 2. The differentially expressed pathways between L and S are mostly different, there are no terms related to amino acid biosynthesis, and many terms related to lipid metabolism and O-antigen biosynthesis (Figure 4E-F). Differentially expressed pathways in L tend to not be differentially expressed in S_B , and vice versa (Figure S15).

There are two pathways that are enriched in both comparisons: flagellar assembly and ribosomal proteins. The changes to flagellar assembly expression is in the opposite direction for S_B and L , where it is up-regulated in S_B but down-regulated in L , suggesting that gene expression for this pathway is ordered $L \downarrow S \downarrow S_B$. In contrast, expression of ribosomal proteins is down-regulated in both L and S_B , perhaps indicating some degree of parallelism involving a fundamental aspect of cell physiology between the two ecotypes. But overall, with the exception of the down-regulation of ribosomal proteins, it appears that the transcriptional changes that differentiate S_B and L from S are quite distinct.

Our RNA-Seq data-set was restricted to monoculture mid-exponential phase culture, so we sought to elucidate gene expression changes throughout the growth cycle, while varying community composition, by leveraging the fluorescent reporters we introduced into the ecotypes, all inserted into the same genomic location. Fluorescence intensity is commonly used to measure protein concentration and promoter activity [73–76]. The genes encoding the fluorescent proteins are under the control of a constitutive σ^{70} promoter, giving a read-out of σ^{70} activity. The net activity of σ^{70} is a useful measure of the global transcriptional state because it is highly responsive to changes in environmental conditions and growth phases. It plays a crucial role in coordinating the expression of genes in response to environmental stresses, nutrient availability, and other external stimuli [77–80]. By monitoring σ^{70} activity, we hope to gain insights into how the cell responds and adapts to different conditions, providing a snapshot of the global transcriptional state.

To this end, we performed an experiment where we mixed 6.5k S 1 with either 6.5k L 1 or S_B 1 at high and low frequencies, after three days of growth in monoculture, and measured their frequencies over time and population-averaged fluorescence intensity at the end of each cycle (Figure S18A-D). We see large, consistent, community composition-dependent shifts in fluorescence intensity for several conditions upon introduction to the community context,

especially noticeable when S is in the minority with L , and when S_B is in the minority with S . Specifically, in both cases, the fluorescence intensity sharply increases after one day of coculture growth, a shift that is maintained for the duration of the experiment. The parallel changes in putative σ^{70} activity across S_B and S reveal that both actively change their transcriptional programs in response to community composition. To a less noticeable degree, we see that the fluorescence intensity of L is lower when it is in the minority with S , again pointing to a degree of composition-dependence.

We measured the fluorescence dynamics over the course of the growth cycle to investigate how the difference arise (Figure S18E-F). We see substantial, parallel changes throughout the cycle, with fluorescence intensity dropping during exponential phase, before increasing again during stationary phase. These data reveal that increased fluorescence intensity at the end of the growth cycle seen when S and S_B are in the minority with L and S respectively accumulates during stationary phase, with the difference mostly disappearing during exponential phase. Together, these data provide evidence that S_B has a transcriptional reaction to the presence of S in the majority that is parallel to how S reacts to the presence of L in the majority.

Discussion

Our study explores the capacity of an evolved microbial community to quickly regenerate ecological diversity following the removal of an ecotype. Our results suggest that even in the case of a community composed of only two strains in a minimal environment, evolution can leave room for alternative diversification processes.

The rediversified ecotype, S_B , demonstrates the robustness of microbial communities to perturbations by sharing several growth traits with the ecotype it replaces, L . For instance, both S_B and L exhibit slower initial growth or longer lag times compared to S across all LTEE timepoints, which may be involved in a trade-off allowing for higher exponential growth rates, as observed in other systems [81]. However, differences between the rediversified and original communities suggest that the mechanism of ecotype coexistence has shifted. Notably, we observe variations in stationary phase responses, survival, and ability to scavenge dead cells, as well as distinct patterns of gene expression. At least in the 6.5k strains, coexistence between S and S_B appears primarily driven by a tradeoff between glucose growth in late exponential phase (where S does better), and the ability to survive in stationary phase, owing to the advantage in scavenging dead cells (where S_B does better). Together, these findings indicate that ecological rediversification in the S - L system may be influenced by a combination of constraints and opportunities. While some traits may evolve nearly deterministically due to strong ecological or physiological constraints, other trait values may more unconstrained. The interplay between contingency and determinism mirrors patterns observed in various other evolving systems, including the LTEE [82–84]. Dissecting why some traits are more evolutionarily constrained during diversification compared to others could be a fruitful avenue for future investigation.

We attempted to determine a potential genetic origin of the S_B phenotype. However, we did not find any consistent mutations shared between the independent S_B clones, relative to their S ancestor. Thus, the S_B phenotype likely either has a large target size, such that many different mutations can cause the same phenotype [85, 86], or it is caused by a non-genetic heritable change. Despite the fact that we did not find any shared mutations, the transcriptional changes of two S_B clones were targeted to the same handful of pathways, predominantly related to amino acid metabolism. This points to parallelism among independent S_B clones, at least on the transcriptional level, if not on the genetic level. Additionally, while the differentially expressed pathways in S_B and L relative to S were generally different, we saw decreased expression of ribosomal proteins in both ecotypes. The fraction of the proteome devoted to ribosomes is known to control many growth traits in bacteria [87, 88], so the similar changes in L and S_B may help to explain the handful of observed similarities in growth traits. One might expect that ribosome expression should be lower in S , due to

its slower exponential growth rate [89, 90]; so the fact that this is not the case may suggest that S_B and L are both allocating their proteome not just to optimize exponential growth rate, but also other growth traits as well.

While we saw that S could rediversify following isolation, we did not see any obvious ecological or phenotypic diversification when L was isolated. There may be several reasons for this. (i) S may have some amount of physiological/ genetic/ metabolic plasticity that allows it to diversify that L lacks. (ii) Diversification of L may happen slowly or rarely, or more quickly only under certain environmental conditions. (iii) Perhaps L can rapidly diversify, but cryptically, where no phenotypic changes are obvious without more extensive phenotyping. It is certainly the case that we would not have found S_B without the obvious changes in colony size. It could be that rediversification is much more common than currently appreciated, but simply not detected. Sequencing technologies, including metagenomic [64] and DNA barcoding-based methods [91], could help to better reveal the full extent of rediversification across microbial communities. In fact, through metagenomic sequencing, we now know that ecological diversification is much more common in the LTEE than previously thought [64].

Our study contributes to the understanding of the ecological consequences of ecotype removal or extinction, which often occurs in natural microbial communities due to sudden environmental shifts [41–47]. The ability of these communities to recover their diversity after such disruptions might be key to maintaining their functions and stability over time. Contrary to the notion that evolutionary processes are too slow to influence ecological recovery, our findings underscore the importance of evolution in the rebound of communities after a disturbance. We used simplified two-ecotype communities, which are ideal for such studies because they are well-documented and amenable to experimental manipulation [26, 59–65]. The methods we developed to investigate rediversification in this simple model could serve as a framework for understanding this process in more complex ecosystems. The presence of alternative eco-evolutionary pathways, even in a maximally reduced community of only two strains, hints at more complex dynamics in richer ecosystems. Ultimately, our work sheds light on the resilience of microbial communities, their ability to recover ecological diversity, and their adaptability to environmental changes. Future research on the processes that control these dynamics is essential for a comprehensive understanding of microbial community function and stability, especially in the face of environmental shifts.

Methods

Growth Conditions and Media

Most of the experiments presented here were performed in Davis Minimal Media (DM) base [5.36 g/L potassium phosphate (dibasic), 2g/L potassium phosphate (monobasic), 1g/L ammonium sulfate, 0.5g/L sodium citrate, 0.01% Magnesium sulfate, 0.0002% Thiamine HCl]. The media used in the LTEE and the competitions shown in Figures 1 and 2 is DM25, that is DM supplement with 25mg/L glucose.

For competition experiments, generally we first inoculated the strain into 1mL LB + 0.2% glucose + 20mM pyruvate (which we found prevented the emergence of the S_B while allowing for robust growth). After overnight growth, we washed the culture 3 times in DM0 (DM without a carbon source added) by centrifuging it at 2500xg for 3 minutes, aspirating the supernatant, and resuspending in DM0. We transferred the washed culture 1:1000 into DM25 in a glass tube. If a strain was isolated directly from a colony, we would instead directly resuspend the colony in DM25. Generally, we grew 1mL cultures in a glass 96 well plate (Thomas Scientific 6977B05). We then grew the culture for 24 hours at 37°C in a shaking incubator. The next day, we transferred all the cultures 1:100 again into 1mL DM25. After another 24 hours of growth under the same conditions, we would mix selected cultures at desired frequencies, then transfer the mixture 1:100 to DM25. After another 24 hours of growth under the same conditions, we would transfer the culture 1:100 to a desired media and start taking flow cytometry measurements—in the competitions of Figures 1 and 2, the media

is DM25, for the competitions of Figure 3, the media is DM supplemented with 200mg/L acetate, 1mg/mL casamino acids, 20mM pyruvate, or 20mM glycerol. For the competitions of Figure 1, we took measurements for 3-4 total days, doing 1:100 serial transfers every 24 hours in DM25; for Figure 2 we took measurements approximately every hour for 8 hours, then another measurement at 24 hours; for Figure 3 we took a second measurement after 8 hours, when the cultures were still in exponential phase. For growth in glucose/acetate media, we grew all strains in DM + 250mg/L acetate + 250mg/L glucose, after three cycles of growth on DM25, measuring OD600 absorbance in a shaking plate reader (SpectraMax 190; Molecular Devices) over the course of 24 hours. For the competitions in the heat-killed cultures, we grew 6.5k *S* 1, *L* 1, and *S_B* 1 cultures overnight in DM2000. We washed all the cultures in DM0 3x, as described above, to eliminate the presence of extracellular metabolites. We then heat-killed a portion of the *S* 1 culture by incubating it at 70°C for 45 minutes. We then mixed 6.5k *S* 1, *L* 1, and *S_B* 1 cultures appropriately, took a flow cytometry measurement, and resuspended them 1:1000 in 1mL of the heat-killed culture. We allowed the cultures to grow at 37°C for 16 hours (the approximate length of stationary phase), and then took another measurement.

Integration of fluorescent proteins

We sought to use flow cytometry to quantify ecotype abundances, which would necessitate that we could differentiate the strains via fluorescence. We decided to integrate fluorescent proteins into a neutral genomic location of our various strains rather than using plasmids, because plasmids can carry a significant metabolic burden, and it is often necessary to add antibiotics to the media to select against plasmid loss. We used a system based on that of Schlechter *et al.* [92] to integrate fluorescent proteins with miniTn7, a transposon that inserts cargo at a putatively neutral intergenic site downstream of *glmS*. Briefly, the system works by mating the recipient strain-of-interest with a donor strain, harboring a plasmid with the miniTn7 proteins, an ampicillin-resistance gene, a temperature-dependent origin of replication, and the cargo flanked by the left and right Tn7 recognition sites. In this case, the cargo consists of a fluorescent protein, under the control of a broad host-range promoter, and a chloramphenicol resistance gene, for selection of integration.

Our protocol for integration proceeded as follows. First, we grew the donor strain with the desired plasmid in LB + 100 μ g/mL carbenicillin + 10 μ g/mL chloramphenicol at 30°C shaken, overnight. We also grew the recipient strain overnight in DM2000 media at 37°C, directly from glycerol stock. The next day, we washed the donor culture by centrifuging it at 2500xg for 3 minutes, aspirating the supernatant, and resuspending in DM0. We then measured the optical density (OD) of both cultures, and mixed about 1 *OD* · mL of each culture on a 20mL LB/agar plate supplemented with 0.2% glucose + 20mM pyruvate. The cultures were allowed to grow into a lawn overnight at 30°C, allowing the donor strain to conjugate with the recipient. Afterwards, we scraped up the lawn and resuspended it in 3mL DM0. We washed the resuspended culture 3 times, as previously described, and then streaked out the culture on a DM2000 + 10 μ g/mL chloramphenicol + agar plate, then allowing the plates to incubate overnight at 37°C. This step simultaneously selects against the presence of the donor (the donor is a proline auxotroph), against the Tn7 plasmid (it has a temperature-sensitive origin of replication), and for integration of the Tn7 cargo (via the chloramphenicol resistance gene). After two days of growth, we restreaked a number of colonies that appeared on DM2000/agar plates for isolation. We then tested for integration of the Tn7 cargo by amplifying and sanger sequencing the junction between the genome and the fluorescent protein insertion (see SI section 3 for oligonucleotide sequences), and by looking for fluorescence via fluorescence microscopy. We confirmed that the plasmid was not present in the colony by testing resistance against carbenicillin. We ensured that the colony was not the donor or a contaminant by checking colony morphologies on tetrazolium-maltose (TM), -arabinose (TA), and -xylose (TX) agar plates. We further confirmed identity

by sanger sequencing the *arcA* and *aspS* loci of the clones we moved forward with (see SI section 3 for oligonucleotide sequences).

We found that the fluorescence provided by the plasmids designed in Schlechter *et al.* [92] were insufficiently strong for our purposes. We also needed two different fluorescent proteins with non-overlapping fluorescence profiles so that we could distinguish the two in our flow cytometer. We decided to use the fluorescent proteins sYFP2 [93] and eBFP2 [94] because they share the same ancestor and are highly homologous, and are thus likely to have the same or similar physiological effects on their host, and they have sufficiently different fluorescence profiles that are compatible with our flow cytometer. Thus, we sought to increase the expression levels of the fluorescent proteins, and add in BFP, by constructing new plasmids. We chose to use the strong, constitutive σ^{70} BBa_J23119 promoter [95] and a ribosome binding site (RBS) designed *in silico* with the Salis lab "RBS calculator" [96], placing them immediately upstream of the fluorescent protein sequences. We used Gibson assembly to construct the plasmids by ordering compatible oligonucleotides with the promoter and RBS sequences on them, and then using the backbone of pMRE-Tn7-133 from Schlechter *et al.* [92] and the eBFP2 gene from pBad-EBFP2 [94] for the BFP plasmid (see SI for plasmid and oligonucleotide information). Final plasmid sequences were confirmed via sanger sequencing.

Flow cytometry

For all population measurements taken with flow cytometry, we used the ThermoFisher Attune Flow Cytometer (2017 model) at the UC Berkeley QB3 Cell and Tissue Analysis Facility (CTAF). For every measurement, we loaded the samples into a round bottom 96 well plate, for use with the autosampler. Typically we diluted the samples 1:5 in DM0, but we changed the dilution rate over the course of the 8 hour within-cycle timecourse. We set the flow cytometer to perform one washing and mixing cycle before each measurement, and ran 50 μ L of bleach through the autosampler in between each measurement to ensure that there was no cross-contamination between wells. We used the "VL1" channel to detect eBFP2 fluorescence, which uses a 405nm laser and a 440/50nm bandpass emission filter. We used the "BL1" channel to detect sYFP2 fluorescence, which uses a 488nm laser and a 530/30nm bandpass emission filter. For the triple competitions shown in Figure 1E, we used a BFP-tagged *S*, a YFP-tagged *S_B*, and a non-fluorescent *L* strain. To estimate the frequency of *L*, we added 5 μ M of Syto62 red fluorescent dye (ThermoFisher S11344) to the sample immediately before measurement. We used the "RL1" channel to detect Syto62 fluorescence, which uses a 637nm laser and a 670/14nm bandpass emission filter. We always used a sample flow rate of 25 μ L/min.

To analyze flow cytometry data, we first perform a hyperlog transform [97] and then created threshold gates to sufficiently separate the "noise cloud" (nonfluorescent particles present even when running blank media) from particles with clear fluorescence. We noticed that in addition to seeing single positive BFP⁺ and YFP⁺ particles, we also see some particles called as fluorescent in both channels (Figure S3). We observed that the proportion of double positive events decreased as a function of fluid flow rate and dilution rate (Figure S4), suggesting that sometimes multiple cells end up in front of the flow cytometry laser at the same time, and are counted as one event. Thus, we sought to correct for this effect. We assume that the probability of a cell ending up in front of the laser is constant per unit time, and uncorrelated in time, i.e. that it is a Poisson process. Thus, for any given window of time, the probability of observing some number of events is distributed as a Poisson distribution. So under this model, the observed BFP or YFP "clouds" will consist of single cells, double cells, triple cells, and so on. Similarly, there are many combinations of BFP/YFP cells that can end up in the double positive cloud. So, in order to get the expectation of the observed frequencies, we add up the contributions of singlets, doublets, triplets, etc by considering the probability of n cells passing in front of the laser together times the probability of all n cells being the same color,

$$f_i^{obs} = \sum_{n=1}^{\infty} p(n \text{ cells}) f_i^n \quad (1)$$

where $i \in \{1, 2\}$. As previously mentioned, $p(n \text{ cells})$ will follow a Poisson distribution, but as we do not observe the case when zero cells pass in front of the laser, we will use a zero-truncated Poisson.

$$f_i^{obs} = \sum_{n=1}^{\infty} \frac{\lambda^n}{n!(e^\lambda - 1)} f_i^n = \frac{e^{\lambda f_i} - 1}{e^\lambda - 1} \quad (2)$$

Where λ is the average number of cells per event. We have two equations (for f_1^{obs} and f_2^{obs}) and two unknowns (λ and f_1), so we can solve for the real frequencies, which we solve for via numerical root-solving. The total cell count N also must be corrected, where $N_{corrected} = N_{observed} \lambda e^\lambda / (e^\lambda - 1)$. The post-correction frequencies appear to be well-reflective of frequencies measured with colony counting (Figure S1). The primary reason why we chose to use a mathematical correction rather than diluting the samples to the point where $\lambda \approx 0$ was for time and efficiency. We found that in order to reduce the number of mixed events to near zero, we would have to run a much larger volume through the flow cytometer, which takes much more time. This is especially problematic for the growth curve experiments in Figure 2, where the dynamics are quite rapid, and long times spent in the flow cytometer would likely distort the data.

Analysis of ecotype dynamics

Once we obtained estimates of strain frequencies and total abundances, we can calculate several downstream metrics of the dynamics. Throughout the manuscript, we estimate the fitness effect of a strain s from the dynamics of ecotype frequencies, $f(t)$, using the model

$$\text{logit } f(t) = st + \text{logit } f_0 + \epsilon_t . \quad (3)$$

We measure time t in units of 24-hour growth cycles, and thus fitness effects are measured in units of 1/cycle. We fit the model using ordinary least squares, jointly estimating s and the intercept f_0 . We calculated p-values for differences in fitness effects as a function of initial ecotype frequency (Figure 1B-D) using a standard two-sample t -test, then performed a standard Benjamini-Hochberg FDR correction, pooled across all of the comparisons.

Once we obtained fitness data to measure growth traits in novel environments (Figure 3), we were first interested in testing how often fitness effects are significantly non-neutral relative to S (i.e. deviate from 0). Thus, we performed standard two-sided, one-sample t -tests on all environment-strain conditions, then corrected the p-values with a Benjamini-Hochberg FDR correction (SI section 5). To test if S_B clones (within a timepoint) had significantly different fitness effects in each condition, we used two-sided, two-sample t -tests, then again corrected with a Benjamini-Hochberg FDR correction. Then, we were interested in testing the hypothesis that the S_B clones within a timepoint cluster together more strongly than with the L clone within the timepoint. Thus, we turned to using a slightly modified version of permutational multivariate analysis of variance (PERMANOVA) [98], to better reflect the structure of our data, where we have multiple biological replicates for each measurement. To calculate the F statistic, we first computed the mean relative fitness effect of each strain in each environment, across biological replicates, \bar{s} . We used total Euclidean distance between mean fitness effects as the metric, i.e. the total squared distance is the sum over all environments of the squared difference in fitness between two strains. We only computed the distance

for the four strains (S_B clones 1-3, L clone) within a timepoint. As previously described [98], and without modification, we used the total sum-of-squares and the within groups sum-of-squares to compute the F statistic, using the distance metric. Then, we needed to estimate a null distribution to compare the F statistic. If we were to estimate the null distribution with the standard method, we would only get 3 values (treating either S_B clone 1, 2, or 3 as the outgroup), which is not sufficient to construct a null distribution. However, the estimated mean fitness effects are calculated from a finite number of biological replicates; with resampling, the mean will change. Thus, we use a parametric resampling scheme to model the variability from sampling. We resampled each mean fitness effect 10,000 times using a Student's t distribution, $s_{rs} = \bar{s} - t\sqrt{\text{var } s/n}$, where s_{rs} is the resampled fitness effect, \bar{s} is the empirical mean fitness effect, $\text{var } s$ is the empirical (unbiased) variance across biological replicates, n is the number of replicates, and $t \sim t_{n-1}$ is drawn from a t -distribution with $n - 1$ degrees of freedom. We get similar results if we resample using a gaussian distribution instead of a t distribution. We then treat either S_B clone 1, 2, or 3 as the outgroup (instead of L), and repeat the multivariate ANOVA procedure to get F statistics for each resampled sample. We concatenate the samples from cases where each of the S_B clones is treated as the outgroup, so that the final size of the null distribution is 30,000 samples. We calculate the p-value as the fraction of values in the null distribution that are larger than the F statistic.

We calculated empirical growth rates (Figures 2, S10) over the course of the 24 hour cycle using the total ecotype abundance data, $n(t)$. For each pair of adjacent time points in a cycle, we used ordinary least squares to extract estimates of the growth rate (r) and its standard error, using the model $\log n(t) = rt + n_0 + \epsilon_t$. Growth rate estimates were compared using Wald's test, and p-values were corrected via a Benjamini-Hochberg FDR correction.

We fit generalized logistic models (Richard's curves) to the 24 hours growth curve abundance data to extract estimates of lag times for each strain and condition (Figure S11) [99]. Denoting the fitted abundance as $\hat{n}(t)$, we use the following form for the generalized logistic model,

$$\hat{n}(t) = a(1 + Te^{-k(t-t_m)})^{-1/T} + b, \quad (4)$$

We jointly infer the parameters a , T , b , k , t_m by using inverse-variance weighted least squares, i.e. $\min \sum_i \sum_j (n_j(t_i) - \hat{n}_j(t_i))^2 / v_{i,j}$, where i labels time points and j labels biological replicates. We use $v_{i,j}$ as the variance of the measurement error, which is taken to be the variance of a Poisson random variable. We implement the global minimization by using the differential evolution optimization algorithm implemented in `scipy` [100]. We used standard bootstrapping to estimate the sampling distributions of the lag times, L , with 1000 resamples. We removed outliers from the bootstrapped distributions by first robustly estimating the standard deviation, $\hat{\sigma}$, of the distribution via the median absolute deviation (MAD), $\hat{\sigma} = \text{med } L - \text{med } L / 0.67449$. Then we counted a bootstrapped replicate as an outlier, and discarded it, if it was more than 3 standard deviations away from the median, $3\hat{\sigma} > L - \text{med } L$. We then used the bootstrapped distributions to compute confidence intervals and p-values.

Whole Genome Sequencing

To perform short-read sequencing of S_B and S clones (see SI), we first grew the clones overnight in 1mL of DM2000, then pelleted the cultures and extracted genomic DNA with the DNeasy Blood and Tissue Kit (Qiagen 69504). We prepared the sample libraries with NEBNext DNA Library Prep kit for Illumina according to the manufacturer's protocol (New England Biolabs E7645). We sequenced the samples with the Illumina 4000 HiSeq 150PE. We used `breseq` (v0.33.2) [101] to compare raw reads to the REL606 genome [102] (GenBank: CP000819.1) and to the S ancestor of each S_B , and then call genetic variants. Read coverage was around 100x across the genome, for all samples. We used default parameters for

the **breseq** pipeline, which uses a bayesian model to call single nucleotide polymorphisms, incorporating information from the FASTQ phred quality score from each read [101].

We attempted to determine if there was any parallelism between 6.5k S_B clone mutations on the level of KEGG annotations, focusing on nonsynonymous and indel mutations. We excluded 6.5k S_B clone 4 from the analysis, as it is a sister to clone 2. We first compiled all KEGG annotations of all genes with nonsynonymous and indel mutations across the 6.5k S_B clones, and computed how many times a gene mapped to a given annotation. For each annotation that appeared, only one gene in our set mapped to it. We then expanded our list to include genes immediately adjacent to intergenic mutations, as well as pseudogenes affected by mutations. In the expanded gene set, we see two genes each map to three different annotations (carbon metabolism, exopolysaccharide biosynthesis, sulfur metabolism). We had planned to implement the multiplicity test to detect parallelism presented in Good et al. (2017) [64], however, they recommend focusing on set items with 3 or more hits to avoid false positives from low counts. We thus do not believe that there is any parallelism between mutations on the level of KEGG annotations.

To perform long-read sequencing of S_B and S clones (see SI), we again grew the clones overnight in 1mL of DM2000, then pelleted the cultures. High-molecular weight DNA extraction was performed via a standard phenol-chloroform extraction and isopropanol precipitation. Distribution of DNA fragment sizes were obtained using the Agilent Femto Pulse System. Fragment size selection was performed using Pippin Prep (Sage Biosciences). The samples were prepared for sequencing with the Nanopore ligation sequencing kit (Oxford Nanopore, SQK-LSK109). The libraries were then sequenced on an Oxford Nanopore MinION. We used **minimap2** [103] and **sniffles** [104] with default parameters to detect structural variants.

RNA Sequencing

6.5k S and L clones 1 and 2 were isolated from REL11555 and REL11556 respectively; 6.5k S_B clones 1 and 2 were the same clones as previously described. Cultures of 6.5k S , S_B , and L clones 1 and 2 were started directly from glycerol stock into 1ml LB + 2g/L glucose + 20mM pyruvate, as a pre-culture. We started two independent cultures for each clone as biological replicates. After overnight growth, the cultures were washed by centrifuging the cultures at $2500\times g$ for 3 minutes, aspirating the supernatant, and resuspending in DM0, repeated three times. Then, the cultures were diluted 1 : 10^{-4} into 1mL fresh DM media supplemented with 4g/L glucose, in glass tubes. After approximately four hours of growth at 37°C , the cultures were again diluted 1 : 50 in 1mL of the same media in glass tubes. The cultures were grown shaken at 37°C . The cultures were grown to mid-exponential phase, i.e. until $OD \sim 0.4$, then the entire culture was immediately centrifuged at $2500\times g$ for 3 minutes to pellet. Immediately after centrifugation, we resuspended the pellets in $25\mu\text{L}$ TES buffer (10 mM Tris-HCl [pH 7.5], 1 mM EDTA, and 100 mM NaCl) and then lysed the pelleted cultures with $250\text{U}/\mu\text{L}$ lysozyme (Ready-Lyse Lysozyme Solution; Lucigen R1804M) at room temperature for 5 minutes. For all subsequent steps, we used Monarch Total RNA Miniprep Kit (New England BioLabs T2010S) according to the standard given protocol for gram-negative bacteria. Samples were eluted in $30\mu\text{L}$ nuclease-free water, and stored at -80°C . The concentration and purity of all RNA samples was quantified using Qubit.

RNAse-free DNase (Invitrogen AM2222) was used to treat the samples for DNA removal. The library preparation was conducted using Illumina’s Stranded Total RNA Prep Ligation with Ribo-Zero Plus kit and 10bp IDT for Illumina indices. Subsequently, the samples were sequenced using NextSeq2000, resulting in $2\times 51\text{bp}$ reads. The process of demultiplexing, quality control, and adapter trimming was carried out using **bcl-convert** (v3.9.3) and **bcl2fast** (v2.20.0.445) (both are proprietary Illumina software for the conversion of bcl files to basecalls). HISAT2 (v2.2.0) [105] was used for read mapping. Reads were mapped to the REL606 genome [102] (GenBank: CP000819.1). The read quantification was performed using the functionality of **featureCounts** (v2.0.1) in **Subread** [106]. All of the above steps in

the pipeline were performed with default parameters, the last two steps also were run with `--very-sensitive` and `-Q 20` tags, respectively. All sequencing and pre-processing steps were performed by SeqCenter, LLC.

After pre-processing, we obtained a matrix of read counts for each gene for each sample. With this table, we used DESeq2 (v1.38.3) [107] to compute fold change in expression between strains and variance-stabilized relative expression values for each gene across samples (blindly with respect to the design matrix), all with default parameters. We used the variance-stabilized relative expression values for the principal components analysis (PCA). We used the `ashr` method (v2.2) [108] with default parameters to shrink and regularize the \log_2 fold changes in expression. We computed \log_2 fold change in expression between samples in two ways, (1) treating the S_B clones as one "strain", and (2) treating the S_B clones as separate, so that we get different fold changes in expression for each clone. Otherwise, for S and L , we pooled data across the two clones and biological replicates when computing fold change in expression. We used the package `clusterProfiler` (v4.6.2) [109] to perform the KEGG gene set enrichment analysis (GSEA) [110]. We used the previously computed \log_2 fold change in expression as the metric to pre-sort the list of genes. We used the `gseKEGG` method along with the parameters `organism="ebr"`, `nPerm=1000000`, `minGSSize=3`, `maxGSSize=800`, `eps=1e-20` to perform the analysis. We also generated the GSEA plots (Figures S16, S17) with `clusterProfiler`.

Code, data, and strain availability

All raw genomic and transcriptomic data has been deposited at the NCBI Sequence Read Archive (SRA), under BioProject accession number PRJNA970313. Code and processed data are available at <https://github.com/joaoascensao/Rediversification>. All newly constructed strains and plasmids presented in this paper are available upon request.

References

- [1] Benton, M. J. Diversification and extinction in the history of life. *Science* **268**, 52–58 (1995).
- [2] Wellborn, G. A. & Langerhans, R. B. Ecological opportunity and the adaptive diversification of lineages. *Ecology and evolution* **5**, 176–95, DOI: [10.1002/ece3.1347](https://doi.org/10.1002/ece3.1347) (2015).
- [3] Burress, E. D. Cichlid fishes as models of ecological diversification: patterns, mechanisms, and consequences. *Hydrobiologia* **748**, 7–27, DOI: [10.1007/s10750-014-1960-z](https://doi.org/10.1007/s10750-014-1960-z) (2015).
- [4] Rabosky, D. L. Diversity-dependence, ecological speciation, and the role of competition in macroevolution. *Annual Review of Ecology, Evolution, and Systematics* **44**, 481–502, DOI: [10.1146/annurev-ecolsys-110512-135800](https://doi.org/10.1146/annurev-ecolsys-110512-135800) (2013).
- [5] Losos, J. B. Adaptive radiation, ecological opportunity, and evolutionary determinism: American society of naturalists eo wilson award address. *The American Naturalist* **175**, 623–639 (2010).
- [6] Stroud, J. T. & Losos, J. B. Ecological opportunity and adaptive radiation. *Annu. Rev. Ecol. Evol. Syst* **47**, 507–532 (2016).
- [7] Whittaker, R. H. Evolution and measurement of species diversity. *Taxon* **21**, 213–251 (1972).

- [8] Schluter, D. *The ecology of adaptive radiation* (OUP Oxford, 2000).
- [9] Friesen, M. L., Saxer, G., Travisano, M. & Doebeli, M. Experimental evidence for sympatric ecological diversification due to frequency-dependent competition in *escherichia coli*. *Evolution* **58**, 245–260 (2004).
- [10] Spencer, C. C., Bertrand, M., Travisano, M. & Doebeli, M. Adaptive diversification in genes that regulate resource use in *escherichia coli*. *PLoS genetics* **3**, e15 (2007).
- [11] Herron, M. D. & Doebeli, M. Parallel evolutionary dynamics of adaptive diversification in *escherichia coli*. *PLoS biology* **11**, e1001490 (2013).
- [12] Dieckmann, U. & Doebeli, M. On the origin of species by sympatric speciation. *Nature* **400**, 354–357 (1999).
- [13] Estrela, S., Diaz-Colunga, J., Vila, J. C., Sanchez-Gorostiaga, A. & Sanchez, A. Diversity begets diversity under microbial niche construction. *bioRxiv* (2022).
- [14] Helling, R. B., Vargas, C. N. & Adams, J. Evolution of *escherichia coli* during growth in a constant environment. *Genetics* **116**, 349–358 (1987).
- [15] Rainey, P. B. & Travisano, M. Adaptive radiation in a heterogeneous environment. *Nature* **394**, 69–72 (1998).
- [16] Rozen, D. E. & Lenski, R. E. Long-term experimental evolution in *escherichia coli*. viii. dynamics of a balanced polymorphism. *The American Naturalist* **155**, 24–35 (2000).
- [17] Brockhurst, M. A., Colegrave, N., Hodgson, D. J. & Buckling, A. Niche occupation limits adaptive radiation in experimental microcosms. *PLoS One* **2**, e193 (2007).
- [18] Gómez, P. & Buckling, A. Real-time microbial adaptive diversification in soil. *Ecology Letters* **16**, 650–655 (2013).
- [19] Schick, A. & Kassen, R. Rapid diversification of *pseudomonas aeruginosa* in cystic fibrosis lung-like conditions. *Proceedings of the National Academy of Sciences* **115**, 10714–10719 (2018).
- [20] Meroz, N., Tovi, N., Sorokin, Y. & Friedman, J. Community composition of microbial microcosms follows simple assembly rules at evolutionary timescales. *Nature communications* **12**, 1–9 (2021).
- [21] Gómez, P. & Buckling, A. Real-time microbial adaptive diversification in soil. *Ecology Letters* **16**, 650–655, DOI: [10.1111/ele.12093](https://doi.org/10.1111/ele.12093) (2013). eprint: <https://onlinelibrary.wiley.com/doi/pdf/10.1111/ele.12093>.
- [22] Folkesson, A. *et al.* Adaptation of *Pseudomonas aeruginosa* to the cystic fibrosis airway: An evolutionary perspective, DOI: [10.1038/nrmicro2907](https://doi.org/10.1038/nrmicro2907) (2012).
- [23] Zhao, S. *et al.* Adaptive Evolution within Gut Microbiomes of Healthy People. *Cell Host and Microbe* **25**, 656–667, DOI: [10.1016/j.chom.2019.03.007](https://doi.org/10.1016/j.chom.2019.03.007) (2019).
- [24] Sousa, A. *et al.* Recurrent Reverse Evolution Maintains Polymorphism after Strong Bottlenecks in Commensal Gut Bacteria. *Molecular Biology and Evolution* **34**, 2879–2892, DOI: [10.1093/MOLBEV/MSX221](https://doi.org/10.1093/MOLBEV/MSX221) (2017).

- [25] M, K. *et al.* Ex uno plures: clonal reinforcement drives evolution of a simple microbial community. *PLoS genetics* **10**, DOI: [10.1371/JOURNAL.PGEN.1004430](https://doi.org/10.1371/JOURNAL.PGEN.1004430) (2014).
- [26] Rozen, D. E., Philippe, N., Arjan de Visser, J., Lenski, R. E. & Schneider, D. Death and cannibalism in a seasonal environment facilitate bacterial coexistence. *Ecology Letters* **12**, 34–44, DOI: [10.1111/j.1461-0248.2008.01257.x](https://doi.org/10.1111/j.1461-0248.2008.01257.x) (2009).
- [27] Treves, D. S., Manning, S. & Adams, J. Repeated evolution of an acetate-crossfeeding polymorphism in long-term populations of *Escherichia coli*. *Molecular Biology and Evolution* **15**, 789–797, DOI: [10.1093/oxfordjournals.molbev.a025984](https://doi.org/10.1093/oxfordjournals.molbev.a025984) (1998).
- [28] Rosenzweig, R. F., Sharp, R. R., Treves, D. S. & Adams, J. Microbial evolution in a simple unstructured environment: genetic differentiation in *Escherichia coli*. *Genetics* **137**, 903–917, DOI: [10.1093/genetics/137.4.903](https://doi.org/10.1093/genetics/137.4.903) (1994).
- [29] Kinnersley, M. A., Holben, W. E. & Rosenzweig, F. E Unibus Plurum: Genomic Analysis of an Experimentally Evolved Polymorphism in *Escherichia coli*. *PLOS Genetics* **5**, e1000713, DOI: [10.1371/journal.pgen.1000713](https://doi.org/10.1371/journal.pgen.1000713) (2009). Publisher: Public Library of Science.
- [30] Meyer, J. R. *et al.* Ecological speciation of bacteriophage lambda in allopatry and sympatry. *Science (New York, N.Y.)* **354**, 1301–1304, DOI: [10.1126/science.aai8446](https://doi.org/10.1126/science.aai8446) (2016).
- [31] Friesen, M. L., Saxer, G., Travisano, M. & Doebeli, M. Experimental evidence for sympatric ecological diversification due to frequency-dependent competition in *Escherichia coli*. *Evolution; International Journal of Organic Evolution* **58**, 245–260 (2004).
- [32] Tyerman, J., Havard, N., Saxer, G., Travisano, M. & Doebeli, M. Unparallel diversification in bacterial microcosms. *Proceedings. Biological Sciences* **272**, 1393–1398, DOI: [10.1098/rspb.2005.3068](https://doi.org/10.1098/rspb.2005.3068) (2005).
- [33] Cooper, T. F. & Lenski, R. E. Experimental evolution with *E. coli* in diverse resource environments. I. Fluctuating environments promote divergence of replicate populations. *BMC Evolutionary Biology* **10**, 11, DOI: [10.1186/1471-2148-10-11](https://doi.org/10.1186/1471-2148-10-11) (2010).
- [34] Frenkel, E. M. *et al.* Crowded growth leads to the spontaneous evolution of semistable coexistence in laboratory yeast populations. *Proceedings of the National Academy of Sciences of the United States of America* **112**, 11306–11311, DOI: [10.1073/pnas.1506184112](https://doi.org/10.1073/pnas.1506184112) (2015).
- [35] Flohr, R. C. E., Blom, C. J., Rainey, P. B. & Beaumont, H. J. E. Founder niche constrains evolutionary adaptive radiation. *Proceedings of the National Academy of Sciences* **110**, 20663–20668, DOI: [10.1073/pnas.1310310110](https://doi.org/10.1073/pnas.1310310110) (2013). Publisher: Proceedings of the National Academy of Sciences.
- [36] Flynn, K. M. *et al.* Evolution of Ecological Diversity in Biofilms of *Pseudomonas aeruginosa* by Altered Cyclic Diguanylate Signaling. *Journal of Bacteriology* **198**, 2608–2618, DOI: [10.1128/JB.00048-16](https://doi.org/10.1128/JB.00048-16) (2016).
- [37] King, T., Ishihama, A., Kori, A. & Ferenci, T. A regulatory trade-off as a source of strain variation in the species *Escherichia coli*. *Journal of Bacteriology* **186**, 5614–5620, DOI: [10.1128/JB.186.17.5614-5620.2004](https://doi.org/10.1128/JB.186.17.5614-5620.2004) (2004).

- [38] Maharjan, R. P. *et al.* The multiplicity of divergence mechanisms in a single evolving population. *Genome Biology* **13**, R41, DOI: [10.1186/gb-2012-13-6-r41](https://doi.org/10.1186/gb-2012-13-6-r41) (2012).
- [39] San Roman, M. & Wagner, A. Diversity begets diversity during community assembly until ecological limits impose a diversity ceiling. *Molecular Ecology* **30**, 5874–5887 (2021).
- [40] Fink, J. W. & Manhart, M. How do microbes grow in nature? The role of population dynamics in microbial ecology and evolution. *EcoEvoRxiv* DOI: [10.32942/X2488N](https://doi.org/10.32942/X2488N) (2023).
- [41] Herren, C. M., Webert, K. C. & McMahon, K. D. Environmental Disturbances Decrease the Variability of Microbial Populations within Periphyton. *mSystems* **1**, 10.1128/msystems.00013–16, DOI: [10.1128/msystems.00013-16](https://doi.org/10.1128/msystems.00013-16) (2016). Publisher: American Society for Microbiology.
- [42] Kim, M., Heo, E., Kang, H. & Adams, J. Changes in Soil Bacterial Community Structure with Increasing Disturbance Frequency. *Microbial Ecology* **66**, 171–181, DOI: [10.1007/s00248-013-0237-9](https://doi.org/10.1007/s00248-013-0237-9) (2013).
- [43] Shade, A. *et al.* Resistance, resilience and recovery: aquatic bacterial dynamics after water column disturbance. *Environmental Microbiology* **13**, 2752–2767, DOI: [10.1111/j.1462-2920.2011.02546.x](https://doi.org/10.1111/j.1462-2920.2011.02546.x) (2011). eprint: <https://onlinelibrary.wiley.com/doi/pdf/10.1111/j.1462-2920.2011.02546.x>.
- [44] Dethlefsen, L. & Relman, D. A. Incomplete recovery and individualized responses of the human distal gut microbiota to repeated antibiotic perturbation. *Proceedings of the National Academy of Sciences of the United States of America* **108 Suppl 1**, 4554–4561, DOI: [10.1073/pnas.1000087107](https://doi.org/10.1073/pnas.1000087107) (2011).
- [45] Jernberg, C., Löfmark, S., Edlund, C. & Jansson, J. K. Long-term ecological impacts of antibiotic administration on the human intestinal microbiota. *The ISME journal* **1**, 56–66, DOI: [10.1038/ismej.2007.3](https://doi.org/10.1038/ismej.2007.3) (2007).
- [46] Jakobsson, H. E. *et al.* Short-term antibiotic treatment has differing long-term impacts on the human throat and gut microbiome. *PloS One* **5**, e9836, DOI: [10.1371/journal.pone.0009836](https://doi.org/10.1371/journal.pone.0009836) (2010).
- [47] Xue, K. S. *et al.* Prolonged delays in human microbiota transmission after a controlled antibiotic perturbation, DOI: [10.1101/2023.09.26.559480](https://doi.org/10.1101/2023.09.26.559480) (2023). Pages: 2023.09.26.559480 Section: New Results.
- [48] Handa, I. T. *et al.* Consequences of biodiversity loss for litter decomposition across biomes. *Nature* **509**, 218–221, DOI: [10.1038/nature13247](https://doi.org/10.1038/nature13247) (2014).
- [49] Philippot, L., Raaijmakers, J. M., Lemanceau, P. & van der Putten, W. H. Going back to the roots: the microbial ecology of the rhizosphere. *Nature Reviews. Microbiology* **11**, 789–799, DOI: [10.1038/nrmicro3109](https://doi.org/10.1038/nrmicro3109) (2013).
- [50] Hewitt, G. The genetic legacy of the Quaternary ice ages. *Nature* **405**, 907–913, DOI: [10.1038/35016000](https://doi.org/10.1038/35016000) (2000). Number: 6789 Publisher: Nature Publishing Group.
- [51] Grant, P. R. & Grant, B. R. Unpredictable Evolution in a 30-Year Study of Darwin’s Finches. *Science* **296**, 707–711, DOI: [10.1126/science.1070315](https://doi.org/10.1126/science.1070315) (2002). Publisher:

American Association for the Advancement of Science.

- [52] Lerner, H. R. L., Meyer, M., James, H. F., Hofreiter, M. & Fleischer, R. C. Multilocus Resolution of Phylogeny and Timescale in the Extant Adaptive Radiation of Hawaiian Honeycreepers. *Current Biology* **21**, 1838–1844, DOI: [10.1016/j.cub.2011.09.039](https://doi.org/10.1016/j.cub.2011.09.039) (2011).
- [53] Genner, M. J. *et al.* Age of Cichlids: New Dates for Ancient Lake Fish Radiations. *Molecular Biology and Evolution* **24**, 1269–1282, DOI: [10.1093/molbev/msm050](https://doi.org/10.1093/molbev/msm050) (2007).
- [54] Doebeli, M. A model for the evolutionary dynamics of cross-feeding polymorphisms in microorganisms. *Population Ecology* **44**, 59–70, DOI: [10.1007/s101440200008](https://doi.org/10.1007/s101440200008) (2002).
- [55] Dieckmann, U. & Doebeli, M. On the origin of species by sympatric speciation. *Nature* **400**, 354–357, DOI: [10.1038/22521](https://doi.org/10.1038/22521) (1999).
- [56] F, P. *et al.* Effects of Beneficial Mutations in pykF Gene Vary over Time and across Replicate Populations in a Long-Term Experiment with Bacteria. *Molecular biology and evolution* **35**, 202–210, DOI: [10.1093/MOLBEV/MSX279](https://doi.org/10.1093/MOLBEV/MSX279) (2018).
- [57] Good, B. H., Martis, S. & Hallatschek, O. Adaptation limits ecological diversification and promotes ecological tinkering during the competition for substitutable resources. *Proceedings of the National Academy of Sciences of the United States of America* **115**, E10407–E10416, DOI: [10.1073/pnas.1807530115](https://doi.org/10.1073/pnas.1807530115) (2018).
- [58] Lenski, R. E. Experimental evolution and the dynamics of adaptation and genome evolution in microbial populations. *ISME Journal* **11**, 2181–2194, DOI: [10.1038/ismej.2017.69](https://doi.org/10.1038/ismej.2017.69) (2017).
- [59] Rozen, D. E. & Lenski, R. E. Long-Term Experimental Evolution in Escherichia coli. VIII. Dynamics of a Balanced Polymorphism. *The American naturalist* **155**, 24–35, DOI: [10.1086/303299](https://doi.org/10.1086/303299) (2000).
- [60] Großkopf, T. *et al.* Metabolic modelling in a dynamic evolutionary framework predicts adaptive diversification of bacteria in a long-term evolution experiment. *BMC evolutionary biology* **16**, 1–15 (2016).
- [61] Rozen, D. E., Schneider, D. & Lenski, R. E. Long-Term Experimental Evolution in Escherichia coli. XIII. Phylogenetic History of a Balanced Polymorphism. *Journal of Molecular Evolution* **61**, 171–180, DOI: [10.1007/s00239-004-0322-2](https://doi.org/10.1007/s00239-004-0322-2) (2005).
- [62] Le Gac, M., Plucain, J., Hindré, T., Lenski, R. E. & Schneider, D. Ecological and evolutionary dynamics of coexisting lineages during a long-term experiment with Escherichia coli. *Proceedings of the National Academy of Sciences of the United States of America* **96**, 10242–7, DOI: [10.1073/pnas.96.18.10242](https://doi.org/10.1073/pnas.96.18.10242) (2012).
- [63] Plucain, J. *et al.* Epistasis and allele specificity in the emergence of a stable polymorphism in Escherichia coli. *Science* **343**, 1366–1369, DOI: [10.1126/science.1248688](https://doi.org/10.1126/science.1248688) (2014).
- [64] Good, B. H., McDonald, M. J., Barrick, J. E., Lenski, R. E. & Desai, M. M. The dynamics of molecular evolution over 60,000 generations. *Nature* **551**, 45–50, DOI: [10.1038/nature24287](https://doi.org/10.1038/nature24287) (2017).

- [65] Ascensao, J. A., Wetmore, K. M., Good, B. H., Arkin, A. P. & Hallatschek, O. Quantifying the local adaptive landscape of a nascent bacterial community. *Nature Communications* 2023 14:1 **14**, 1–19, DOI: [10.1038/s41467-022-35677-5](https://doi.org/10.1038/s41467-022-35677-5) (2023).
- [66] Doebeli, M. A model for the evolutionary dynamics of cross-feeding polymorphisms in microorganisms. *Population Ecology* **44**, 59–70 (2002).
- [67] Vasi, F. K., Travisano, M. & Lenski, R. E. Long-term experimental evolution in *Escherichia coli*. ii. changes in life-history traits during adaptation to a seasonal environment. *The American Naturalist* **144**, 432–456, DOI: [10.1086/285685](https://doi.org/10.1086/285685) (1994).
- [68] Holms, H. Flux analysis and control of the central metabolic pathways in *Escherichia coli*. *MICROBIOLOGY REVIEWS ELSEVIER FEMS Microbiology Reviews* **19**, 85–116, DOI: [10.1111/j.1574-6976.1996.tb00255.x](https://doi.org/10.1111/j.1574-6976.1996.tb00255.x) (1996).
- [69] Mukherjee, A. *et al.* Coexisting ecotypes in long-term evolution emerged from interacting trade-offs. *Nature Communications* **14**, 3805, DOI: [10.1038/s41467-023-39471-9](https://doi.org/10.1038/s41467-023-39471-9) (2023). Number: 1 Publisher: Nature Publishing Group.
- [70] Sniegowski, P. D., Gerrish, P. J. & Lenski, R. E. Evolution of high mutation rates in experimental populations of *E. coli*. *Nature* **387**, 703–705, DOI: [10.1038/42701](https://doi.org/10.1038/42701) (1997).
- [71] Favate, J. S., Liang, S., Cope, A. L., Yadavalli, S. S. & Shah, P. The landscape of transcriptional and translational changes over 22 years of bacterial adaptation. *eLife* **11**, e81979, DOI: [10.7554/eLife.81979](https://doi.org/10.7554/eLife.81979) (2022).
- [72] Kanehisa, M. & Goto, S. KEGG: Kyoto Encyclopedia of Genes and Genomes. *Nucleic Acids Research* **28**, 27–30, DOI: [10.1093/NAR/28.1.27](https://doi.org/10.1093/NAR/28.1.27) (2000).
- [73] Lo, C.-A. *et al.* Quantification of Protein Levels in Single Living Cells. *Cell Reports* **13**, 2634–2644, DOI: [10.1016/j.celrep.2015.11.048](https://doi.org/10.1016/j.celrep.2015.11.048) (2015).
- [74] Kannan, S., Sams, T., Maury, J. & Workman, C. T. Reconstructing Dynamic Promoter Activity Profiles from Reporter Gene Data. *ACS Synthetic Biology* **7**, 832–841, DOI: [10.1021/acssynbio.7b00223](https://doi.org/10.1021/acssynbio.7b00223) (2018). Publisher: American Chemical Society.
- [75] Kelly, J. R. *et al.* Measuring the activity of BioBrick promoters using an in vivo reference standard. *Journal of Biological Engineering* **3**, 4, DOI: [10.1186/1754-1611-3-4](https://doi.org/10.1186/1754-1611-3-4) (2009).
- [76] Ducrest, A.-L., Amacker, M., Lingner, J. & Nabholz, M. Detection of promoter activity by flow cytometric analysis of GFP reporter expression. *Nucleic Acids Research* **30**, e65 (2002).
- [77] Reppas, N. B., Wade, J. T., Church, G. M. & Struhl, K. The transition between transcriptional initiation and elongation in *E. coli* is highly variable and often rate limiting. *Molecular Cell* **24**, 747–757, DOI: [10.1016/j.molcel.2006.10.030](https://doi.org/10.1016/j.molcel.2006.10.030) (2006).
- [78] Ishihama, A. Functional Modulation of *Escherichia coli* RNA Polymerase. *Annual Review of Microbiology* **54**, 499–518, DOI: [10.1146/annurev.micro.54.1.499](https://doi.org/10.1146/annurev.micro.54.1.499) (2000).
_eprint: <https://doi.org/10.1146/annurev.micro.54.1.499>.
- [79] Sharma, U. K. & Chatterji, D. Transcriptional switching in *Escherichia coli* during stress and starvation by modulation of σ^{70} activity. *FEMS Microbiology Reviews* **34**,

- 646–657, DOI: [10.1111/j.1574-6976.2010.00223.x](https://doi.org/10.1111/j.1574-6976.2010.00223.x) (2010).
- [80] Nyström, T. MicroReview: Growth versus maintenance: a trade-off dictated by RNA polymerase availability and sigma factor competition? *Molecular Microbiology* **54**, 855–862, DOI: [10.1111/j.1365-2958.2004.04342.x](https://doi.org/10.1111/j.1365-2958.2004.04342.x) (2004). eprint: <https://onlinelibrary.wiley.com/doi/pdf/10.1111/j.1365-2958.2004.04342.x>.
- [81] Basan, M. *et al.* A universal trade-off between growth and lag in fluctuating environments. *Nature* **584**, 470–474, DOI: [10.1038/s41586-020-2505-4](https://doi.org/10.1038/s41586-020-2505-4) (2020).
- [82] Blount, Z. D., Lenski, R. E. & Losos, J. B. Contingency and determinism in evolution: Replaying life’s tape. *Science* **362**, DOI: [10.1126/science.aam5979](https://doi.org/10.1126/science.aam5979) (2018).
- [83] Beatty, J. Replaying Life’s Tape. *The Journal of Philosophy* **103**, 336–362 (2006). Publisher: Journal of Philosophy, Inc.
- [84] Gould, S. J. *Wonderful life* (WW Norton, New York, NY, 1989).
- [85] Besnard, F., Picao-Osorio, J., Dubois, C. & Félix, M. A. A broad mutational target explains a fast rate of phenotypic evolution. *eLife* **9**, 1–70, DOI: [10.7554/ELIFE.54928](https://doi.org/10.7554/ELIFE.54928) (2020).
- [86] Boyle, E. A., Li, Y. I. & Pritchard, J. K. An Expanded View of Complex Traits: From Polygenic to Omnigenic. *Cell* **169**, 1177–1186, DOI: [10.1016/J.CELL.2017.05.038](https://doi.org/10.1016/J.CELL.2017.05.038) (2017).
- [87] Scott, M. & Hwa, T. Bacterial growth laws and their applications. *Current Opinion in Biotechnology* **22**, 559–565, DOI: [10.1016/j.copbio.2011.04.014](https://doi.org/10.1016/j.copbio.2011.04.014) (2011).
- [88] Erickson, D. W. *et al.* A global resource allocation strategy governs growth transition kinetics of Escherichia coli. *Nature* **551**, 119–123, DOI: [10.1038/nature24299](https://doi.org/10.1038/nature24299) (2017).
- [89] Forchhammer, J. & Lindahl, L. Growth rate of polypeptide chains as a function of the cell growth rate in a mutant of Escherichia coli 15. *Journal of Molecular Biology* **55**, 563–568, DOI: [10.1016/0022-2836\(71\)90337-8](https://doi.org/10.1016/0022-2836(71)90337-8) (1971).
- [90] Scott, M., Gunderson, C. W., Mateescu, E. M., Zhang, Z. & Hwa, T. Interdependence of cell growth and gene expression: Origins and consequences. *Science* **330**, 1099–1102, DOI: [10.1126/science.1192588](https://doi.org/10.1126/science.1192588) (2010).
- [91] Levy, S. F. *et al.* Quantitative evolutionary dynamics using high-resolution lineage tracking. *Nature* **519**, 181–186, DOI: [10.1038/nature14279](https://doi.org/10.1038/nature14279) (2015).
- [92] Schlechter, R. O. *et al.* Chromatic Bacteria - A Broad Host-Range Plasmid and Chromosomal Insertion Toolbox for Fluorescent Protein Expression in Bacteria. *Frontiers in microbiology* **9**, DOI: [10.3389/FMICB.2018.03052](https://doi.org/10.3389/FMICB.2018.03052) (2018).
- [93] Kremers, G. J., Goedhart, J., Van Munster, E. B. & Gadella, T. W. Cyan and yellow super fluorescent proteins with improved brightness, protein folding, and FRET Förster radius. *Biochemistry* **45**, 6570–6580, DOI: [10.1021/BI0516273](https://doi.org/10.1021/BI0516273) (2006).
- [94] Ai, H. W., Shaner, N. C., Cheng, Z., Tsien, R. Y. & Campbell, R. E. Exploration of new chromophore structures leads to the identification of improved blue fluorescent proteins. *Biochemistry* **46**, 5904–5910, DOI: [10.1021/BI700199G](https://doi.org/10.1021/BI700199G) (2007).

- [95] Part:BBa J23119 - parts.igem.org.
- [96] Reis, A. C. & Salis, H. M. An automated model test system for systematic development and improvement of gene expression models. *ACS Synthetic Biology* **9**, 3145–3156, DOI: [10.1021/ACSSYNBIO.0C00394/SUPPL_{_}FILE/SB0C00394_{_}SI_{_}006.XLSX](https://doi.org/10.1021/ACSSYNBIO.0C00394/SUPPL_{_}FILE/SB0C00394_{_}SI_{_}006.XLSX) (2020).
- [97] Bagwell, C. B. Hyperlog-a flexible log-like transform for negative, zero, and positive valued data. *Cytometry. Part A: The Journal of the International Society for Analytical Cytology* **64**, 34–42, DOI: [10.1002/cyto.a.20114](https://doi.org/10.1002/cyto.a.20114) (2005).
- [98] Anderson, M. J. A new method for non-parametric multivariate analysis of variance. *Austral Ecology* **26**, 32–46, DOI: [10.1111/j.1442-9993.2001.01070.pp.x](https://doi.org/10.1111/j.1442-9993.2001.01070.pp.x) (2001). eprint: <https://onlinelibrary.wiley.com/doi/pdf/10.1111/j.1442-9993.2001.01070.pp.x>.
- [99] Zwietering, M. H., Jongenburger, I., Rombouts, F. M. & van 't Riet, K. Modeling of the Bacterial Growth Curve. *Applied and Environmental Microbiology* **56**, 1875–1881 (1990).
- [100] Virtanen, P. *et al.* SciPy 1.0: Fundamental Algorithms for Scientific Computing in Python. *Nature Methods* **17**, 261–272, DOI: [10.1038/s41592-019-0686-2](https://doi.org/10.1038/s41592-019-0686-2) (2020).
- [101] Deatherage, D. E. & Barrick, J. E. Identification of mutations in laboratory-evolved microbes from next-generation sequencing data using breseq. *Methods in molecular biology (Clifton, N.J.)* **1151**, 165–188, DOI: [10.1007/978-1-4939-0554-6_{_}12](https://doi.org/10.1007/978-1-4939-0554-6_{_}12) (2014).
- [102] Jeong, H. *et al.* Genome Sequences of Escherichia coli B strains REL606 and BL21(DE3). *Journal of Molecular Biology* **394**, 644–652, DOI: [10.1016/J.JMB.2009.09.052](https://doi.org/10.1016/J.JMB.2009.09.052) (2009).
- [103] Li, H. Minimap2: Pairwise alignment for nucleotide sequences. *Bioinformatics* **34**, 3094–3100, DOI: [10.1093/bioinformatics/bty191](https://doi.org/10.1093/bioinformatics/bty191) (2018).
- [104] Sedlazeck, F. J. *et al.* Accurate detection of complex structural variations using single-molecule sequencing. *Nature Methods* **15**, 461–468, DOI: [10.1038/s41592-018-0001-7](https://doi.org/10.1038/s41592-018-0001-7) (2018).
- [105] Kim, D., Paggi, J. M., Park, C., Bennett, C. & Salzberg, S. L. Graph-based genome alignment and genotyping with HISAT2 and HISAT-genotype. *Nature biotechnology* **37**, 907–915, DOI: [10.1038/S41587-019-0201-4](https://doi.org/10.1038/S41587-019-0201-4) (2019).
- [106] Liao, Y., Smyth, G. K. & Shi, W. featureCounts: an efficient general purpose program for assigning sequence reads to genomic features. *Bioinformatics (Oxford, England)* **30**, 923–930, DOI: [10.1093/BIOINFORMATICS/BTT656](https://doi.org/10.1093/BIOINFORMATICS/BTT656) (2014).
- [107] Love, M. I., Huber, W. & Anders, S. Moderated estimation of fold change and dispersion for RNA-seq data with DESeq2. *Genome Biology* **15**, 550, DOI: [10.1186/s13059-014-0550-8](https://doi.org/10.1186/s13059-014-0550-8) (2014).
- [108] Stephens, M. False discovery rates: a new deal. *Biostatistics* **18**, 275–294, DOI: [10.1093/BIOSTATISTICS/KXW041](https://doi.org/10.1093/BIOSTATISTICS/KXW041) (2017).
- [109] Wu, T. *et al.* clusterProfiler 4.0: A universal enrichment tool for interpreting omics data. *The Innovation* **2**, 100141, DOI: [10.1016/J.XINN.2021.100141](https://doi.org/10.1016/J.XINN.2021.100141) (2021).

- [110] Subramanian, A. *et al.* Gene set enrichment analysis: A knowledge-based approach for interpreting genome-wide expression profiles. *Proceedings of the National Academy of Sciences* **102**, 15545–15550, DOI: [10.1073/pnas.0506580102](https://doi.org/10.1073/pnas.0506580102) (2005).

Acknowledgements

We thank Adam Arkin, Morgan Price, Benjamin Good, Tanush Jagdish, Michael Desai, Jeff Barrick, Dominique Schneider, and all members of the Hallatschek lab (past and present) for helpful comments and advice on the project. We thank Richard Lenski for sending us the LTEE-derived strains and populations, along with experimental advice and feedback. Research reported in this publication was supported by a National Science Foundation CAREER Award (1555330). This work was supported by the National Institute of General Medical Sciences of the NIH under award R01GM115851 and by a Humboldt Professorship of the Alexander von Humboldt Foundation. JAA acknowledges support from an NSF graduate research fellowship, a Berkeley fellowship (from UC Berkeley), and Lloyd and Brodie scholarships (from UC Berkeley Dept of Bioengineering). We thank Mary West of the Cell and Tissue Analysis Facility (CTAF) at UC Berkeley. This work was performed in part in the QB3 CTAF, that provided the ThermoFisher Attune Flow Cytometer (2017 model). RNA sequencing and processing was performed by SeqCenter, LLC. Nanopore library preparation and genomic sequencing along with Illumina sequencing was performed by the Vincent J. Coates Genomics Sequencing Laboratory at UC Berkeley, supported by NIH S10 OD018174 Instrumentation Grant.

Competing Interests Statement

The authors declare no competing interests.

Chapter 4: Large genotype frequency fluctuations are linked to decorrelated offspring number stochasticity

Abstract

Understanding the factors that drive population fluctuations is crucial for predicting and controlling ecological and evolutionary dynamics. Our group and others have observed large population fluctuations that are difficult to explain through genetic drift, thought to be the primary source of genotype frequency fluctuations. We developed a model to delve deeper into this issue, focusing on the dynamics of genotypes within a community. Genetic drift generically arises from independent offspring number fluctuations. However, in our model, when offspring fluctuations are correlated between individuals, fluctuations appear with distinctive scaling behaviors. The correlated offspring fluctuations can strongly affect the total population abundance, and can also affect the genotype frequency if the correlated fluctuations between genotypes are sufficiently decoupled from each other. We thus refer to these frequency fluctuations as "decoupling fluctuations". Empirical measurements using model microbial populations quantitatively supported our model, revealing that decoupling fluctuations between strains can lead to frequency fluctuations far larger than those from genetic drift. By measuring densely sampled intra-cycle time-courses across many replicates, we show that initially close trajectories exponentially diverge from each other, suggesting that underlying chaotic dynamics cause the observed correlated offspring numbers between individuals. Subtle environmental fluctuations can be amplified by the chaotic dynamics, causing batch correlations between replicates grown in the same environment. We also explored the evolutionary implications of these decoupling fluctuations, showing that they can significantly influence the fixation probability of a strain and the site frequency spectrum. Notably, decoupling fluctuations arise from a sufficiently generic mechanism such that we expect they are common across biological populations, strongly affecting evolutionary dynamics. Overall, our findings highlight the importance of considering correlated fluctuations in understanding population dynamics and their evolutionary consequences.

Introduction

The process of evolution is deeply shaped by the interplay between the deterministic and stochastic forces acting on populations. Natural selection pushes allele frequencies up or down in the population, depending on the relative allele fitness, while genetic drift causes random allele frequency fluctuations, with no preferred direction [1–5]. Theoretical population genetics has provided many examples of how natural selection and genetic drift can interact with each other in complex ways. For example, the probability that a mutant will fix, or take over, in a population is determined primarily by dynamics dominated by genetic drift at low mutant frequencies, along with dynamics dominated by natural selection at high frequencies [3, 6, 7]. The transition point between the two regimes is set by the relative strength of selection and drift. Even in purely neutral scenarios, where natural selection is not present, genetic drift can cause surprisingly complex dynamics. For example, while new mutations increase genetic diversity in a population, genetic drift can cause mutants to go extinct, decreasing diversity. The interaction leaves behind a characteristic power-law spectrum of the fraction of mutants in a population [8].

Direct and precise measurements of population stochasticity have recently become possible, allowing us to compare experimental observation with theoretical expectations. These measurements, primarily in microbial populations, have given us a deeper understanding of

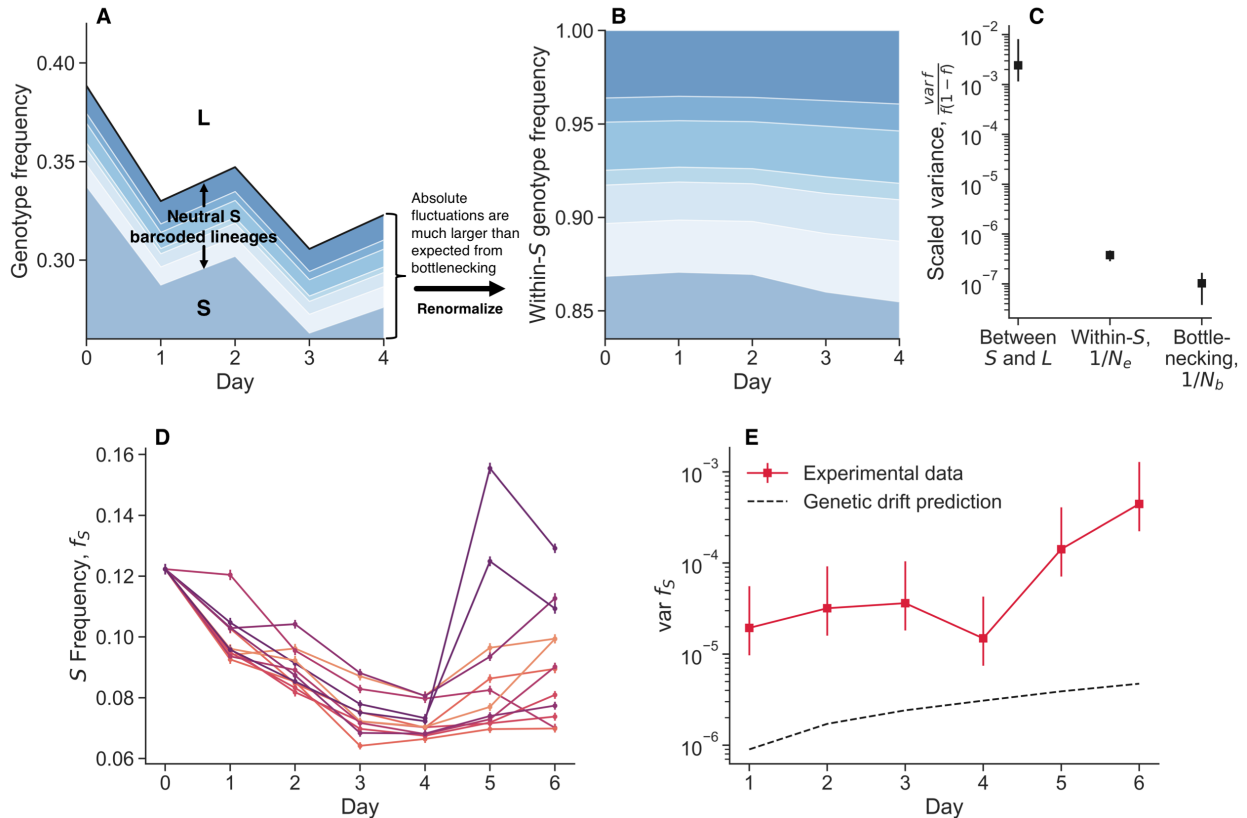


Fig. 1 Observation of large genotype frequency fluctuations. (**A**, **B**) Randomly barcoded libraries of *E. coli* strains *S* and *L* were propagated together in their native serial dilution environment (previously reported data [16]). In the muller plot representation of lineage sizes, we see that the total frequency of *S* relative to *L* shows large fluctuations. However, neutral barcoded lineages within *S* show substantially smaller fluctuations relative to each other. (**C**) By quantifying the strength of fluctuations, we see that total frequency fluctuations between *S* and *L* are several orders of magnitude larger than fluctuations between neutral lineages and expected fluctuations from bottlenecks. (**D**, **E**) We propagated replicate cocultures of *S* and *L* strains together, after splitting them from the same mother culture at day zero. We see that even after one day of propagation, there is already more variance between replicates than expected from genetic drift, and the variance accumulates over time. Note that the experiments in panels **A-C** and in **D-E** were performed at different culture volumes (800mL versus 1mL), but at the same daily dilution regime.

how genetic drift arises from the behaviors and interactions of individuals within the population [9–11]. However, groups often observe anomalous fluctuations in laboratory microbial populations that are neither consistent with genetic drift nor with measurement error [12–15]. These fluctuations are often too large to be easily explained by genetic drift, and share other unexpected features, such as batch correlations [13]. The microbial populations are grown under tightly controlled laboratory conditions, so the presence of these large fluctuations is currently unexplained. It is possible that a new source of fluctuations, aside from genetic drift, must be invoked to explain the fluctuations, which could alter the evolution of these populations.

To explore the nature of these frequency fluctuations, we turned to using strains isolated from the *E. coli* Long Term Evolution Experiment (LTEE). The LTEE is a well-known model system in experimental evolution, that has been propagating and evolving populations of *E. coli* for over 70,000 generations [17]. As a simple system, we used two LTEE-derived strains that have coevolved with each other, referred to as *S* and *L* [18–22]. *S* and *L* diverged from each other early in the LTEE evolution, around 6.5k generations, where *S* emerged as an ecologically-distinct, but closely related strain that partially invaded the initially

L -dominated population [22, 23]. They are a useful model system because they are well-characterized, and they differ significantly even right after they diverged from one another at 6.5k generations.

We propagated 6.5k S and L clones (tagged with fluorescent proteins[24]) together over several days in coculture and precisely measured the relative strain frequency with flow cytometry. We observed large genotype frequency fluctuations; independent biological replicates, grown in the exact same environments, fluctuated apparently randomly, with frequency displacements of up to several percent (Figure 1A). Measurement error is not strong enough to fully account for the observed strength of the fluctuations. It also cannot be explained by genetic drift. The strength of genetic drift is controlled by a parameter known as the effective population size, N_e . The variance induced by genetic drift from one time point to the next is $\text{var } f' = f(1-f)/N_e$ [8]. We previously [16] obtained estimates of N_e for the S and L clones by measuring the fluctuations of many neutrally-barcoded variants of S and L , across both monoculture and coculture conditions. The estimates were consistent with an effective population size that was an $O(1)$ factor smaller than the census bottleneck population size, $N_e \approx 5 \cdot 10^4/mL$. Given the estimated N_e , genetic drift is too weak to account for the strength of the observed fluctuations (Figure 1BC). In fact, N_e would have to be several orders of magnitude smaller to account for the fluctuation strength. We obtained the N_e estimate with barcoded variants at a low frequency, $f \lesssim 10^{-3}$, and used the within strain frequency fluctuations rather than between strain fluctuations. Thus, we hypothesized that the observed large frequency fluctuations were either caused by a source of fluctuations that is only detectable at high frequencies, or is something unique to between-strain fluctuations. We built a mathematical model of population fluctuations to quantify possible sources of fluctuations.

Results

Model of population fluctuations

To model the process of population fluctuations, we first consider a simple population consisting of one strain, where all individuals are identical. The change in population size of a strain μ from size N_μ in the current time point to size N'_μ in the next time point can be decomposed as

$$\Delta N_\mu \equiv N'_\mu - N_\mu = \sum_{i=1}^{N_\mu} n'_{\mu,i} - n_{\mu,i} \equiv \sum_{i=1}^{N_\mu} \Delta n_{\mu,i}, \quad (1)$$

where $\Delta n_{\mu,i} \in [-1, 0, 1, \dots]$, $i \in [1, N_\mu]$ is -1 plus the offspring number of the i^{th} cell of the N_μ cells of the μ strain that exist at the current time step. We know that if all cells behave the same way, we have to demand

$$\langle \Delta n_{\mu,i} \Delta n_{\mu,j} \rangle = \begin{cases} c_{\mu,0} & \text{for } i = j \\ c_{\mu,1} & \text{for } i \neq j \end{cases} \quad (2)$$

This is the only mathematical form of the covariance parameters that won't change if we relabel the cells—a symmetry argument that can easily be extended to multiple strains. This assumes that the offspring number distributions have finite covariances, i.e. are not heavy-tailed. Note that $c_1 < c_0$ follows from $0 < \langle (\Delta n_i - \Delta n_j)^2 \rangle = 2c_0 - 2c_1$.

We can express the variance in total population size in terms of c_0 and c_1 ,

$$\text{var}(N'_\mu) = (c_{\mu,0} - c_{\mu,1})N_\mu + c_{\mu,1}N_\mu^2. \quad (3)$$

The form of this variance scaling has been previously noted [25, 26]. Power law mean-variance scaling of population abundance has been widely observed in ecology, where it is

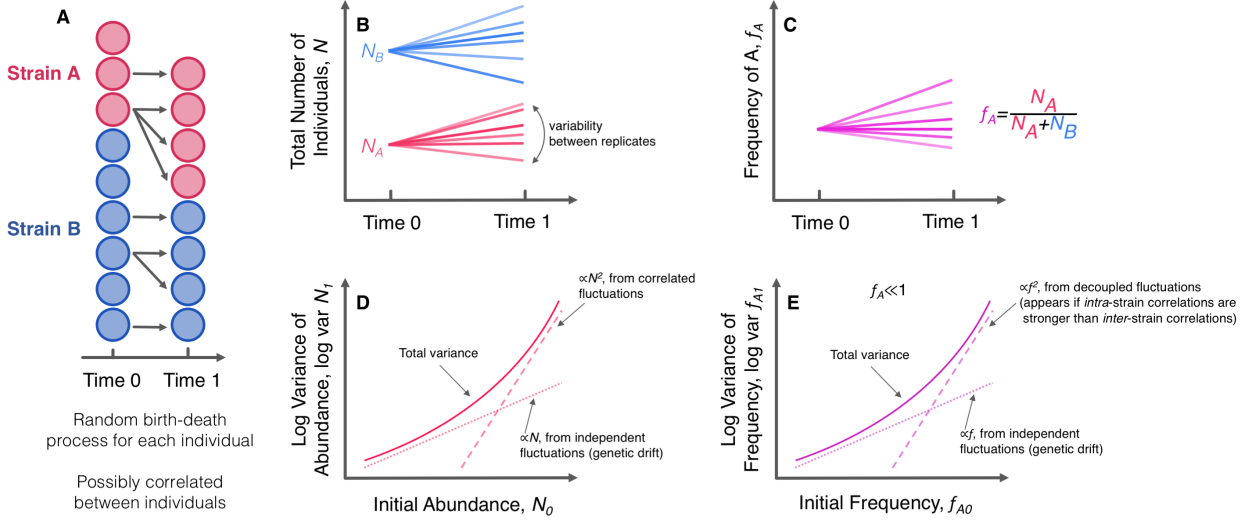


Fig. 2 Model of population fluctuations. (A) We consider a population of individuals, subdivided into two strains. At time zero, there are a specified number of individuals in each strain. After some period of time, each individual has left behind some random number of descendants, drawn from a distribution that may be correlated between individuals. (B, C) The abundance of populations and relative frequencies of strains will generally differ across different instances/replicates, due to the random nature of the process. (D, E) Our model suggests specific scaling behaviors for both the variance of a total number of individuals in each strain and variance of the relative frequencies. Specifically, there is a linearly scaling component caused by independent fluctuations (genetic drift), and a quadratically scaling component caused by fluctuations correlated between individuals. The quadratically scaling fluctuations will appear in abundance trajectories if there are correlated fluctuations, but they will only appear in frequency trajectories if *intra*-strain correlations are stronger than *inter*-strain correlations.

known as Taylor's power law [27–30]. For large enough values of N_μ , the distribution of N'_μ will converge in distribution to a gaussian random variable, because of the central limit theorem. So the fluctuations of N'_μ will solely depend on the variance, $\text{var}(N'_\mu)$.

We can now extend the analysis to a population consisting of two strains labeled A and B , possibly with non-identical properties (Figure 2A). Extending the symmetry argument from above, we now require five covariance parameters to fully describe the population,

$$\langle \Delta n_{\mu,i} \Delta n_{\nu,j} \rangle = \begin{cases} c_{0A} & \text{for } i = j \text{ and } \mu = \nu = A \\ c_{0B} & \text{for } i = j \text{ and } \mu = \nu = B \\ c_{1A} & \text{for } i \neq j \text{ and } \mu = \nu = A \\ c_{1B} & \text{for } i \neq j \text{ and } \mu = \nu = B \\ c_{AB} & \text{for } i \neq j \text{ and } \mu \neq \nu \end{cases} \quad (4)$$

The expression for the variance of the total population size for each strain is the same as in equation 3. The covariance of the total population sizes between strains is,

$$\text{cov}(N'_A, N'_B) = c_{AB} N_A N_B = c_{AB} N_{tot}^2 f_A (1 - f_A). \quad (5)$$

Where $N_{tot} = N_A + N_B$ is the total population size, and $f_A = N_A / (N_A + N_B)$ is the frequency of strain A in the population. The frequency of a strain will also change from one time point to the next, induced by the fluctuations of individuals. The expected frequency variance at the next time point can be written as,

$$\text{var}(f'_A) = \left\langle \left(\frac{\sum_{i=1}^{N_A} 1 + \Delta n_{A,i}}{\sum_{i=1}^{N_A} 1 + \Delta n_{A,i} + \sum_{j=1}^{N_B} 1 + \Delta n_{B,j}} - \frac{N_A}{N_{tot}} \right)^2 \right\rangle \quad (6)$$

If we assume that the frequency deviations are small, we can expand in the deviations to obtain,

$$\text{var}(f'_A) \approx f_A^2 \left\langle \left(\frac{\sum_{i=1}^{N_A} \Delta n_{A,i}}{N_A} - \frac{\sum_{i=1}^{N_A} \Delta n_{A,i} + \sum_{j=1}^{N_B} \Delta n_{B,j}}{N_{tot}} \right)^2 \right\rangle \quad (7)$$

$$\begin{aligned} &= \frac{f_A(1-f_A)}{N_{tot}} [(c_{0A} - c_{1A})(1-f_A) + (c_{0B} - c_{1B})f_A] \\ &+ \underbrace{(c_{1A} + c_{1B} - 2c_{AB})}_{=\delta} f_A^2 (1-f_A)^2. \end{aligned} \quad (8)$$

Similar forms for the frequency variance were found by Takahata et al. (1975)[31] and Melbinger and Vergassola (2015)[32]; however, their models are both special cases of our model, and our model can be derived in a more generic way. The new composite parameter δ quantifies the degree of decoupling between the two strains. If the strains are identical such that $c_{1A} = c_{1B} = c_{AB}$, then the quadratically-scaling fluctuations will vanish. These fluctuations will only appear if individuals *within* a strain are more correlated with each other compared to individuals *between* strains.

We note that if we consider the case where $c_{0A} - c_{1A} = c_{0B} - c_{1B}$, then we can simplify equation 8,

$$\text{var}(f'_A) = \frac{f_A(1-f_A)}{N_e} + \delta f_A^2 (1-f_A)^2. \quad (9)$$

Where the effective population size is defined as $N_e = N_{tot}/(c_{0A} - c_{1A})$. This form of the variance of strain frequencies clearly shows that it is composed of two components. The first component arises from independent fluctuations of individuals, linearly scales with frequency, and corresponds to classical genetic drift. The second, quadratically scaling part arises when individual fluctuations between strains are decoupled to a degree, thus we call them "decoupling fluctuations". Elsewhere in the literature, similar fluctuations have been described as "fluctuating selection" [31, 32]. However, the mechanism through which these fluctuations arise in our model does not depend on invoking selection. Various other mechanisms [27–30] can cause the correlated individual fluctuations that are linked to Taylor's power law abundance fluctuations that scale $\text{var } N \propto N^2$, including inherently chaotic dynamics [33] and dispersal [34].

Empirical fluctuation scaling measurements

Our model of population fluctuations suggests that measuring the scaling of abundance and strain frequency fluctuations with respect to initial abundance and strain frequency may provide insight on the nature of those fluctuations. Thus, we sought to measure those relationships in the *S* and *L* coculture system, measuring population abundance via flow cytometry (see Methods). Briefly, we initially grow each strain in monoculture for several serial dilution cycles, before mixing the two strains together at a defined frequency. After one more growth cycle, we take a flow cytometry measurement of the population, and then split it into biological replicates (Figure 2BC). After another growth cycle, we again take flow cytometry measurements of all replicates, and then calculate variances across replicates.

We performed the described experiment, starting *S* in the minority, and varying the initial frequency over about two orders of magnitude, and using 16 biological replicate per initial frequency. Once we calculate the frequency variance across replicates, we see that the variance clearly scales like $\text{var } f_S \sim f_S^2$ (Figure 3A). From equation 9, we see that the quadratically scaling frequency fluctuations are predicted to occur at small frequencies $f_S \ll 1$, so that the $1 - f_S$ nonlinearity is negligible, but large enough so that the effect of genetic drift is

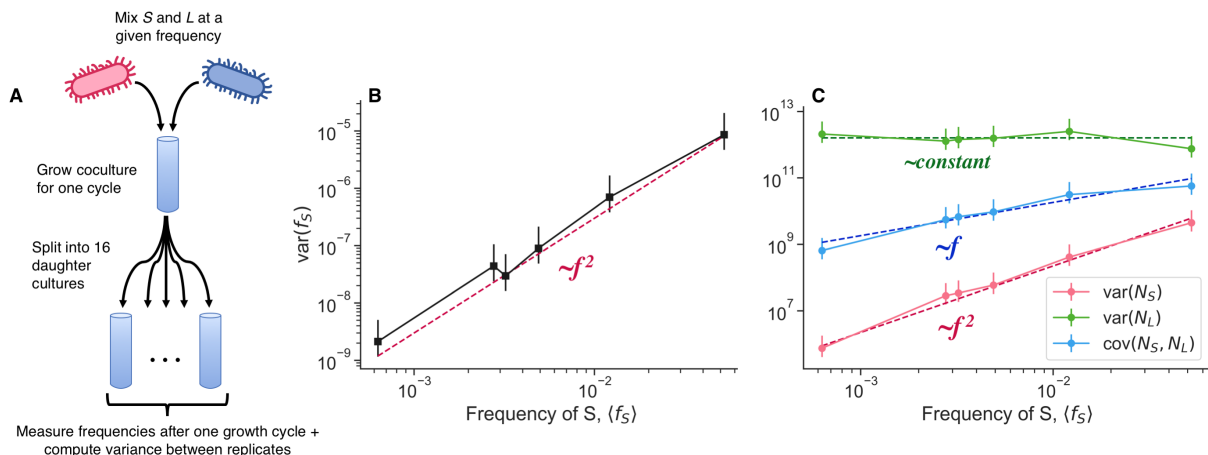


Fig. 3 Empirical scaling of population fluctuations. (A) After growing S and L together at defined relative frequencies, we split the cocultures into 16 biological replicates. We then grew the culture for another cycle, and measured the variation across cocultures. We measured (B) variance of genotype frequency along with (C) variance and covariance of absolute abundance. The points represent experimental measurements, and the dashed lines are fitted lines with the indicated scaling. All of the scaling relationships are consistent with our model of population fluctuations. Error bars represent 95% CIs.

negligible, $f_S \gg 1/(N_e\delta)$ (slightly different expression when the genetic drift parameters differ between strains). Thus, it appears that the data falls into this regime. There is some evidence that the lowest data point in Figure 3A may fall into the cross-over between the linear and quadratic regimes, but it is not completely clear. We compared the variance to the mean frequency, instead of the frequency at the beginning of the cycle, because the within-cycle frequency dynamics show that the mean frequency is a better measure of the frequency right because variance starts to accumulate (Figure 4). But either comparison does not change the scaling behavior significantly.

We also measured the scaling behavior of the variance of the absolute abundance of S and L , $\text{var}(N_S)$ (and $\text{var}(N_L)$ respectively, and the covariance between the two strains $\text{cov}(N_S, N_L)$ (Figure 3B). Consistently, S abundance scales like $\text{var}(N_S) \sim f_S^2$, L abundance stays approximately constant, and the covariance scales like $\text{cov}(N_S, N_L) \sim f_S$. Given the regime the data lies in, these scaling behaviors are consistent with equations 3 and 5. We also measured total abundance fluctuations as a function of initial population sizes, by varying the volume of the culture while holding the dilution rate constant. We also found that $\text{var}(N') \propto N^2$, in both monoculture and coculture conditions, also consistent with equation 3. This indicates that the abundance fluctuations are present even in the absence of coculture conditions.

These data very clearly indicate that the large frequency fluctuations we see cannot be explained by independent fluctuations of individuals, i.e. genetic drift. Instead, fluctuations must be correlated across individuals. Furthermore, the data indicate that it is not the case that the fluctuations predominantly arise from only one strain; S and L abundance fluctuations are of about the same magnitude, with S perhaps fluctuating slightly more by an $O(1)$ factor. The correlation between S and L abundance fluctuations $\rho_{AB} = c_{AB}/\sqrt{c_{1A}c_{1B}}$ is over 90%, demonstrating that a slight decoupling in correlated fluctuations between strains is sufficient to generate noticeable decoupling fluctuations.

The form of frequency fluctuation scaling also appears in other datasets collected by independent groups. Venkataram et al.(2016) [12] used a barcoding system to track frequency trajectories of many adaptive variants of *S. cerevisiae* yeast. They also find large frequency fluctuations when adaptive variants are at high frequencies. They see that variance in frequency across time points scales like $\sim f$ at low frequencies and $\sim f^2$ at high frequencies,

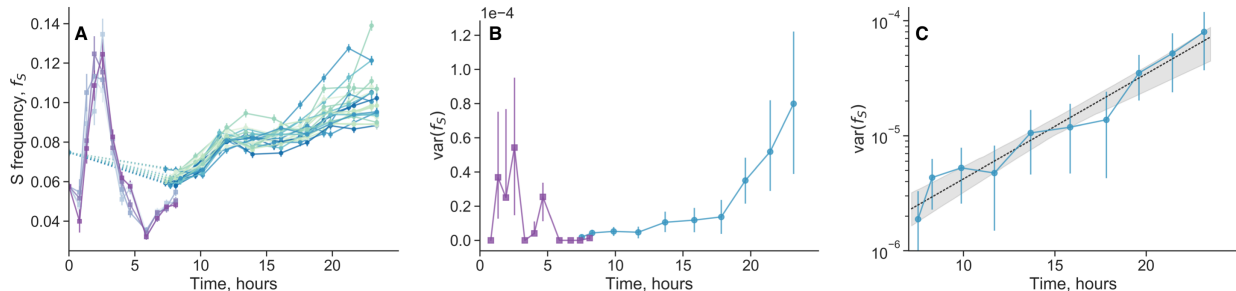


Fig. 4 Within-cycle chaotic dynamics of strain frequencies. **(A)** After splitting cocultures of S and L into multiple biological replicates, we measured strain frequencies over the course of a twenty-four hour cycle (purple lines: 5 replicates; blue/green lines: 23 replicates). Each line represents a biological replicate. **(B)** Quantifying the variance across replicates over time, we see that the variance peaks both in the first 5 hours, and at the end of the cycle. However, the initial variance is not maintained beyond the first 5 hours, suggesting that the later accumulation of variance is the primary contributor to the decoupling fluctuations. **(C)** We plotted the variance (after 7 hours) on a semilog scale, revealing that the variance appears to increase exponentially over time. The black dashed line represents the exponential fit. Exponentially increasing variance between initially close replicates is indicative of chaotic dynamics. All error bars represents 95% CIs.

again consistent with equation 8. While Venkataram et al. only measured relative frequencies and did not collect total abundance data, the frequency fluctuation scaling suggests that decoupling fluctuations might be ubiquitous across systems.

Overall, the data quantitatively supports our model of population fluctuations, where decoupled fluctuations between strains can give rise to frequency fluctuations far larger than from genetic drift.

Within-cycle growth measurements reveal chaotic dynamics

Populations derived from the *E. coli* LTEE are grown in a serial dilution, glucose minimal media environment, such that the populations are transferred at a 1:100 dilution into fresh media every twenty-four hours. This set-up creates a seasonally-varying environment, where the populations are switching strategies throughout a cycle as it proceeds from feast to famine and back again [20, 35, 36]. We reasoned that the within-cycle dynamics of replicate cultures could help to reveal the origin of decoupling fluctuations. We find evidence that underlying chaotic dynamics are the source of the birth-death correlations between individuals and decoupling fluctuations.

Thus, we measured the population dynamics of S and L coculture over the course of the twenty-four growth cycle. In a similar process as previously described, after several initial monoculture growth cycles, we mixed S and L such that S initially occupies around 5% of the population. After one more growth cycle in coculture, we split the culture into multiple, independent biological replicates, and started to take population measurements over defined time increments via flow cytometry. We grew all of the populations together in a shaking 37°C water bath, to minimize the effects of any potential environmental fluctuations. We measured the dynamics of the first eight hours and those of the last sixteen hours separately (on different days), because we found that the two periods had distinct experimental design requirements. This is primarily because the first eight hours (i.e. during exponential phase) is the period of the fastest dynamics, so we had to use both fewer biological replicates and a more dense sampling strategy (see Methods for details).

We first look at a representation of the raw data of the within-cycle population dynamics, the dynamics of S frequency, f_s (Figure 4A). We see relatively complex dynamics, especially in the first eight hours. As previously described, [24] the dynamics can be explained by differences in lag time, exponential growth, and stationary phase behavior. The frequency of S initially increases because it "wakes up" from lag phase earlier than L . However, L has a higher growth rate on glucose, so f_s starts to decline once it wakes up. Then after a

transition period, f_S starts to increase again due to a stationary phase advantage and better growth on acetate [20, 24, 37].

We quantify the variance between replicates, and observe that there are periods of increased variance in approximately the first 5 hours, and the last 7 hours (Figure 4B). The increased variance between replicates in the first 5 hours may be caused by higher measurement error or fast dynamics, but its origin is still not clear. The fact that the variance drops close to zero by eight hours, instead of accumulating, suggests a non-biological origin to explain the initial variance. In contrast, after a period where the variance does not increase much, we see a steady accumulation of variance later in the cycle. Specifically, the variance appears to be increasing exponentially at a constant rate, from around 7 hours to the end of the 24 hour cycle (Figure 4C). The data fits an exponential trajectory better than linear or various other non-linear models.

Exponentially increasing variance between replicates that are initially close to each other is significant because it is indicative of chaotic dynamics. Chaotic dynamics are classically indicated by extreme sensitivity to tiny perturbations (and a bounded phase space), such that small differences in the initial conditions exponentially increase over time. The observation of exponentially increasing variance is equivalent to the observation of pairwise exponential divergence.

We used another standard method to detect chaotic dynamics and infer a largest Lyapunov exponent [38]. We inferred a Lyapunov exponent of 0.15 hr^{-1} (95% CI: [0.119, 0.184]), which is significantly positive ($p = 0.006$). This is consistent with the Lyapunov exponent estimated from the exponentially increasing variance, 0.11 hr^{-1} (95% CI: [0.072, 0.140]). The inverse of the Lyapunov exponent (“Lyapunov time”) represents a characteristic timescale of the system, effectively representing how long a system will appear to be predictable. The Lyapunov time is approximately 5-10 hours, implying that trajectories appear to be stochastic on longer timescales.

The replicate cultures were all grown in the same shaking water bath, and seeded from the same mother culture, so initial variance between cultures should arise from the initial bottleneck, i.e. $\text{var } f(0) = f(1-f)/N_b \approx 4.8 \cdot 10^{-7}$. The exponential fit of the variance from 7 to 24 hours can give a prediction for the initial variance, if exponential growth was constant over the timecourse. Intriguingly, the prediction is very similar to the variance induced by the bottleneck, $\text{var } f(0) = (5.2 \pm 1.2) \cdot 10^{-7}$. This raises the possibility that variance is accumulating in a steady manner over the timecourse, including during exponential phase. However, this possibility would be obscured by the fast dynamics in exponential phase, which makes it difficult to accurately measure how variance is changing over time.

Together, these data suggest that decoupling fluctuations originate from underlying chaotic dynamics. The overnight timecourses were necessary to reveal chaos, because the system shows a relatively fast lyapunov time of approximately 5-10 hours, so timepoints taken every 24 hours appear effectively stochastic.

Evolutionary implications of decoupling fluctuations

As fluctuations from genetic drift have strong effects on evolutionary outcomes, it is reasonable to expect that the presence of decoupling fluctuations may also have evolutionary implications. To study the implications of decoupling fluctuations, we consider our model in the limit of continuous time and individuals under constant selection,

$$\begin{aligned} \partial_t f = & [s - c_{1A}f + c_{1B}(1-f) - c_{AB}(1-2f)] f(1-f) \\ & + \sqrt{f(1-f) [\kappa_A(1-f) + \kappa_B f] + \delta f^2(1-f)^2} \eta(t) . \end{aligned} \quad (10)$$

Where $\eta(t)$ is standard gaussian white noise, $\langle \eta(t) \rangle = 0$ and $\langle \eta(t)\eta(t') \rangle = \delta(t-t')$. Takahata et al. (1975)[31] and Melbinger and Vergassola (2015)[32] studied similar stochastic

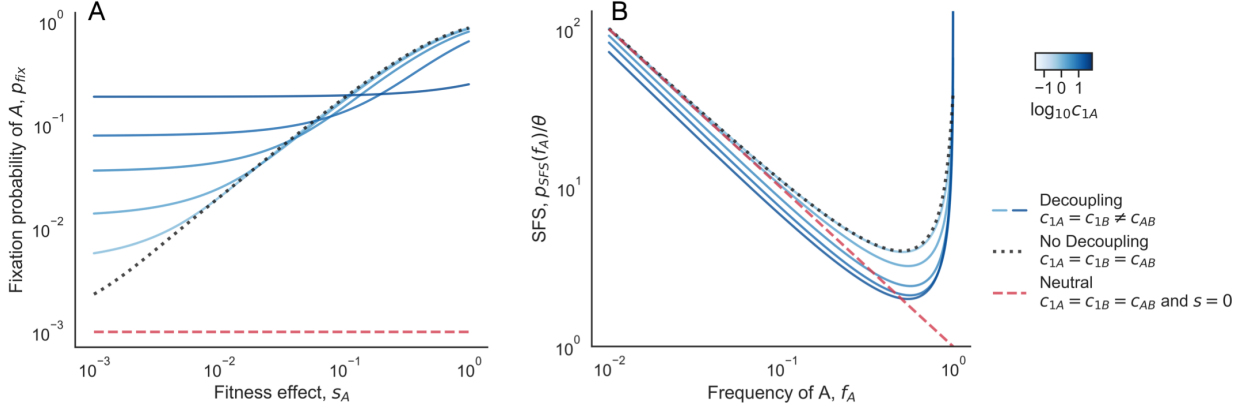


Fig. 5 Theoretical predictions of the evolutionary implications of decoupling fluctuations. **(A)** The fixation probability of strain A , when in coculture with strain B , as a function of the fitness effect of A . **(B)** The site frequency spectrum as a function of the frequency. In both plots, the blue lines represent quantities with decoupling fluctuations, across different values of c_{1A} . The black dotted lines represent the case where there are no decoupling fluctuations, but there is still natural selection. The red dashed lines represents the case where there is neither decoupling fluctuations nor natural selection. Across both plots, $c_{1A} = c_{1B}$, $\rho_{AB} = 0.5$, $\kappa_A = \kappa_B = 10^{-3}$. In **(A)**, $f_{A,0} = 10^{-3}$, and in **(B)**, $s_A = 0.02$.

processes, but we consider the more general form. We have combined several parameters for notational simplicity,

$$\kappa_A = (c_{0A} - c_{1A}) / N_{tot} \quad (11)$$

$$\kappa_B = (c_{0B} - c_{1B}) / N_{tot} . \quad (12)$$

Fixation probability

We first consider the fixation probability of strain A in our two-strain community, i.e. the probability that A completely takes over the population, or that B goes extinct. By applying the Kolmogorov backwards equation that corresponds to equation 10, we find the fixation probability of strain A in terms of the initial strain frequency $f_{A,0}$,

$$p_{fix} = \frac{\left(\frac{\beta + \delta(1 - 2f_{A,0}) - \kappa_A + \kappa_B}{\beta - \delta(1 - 2f_{A,0}) + \kappa_A - \kappa_B} \right)^{\gamma/\beta} - \left(\frac{\beta + \delta - \kappa_A + \kappa_B}{\beta - \delta + \kappa_A - \kappa_B} \right)^{\gamma/\beta}}{\left(\frac{\beta - \delta - \kappa_A + \kappa_B}{\beta + \delta + \kappa_A - \kappa_B} \right)^{\gamma/\beta} - \left(\frac{\beta + \delta - \kappa_A + \kappa_B}{\beta - \delta + \kappa_A - \kappa_B} \right)^{\gamma/\beta}} . \quad (13)$$

Which is in terms of new compound parameters,

$$\beta = \sqrt{(\kappa_A - \kappa_B)^2 + \delta(\delta + 2(\kappa_A + \kappa_B))} \quad (14)$$

$$\gamma = 2s - c_{1A} + c_{1B} + \kappa_A - \kappa_B \quad (15)$$

In the limit of weak correlated fluctuations and when $\kappa_A = \kappa_B$, we find that p_{fix} reduces to the classical fixation probability of a mutant under constant selection[8], as expected. When correlated fluctuations are stronger, and when $f_{A,0} \ll 1$, we see that the fixation probability is higher at low s compared to the case without decoupling fluctuations (Figure 5A). This is an effect of the effective negative frequency-dependent selection arising from the correlated fluctuations[31, 32]—the strain A has an effective positive relative fitness at low frequencies, the crucial period for new mutations when they are most at risk for extinction. Thus, selection is not effective when $s \ll c_{1B} - c_{AB}$.

Site frequency spectrum

The site frequency spectrum (SFS) is a commonly used summary of the genetic diversity within a population. It describes the expected density of derived alleles at a given frequency; specifically $p_{SFS}(f)df$ is the number of derived alleles in the frequency range $[f - df/2, f + df/2]$ [39]. Different dynamical processes can leave different characteristic signatures on the site frequency spectrum, so empirical site frequency spectra are often measured to infer aspects of the underlying evolutionary dynamics.

We calculate the SFS for alleles effected by decoupling fluctuations by leveraging previously described approaches [40]. We find a general closed form solution for the SFS in terms of the frequency of alleles with parameters from A ,

$$p_{SFS}(f_A) = \theta \frac{\phi(f_A) - \phi(1)}{(1 - \phi(1))(1 - f_A)f_A} \quad (16)$$

$$\phi(f_A) = \left(\frac{(\beta + \delta - \kappa_A + \kappa_B)(\beta - \delta(1 - 2f_A) + \kappa_A - \kappa_B)}{(\beta - \delta + \kappa_A - \kappa_B)(\beta + \delta(1 - 2f_A) - \kappa_A + \kappa_B)} \right)^{\gamma/\beta}. \quad (17)$$

Where $\theta = N_{tot}\mu$ is the population mutation rate. Again, we find that in the limit of weak correlated fluctuations and when $\kappa_A = \kappa_B$, equation 16 reduces to the classical expression[8] for the site frequency spectrum for mutations under constant selection, i.e.

$$p_{SFS}^{class}(f_A) = \theta \frac{e^{2s/\kappa_A}(1 - e^{-2s(1-f_A)/\kappa_A})}{(e^{2s/\kappa_A} - 1)f_A(1 - f_A)}. \quad (18)$$

We see that at low frequencies, the SFS both with and without decoupling fluctuations decays as $\sim 1/f$, which is also the expectation for purely neutral alleles [8] (Figure 5B). The major difference between the SFS with and without decoupling fluctuations lies in the uptick at high frequencies, where the uptick rises more quickly when the decoupling mutations are present (Figure 5B). Specifically, the asymptotic scaling behavior of the SFS as $f_A \rightarrow 1$ is,

$$p_{SFS}^{class}(f_A) \sim f_A^{\frac{s - \kappa_A}{\kappa_A}} \quad (19)$$

In contrast, in the presence of decoupling mutations, we find a different asymptotic scaling behavior,

$$p_{SFS}(f_A) \sim f_A^{\frac{s + \kappa_A - 2\kappa_B + c_{1B} - c_{AB}}{\kappa_B}} \quad (20)$$

Thus, the shape of the SFS at large frequencies can be strongly affected by the presence of decoupling fluctuations. The magnitude of the power-law exponent is not sufficient to distinguish the effects of constant selection and decoupling fluctuations.

Discussion

In this study, we identified significant population fluctuations that are much larger than what can be attributed to genetic drift or measurement error. We constructed a simple and generic model of population fluctuations, revealing that their magnitude is the sum of linearly-scaling genetic drift, and quadratically-scaling decoupling fluctuations. While genetic drift arises from independent individual fluctuations, decoupling fluctuations arise when individuals are more correlated *within* strains compared to *between* strains. By measuring the scaling relationships of the population fluctuations, we showed that the observed large fluctuations were indeed caused by the presence of decoupling fluctuations.

Population abundance fluctuations are a well known, near-universal feature of populations across the tree of life, many of which follow Taylor's power law [27–30]. Our model

provides a general description of abundance fluctuations with few assumptions—namely it just requires that populations must be large enough so that the central limit theorem applies, and descendant number variances are finite. The scaling behavior of abundance and frequency variance over time will be valid for any population dynamics where the assumptions apply. The presence of ubiquitous abundance fluctuations suggests that correlated fluctuations between individuals are common. Importantly, our model predicts that any population composed of two or more strains that have sufficiently decoupled individual fluctuations will experience decoupling fluctuations. Because many populations experience abundance fluctuations with a Taylor’s law exponent near 2 [cite], we expect that decoupling frequency fluctuations should be common if offspring number correlations are at least partly genetically determined, and thus able to be changed by mutation.

In our system, the correlated birth-death fluctuations, and decoupling fluctuations in frequencies, appear to be caused by underlying chaotic dynamics, as demonstrated by the exponential divergence of nearby trajectories. The fluctuations appear even under the most tightly controlled environment we could create—among replicates from the same mother culture in the same shaking water bath. Chaotic dynamics are known to be possible even in simple, single-strain populations, caused by e.g. overcompensation [41, 42]. Thus, we believe that these decoupling fluctuations are inescapable, and a fundamental aspect of the system. The underlying source of the fluctuations in other, related microbial systems [12–15] remains unclear. A number of mechanisms are known to cause abundance fluctuations [27–33]. However, the recently reported extreme sensitivity of barcoded yeast populations to subtle variations in the environment [13] is consistent with chaotic dynamics. Chaotic abundance dynamics have been suggested to be common among wild populations [43], and have been demonstrated in a number of carefully controlled laboratory [44–47] and field [48–50] systems. Together, this opens the possibility that chaotic dynamics are also common in experimental microbial populations, and could play an important role in evolutionary dynamics by influencing genotype frequency dynamics across different systems.

The results of our study have implications for the inference of fitness effects in microbial populations. Subtle environmental fluctuations can be amplified by the chaotic dynamics, which can cause batch correlations among replicates grown in the same conditions. These batch correlations may be mistaken for a genuine fitness effect, especially if the autocorrelation time of the environment is on a similar timescale as the evolution experiment. Thus, special care must be taken when designing experiments to measure genotype fitness effects. For example, experimenters could perform biological replicates separately on different sets of days, or continuously measure environmental variables (e.g. temperature, humidity) over the time course to quantify the effect of environmental fluctuations.

A number of emergent effects on evolution could arise from the presence of decoupling fluctuations. For example, we showed that the fixation probability can be drastically shifted by the presence of decoupling fluctuations; thus, the fate of a mutant will not only depend on its fitness effect, but also on its decoupling parameters. The distribution of mutant fitness effects (DFE) is currently thought to largely shape the evolutionary dynamics [51, 52]. But the DFE may (partially) lose its predictive power in the face of decoupling fluctuations; we may need to consider a more general joint distribution, between fitness effects, drift effects, and decoupling parameters, especially if the joint distribution has non-trivial structure.

In our theoretical analysis, we focused on the strong selection-weak mutation regime, where beneficial mutations rise and fix before another establishes. However, it is still unclear how decoupling fluctuations would change the dynamics under other regimes, for example in the clonal interference regime [53]. Additionally, broad-tail offspring number distributions can emerge out of a diverse array of growth processes [54–56], but their effects on dynamics may change if such distributions could be correlated across individuals. Both extensions are likely fruitful avenues for future work.

Overall, we presented experimental measurements for the scaling behavior of population fluctuations, and showed that we could explain them through a generic and extendable

theoretical framework. We found that decoupling fluctuations affecting genotype frequencies can arise quite generally, through a number of mechanisms, so we believe that they may be common across systems.

Methods

Growth conditions, media, and strains

All of the experiments presented here were performed in Davis Minimal Media (DM) base [5.36 g/L potassium phosphate (dibasic), 2g/L potassium phosphate (monobasic), 1g/L ammonium sulfate, 0.5g/L sodium citrate, 0.01% Magnesium sulfate, 0.0002% Thiamine HCl]. The media used in the LTEE and all experiments presented here is DM25, that is DM supplement with 25mg/L glucose. For coculture experiments, we first inoculated the desired strain into 1mL LB + 0.2% glucose + 20mM pyruvate. After overnight growth, we washed the culture 3 times in DM0 (DM without a carbon source added) by centrifuging it at 2500 xg for 3 minutes, aspirating the supernatant, and resuspending in DM0. We transferred the washed culture 1:1000 into 1mL DM25 in a glass tube. Generally, we grew 1mL cultures in a glass 96 well plate (Thomas Scientific 6977B05). We then grew the culture for 24 hours at 37°C in a shaking incubator. The next day, we transferred the cultures 1:100 again into 1mL DM25. After another 24 hours of growth under the same conditions, we would mix selected cultures at desired frequencies, then transfer the mixture 1:100 to DM25. After another 24 hours of growth under the same conditions, we proceed with the experiment and start collecting measurements.

We used strains with fluorescent proteins inserted at the *attTn7* locus, integrated via a miniTn7 transposon system, as previously reported [24]. The 6.5k *S* strain was tagged with eBFP2, the 6.5k *L* strain was tagged with sYFP2, REL606 was tagged with sYFP2, and the REL606 Δ *pykF* mutant was tagged with mScarlet-I.

Flow cytometry

For all population measurements taken with flow cytometry, we used the ThermoFisher Attune Flow Cytometer (2017 model) at the UC Berkeley QB3 Cell and Tissue Analysis Facility (CTAF). For every measurement, we loaded the samples into a round bottom 96 well plate, for use with the autosampler. We set the flow cytometer to perform one washing and mixing cycle before each measurement, and ran 50 μ L of bleach through the autosampler in between each measurement to ensure that there was no cross-contamination between wells. We used the "VL1" channel to detect eBFP2 fluorescence, which uses a 405nm laser and a 440/50nm bandpass emission filter. We used the "BL1" channel to detect sYFP2 fluorescence, which uses a 488nm laser and a 530/30nm bandpass emission filter. We used the "YL2" channel to detect mScarlet-I fluorescence, which uses a 561nm laser and a 620/15nm bandpass emission filter. We used a previously described and validated analysis framework [24] to extract cell counts and strain frequencies from raw flow cytometry data.

Within-cycle timecourses

After the initial growth cycles of fluorescently tagged *S* and *L* as previously described, we mixed the strains together such that the relative frequency of *S* was around 6%. We grew the coculture for one more cycle in DM25, then took a flow cytometry measurement at the end of the 24 hour cycle, which we took as time 0. We then immediately inoculated new replicate cultures from the overnight mother culture by diluting the culture 1:100 into DM25 (e.g. 300 μ L of culture + 30mL of DM25), vortexing the mixture well, and then splitting the resulting mixture into 1mL cultures in individual wells of a glass 96 well plate. We used 5 biological replicates for the 8 hour time-course and 23 replicates for the 24 hour time-course. We secured the 96 well plate in a 37°C water bath, shaking at 180rpm. We briefly removed the plate at designated time intervals (about every 30 minutes and 2 hours for the 8

and 24 hour time course, respectively) to subsample approximately 50 μ L of culture for flow cytometry measurements. Subsamples were discarded after measurement. Exact times of plate sampling were documented. We subsampled the cultures from the 24 hour time course in two batches (one of 11, one of 12), where we subsampled the second batch immediately after the flow cytometry measurement of the first batch was finished. We utilized the batch structure to minimize the amount of time subsample have to wait outside of the water bath to be measured by the flow cytometer.

Following data processing, we computed the variance between biological replicates at the same time points. For the 24 hour time-course, we first computed the variance among all samples in the same batch for each time point, then averaged the variance between the two batches at the same time point, because the batches were taken at slightly different actual times. The confidence intervals for variance measurements were computed with standard asymptotic formulas. We fit a simple exponential to the variance trajectory after 7 hours by first log-transforming the variances (as an approximate variance-stabilizing transform), and then performing linear ordinary least squares regression. Confidence intervals for the regression were obtained by resampling trajectories of biological replicates with replacement (standard bootstrapping), computing the variance in the same manner as previously described, and performing the regression again.

References

- [1] Fisher, R. A. XXI.—On the Dominance Ratio. *Proceedings of the Royal Society of Edinburgh* **42**, 321–341, DOI: [10.1017/S0370164600023993](https://doi.org/10.1017/S0370164600023993) (1923). Publisher: Royal Society of Edinburgh Scotland Foundation.
- [2] Haldane, J. B. S. A Mathematical Theory of Natural and Artificial Selection, Part V: Selection and Mutation. *Mathematical Proceedings of the Cambridge Philosophical Society* **23**, 838–844, DOI: [10.1017/S0305004100015644](https://doi.org/10.1017/S0305004100015644) (1927). Publisher: Cambridge University Press.
- [3] Kimura, M. On the probability of fixation of mutant genes in a population. *Genetics* **47**, 713–719, DOI: [10.1093/genetics/47.6.713](https://doi.org/10.1093/genetics/47.6.713) (1962).
- [4] Uecker, H. & Hermisson, J. On the Fixation Process of a Beneficial Mutation in a Variable Environment. *Genetics* **188**, 915–930, DOI: [10.1534/genetics.110.124297](https://doi.org/10.1534/genetics.110.124297) (2011).
- [5] Barrick, J. E. & Lenski, R. E. Genome dynamics during experimental evolution. *Nature Reviews Genetics* **14**, 827–839, DOI: [10.1038/nrg3564](https://doi.org/10.1038/nrg3564) (2013). Number: 12 Publisher: Nature Publishing Group.
- [6] Kimura, M. Diffusion Models in Population Genetics. *Journal of Applied Probability* **1**, 177–232, DOI: [10.2307/3211856](https://doi.org/10.2307/3211856) (1964). Publisher: Applied Probability Trust.
- [7] Ohta, T. Slightly Deleterious Mutant Substitutions in Evolution. *Nature* **246**, 96–98, DOI: [10.1038/246096a0](https://doi.org/10.1038/246096a0) (1973). Number: 5428 Publisher: Nature Publishing Group.
- [8] Ewens, W. J. *Mathematical Population Genetics 1: Theoretical Introduction* (Springer Science & Business Media, 2004).
- [9] Yu, Q. *et al.* Mutability of demographic noise in microbial range expansions. *The ISME Journal* **15**, 2643–2654, DOI: [10.1038/s41396-021-00951-9](https://doi.org/10.1038/s41396-021-00951-9) (2021). Number: 9 Publisher: Nature Publishing Group.

- [10] Yu, Q. *et al.* Lineage frequency time series reveal elevated levels of genetic drift in SARS-CoV-2 transmission in England, DOI: [10.1101/2022.11.21.517390](https://doi.org/10.1101/2022.11.21.517390) (2022). Pages: 2022.11.21.517390 Section: New Results.
- [11] Gralka, M. *et al.* Allele surfing promotes microbial adaptation from standing variation. *Ecology Letters* **19**, 889–898, DOI: [10.1111/ele.12625](https://doi.org/10.1111/ele.12625) (2016).
- [12] Venkataram, S. *et al.* Development of a Comprehensive Genotype-to-Fitness Map of Adaptation-Driving Mutations in Yeast. *Cell* **166**, 1585–1596.e22, DOI: [10.1016/j.cell.2016.08.002](https://doi.org/10.1016/j.cell.2016.08.002) (2016).
- [13] Kinsler, G. *et al.* Extreme Sensitivity of Fitness to Environmental Conditions: Lessons from #1BigBatch. *Journal of Molecular Evolution* **91**, 293–310, DOI: [10.1007/s00239-023-10114-3](https://doi.org/10.1007/s00239-023-10114-3) (2023).
- [14] Kinsler, G., Geiler-Samerotte, K. & Petrov, D. Fitness variation across subtle environmental perturbations reveals local modularity and global pleiotropy of adaptation. *eLife* **9**, 1–52, DOI: [10.7554/ELIFE.61271](https://doi.org/10.7554/ELIFE.61271) (2020).
- [15] McGee, R. S., Kosterlitz, O., Kaznatcheev, A., Kerr, B. & Bergstrom, C. T. The cost of information acquisition by natural selection, DOI: [10.1101/2022.07.02.498577](https://doi.org/10.1101/2022.07.02.498577) (2022). Pages: 2022.07.02.498577 Section: New Results.
- [16] Ascensao, J. A., Wetmore, K. M., Good, B. H., Arkin, A. P. & Hallatschek, O. Quantifying the local adaptive landscape of a nascent bacterial community. *Nature Communications* **14**, 248, DOI: [10.1038/s41467-022-35677-5](https://doi.org/10.1038/s41467-022-35677-5) (2023). Number: 1 Publisher: Nature Publishing Group.
- [17] Lenski, R. E. Experimental evolution and the dynamics of adaptation and genome evolution in microbial populations. *ISME Journal* **11**, 2181–2194, DOI: [10.1038/ismej.2017.69](https://doi.org/10.1038/ismej.2017.69) (2017).
- [18] Rozen, D. E. & Lenski, R. E. Long-Term Experimental Evolution in *Escherichia coli*. VIII. Dynamics of a Balanced Polymorphism. *The American naturalist* **155**, 24–35, DOI: [10.1086/303299](https://doi.org/10.1086/303299) (2000).
- [19] Rozen, D. E., Schneider, D. & Lenski, R. E. Long-Term Experimental Evolution in *Escherichia coli*. XIII. Phylogenetic History of a Balanced Polymorphism. *Journal of Molecular Evolution* **61**, 171–180, DOI: [10.1007/s00239-004-0322-2](https://doi.org/10.1007/s00239-004-0322-2) (2005).
- [20] Rozen, D. E., Philippe, N., Arjan de Visser, J., Lenski, R. E. & Schneider, D. Death and cannibalism in a seasonal environment facilitate bacterial coexistence. *Ecology Letters* **12**, 34–44, DOI: [10.1111/j.1461-0248.2008.01257.x](https://doi.org/10.1111/j.1461-0248.2008.01257.x) (2009).
- [21] Le Gac, M., Plucain, J., Hindré, T., Lenski, R. E. & Schneider, D. Ecological and evolutionary dynamics of coexisting lineages during a long-term experiment with *Escherichia coli*. *Proceedings of the National Academy of Sciences* **109**, 9487–9492 (2012).
- [22] Plucain, J. *et al.* Epistasis and allele specificity in the emergence of a stable polymorphism in *Escherichia coli*. *Science* **343**, 1366–1369 (2014).
- [23] Good, B. H., McDonald, M. J., Barrick, J. E., Lenski, R. E. & Desai, M. M. The dynamics of molecular evolution over 60,000 generations. *Nature* **551**, 45–50, DOI: [10.1038/nature24287](https://doi.org/10.1038/nature24287) (2017).

- [24] Ascensao, J. A. *et al.* Rediversification Following Ecotype Isolation Reveals Hidden Adaptive Potential, DOI: [10.1101/2023.05.03.539206](https://doi.org/10.1101/2023.05.03.539206) (2023). Pages: 2023.05.03.539206 Section: New Results.
- [25] Bartlett, M. S. Some Notes on Insecticide Tests in the Laboratory and in the Field. *Supplement to the Journal of the Royal Statistical Society* **3**, 185, DOI: [10.2307/2983670](https://doi.org/10.2307/2983670) (1936).
- [26] Ballantyne IV, F. & J. Kerkhoff, A. The observed range for temporal mean-variance scaling exponents can be explained by reproductive correlation. *Oikos* **116**, 174–180, DOI: [10.1111/j.2006.0030-1299.15383.x](https://doi.org/10.1111/j.2006.0030-1299.15383.x) (2007). eprint: <https://onlinelibrary.wiley.com/doi/pdf/10.1111/j.2006.0030-1299.15383.x>.
- [27] Cobain, M. R. D., Brede, M. & Trueman, C. N. Taylor’s power law captures the effects of environmental variability on community structure: An example from fishes in the North Sea. *Journal of Animal Ecology* **88**, 290–301, DOI: [10.1111/1365-2656.12923](https://doi.org/10.1111/1365-2656.12923) (2019). eprint: <https://onlinelibrary.wiley.com/doi/pdf/10.1111/1365-2656.12923>.
- [28] Cohen, J. E. & Xu, M. Random sampling of skewed distributions implies Taylor’s power law of fluctuation scaling. *Proceedings of the National Academy of Sciences* **112**, 7749–7754, DOI: [10.1073/pnas.1503824112](https://doi.org/10.1073/pnas.1503824112) (2015). Publisher: Proceedings of the National Academy of Sciences.
- [29] Xu, M. Taylor’s power law: before and after 50 years of scientific scrutiny (2016). ArXiv:1505.02033 [q-bio].
- [30] Eisler, Z., Bartos, I. & Kertész, J. Fluctuation scaling in complex systems: Taylor’s law and beyond1. *Advances in Physics* **57**, 89–142, DOI: [10.1080/00018730801893043](https://doi.org/10.1080/00018730801893043) (2008).
- [31] Takahata, N., Ishii, K. & Matsuda, H. Effect of temporal fluctuation of selection coefficient on gene frequency in a population. *Proceedings of the National Academy of Sciences* **72**, 4541–4545, DOI: [10.1073/pnas.72.11.4541](https://doi.org/10.1073/pnas.72.11.4541) (1975).
- [32] Melbinger, A. & Vergassola, M. The Impact of Environmental Fluctuations on Evolutionary Fitness Functions. *Scientific Reports* **5**, 15211, DOI: [10.1038/srep15211](https://doi.org/10.1038/srep15211) (2015). Number: 1 Publisher: Nature Publishing Group.
- [33] Perry, J. N. Chaotic Dynamics can Generate Taylor’s Power Law. *Proceedings: Biological Sciences* **257**, 221–226 (1994). Publisher: The Royal Society.
- [34] Shi, P.-J., Sandhu, H. S. & Reddy, G. V. P. Dispersal distance determines the exponent of the spatial Taylor’s power law. *Ecological Modelling* **335**, 48–53, DOI: [10.1016/j.ecolmodel.2016.05.008](https://doi.org/10.1016/j.ecolmodel.2016.05.008) (2016).
- [35] Vasi, F., Travisano, M. & Lenski, R. E. Long-Term Experimental Evolution in *Escherichia coli*. II. Changes in Life-History Traits During Adaptation to a Seasonal Environment. <https://doi.org/10.1086/285685> **144**, 432–456, DOI: [10.1086/285685](https://doi.org/10.1086/285685) (1994).
- [36] Rocabert, C., Knibbe, C., Consuegra, J., Schneider, D. & Beslon, G. Beware batch culture: Seasonality and niche construction predicted to favor bacterial adaptive diversification. *PLOS Computational Biology* **13**, e1005459, DOI: [10.1371/journal.pcbi.1005459](https://doi.org/10.1371/journal.pcbi.1005459) (2017).

- [37] Großkopf, T. *et al.* Metabolic modelling in a dynamic evolutionary framework predicts adaptive diversification of bacteria in a long-term evolution experiment. *BMC Evolutionary Biology* **16**, 163, DOI: [10.1186/s12862-016-0733-x](https://doi.org/10.1186/s12862-016-0733-x) (2016).
- [38] Rosenstein, M. T., Collins, J. J. & De Luca, C. J. A practical method for calculating largest Lyapunov exponents from small data sets. *Physica D: Nonlinear Phenomena* **65**, 117–134, DOI: [10.1016/0167-2789\(93\)90009-P](https://doi.org/10.1016/0167-2789(93)90009-P) (1993).
- [39] Kimura, M. The Number of Heterozygous Nucleotide Sites Maintained in a Finite Population Due to Steady Flux of Mutations. *Genetics* **61**, 893–903 (1969).
- [40] Evans, S. N., Shvets, Y. & Slatkin, M. Non-equilibrium theory of the allele frequency spectrum. *Theoretical Population Biology* **71**, 109–119, DOI: [10.1016/j.tpb.2006.06.005](https://doi.org/10.1016/j.tpb.2006.06.005) (2007).
- [41] May, R. M. Biological Populations with Nonoverlapping Generations: Stable Points, Stable Cycles, and Chaos. *Science* **186**, 645–647, DOI: [10.1126/science.186.4164.645](https://doi.org/10.1126/science.186.4164.645) (1974). Publisher: American Association for the Advancement of Science.
- [42] DeAngelis, D. L. & Waterhouse, J. C. Equilibrium and Nonequilibrium Concepts in Ecological Models. *Ecological Monographs* **57**, 1–21, DOI: [10.2307/1942636](https://doi.org/10.2307/1942636) (1987). eprint: <https://onlinelibrary.wiley.com/doi/pdf/10.2307/1942636>.
- [43] Rogers, T., Johnson, B. & Munch, S. Chaos is not rare in natural ecosystems. preprint, In Review (2021). DOI: [10.21203/rs.3.rs-888047/v1](https://doi.org/10.21203/rs.3.rs-888047/v1).
- [44] Costantino, R. F., Desharnais, R. A., Cushing, J. M. & Dennis, B. Chaotic Dynamics in an Insect Population. *Science* **275**, 389–391, DOI: [10.1126/science.275.5298.389](https://doi.org/10.1126/science.275.5298.389) (1997). Publisher: American Association for the Advancement of Science.
- [45] Benincà, E. *et al.* Chaos in a long-term experiment with a plankton community. *Nature* **451**, 822–825, DOI: [10.1038/nature06512](https://doi.org/10.1038/nature06512) (2008). Number: 7180 Publisher: Nature Publishing Group.
- [46] Becks, L., Hilker, F. M., Malchow, H., Jürgens, K. & Arndt, H. Experimental demonstration of chaos in a microbial food web. *Nature* **435**, 1226–1229, DOI: [10.1038/nature03627](https://doi.org/10.1038/nature03627) (2005). Number: 7046 Publisher: Nature Publishing Group.
- [47] Graham, D. W. *et al.* Experimental demonstration of chaotic instability in biological nitrification. *The ISME Journal* **1**, 385–393, DOI: [10.1038/ismej.2007.45](https://doi.org/10.1038/ismej.2007.45) (2007). Number: 5 Publisher: Nature Publishing Group.
- [48] Benincà, E., Ballantine, B., Ellner, S. P. & Huisman, J. Species fluctuations sustained by a cyclic succession at the edge of chaos. *Proceedings of the National Academy of Sciences* **112**, 6389–6394, DOI: [10.1073/pnas.1421968112](https://doi.org/10.1073/pnas.1421968112) (2015). Publisher: Proceedings of the National Academy of Sciences.
- [49] Tilman, D. & Wedin, D. Oscillations and chaos in the dynamics of a perennial grass. *Nature* **353**, 653–655, DOI: [10.1038/353653a0](https://doi.org/10.1038/353653a0) (1991). Number: 6345 Publisher: Nature Publishing Group.
- [50] Ushio, M. *et al.* Fluctuating interaction network and time-varying stability of a natural fish community. *Nature* **554**, 360–363, DOI: [10.1038/nature25504](https://doi.org/10.1038/nature25504) (2018). Number: 7692 Publisher: Nature Publishing Group.

- [51] Good, B. H., Rouzine, I. M., Balick, D. J., Hallatschek, O. & Desai, M. M. Distribution of fixed beneficial mutations and the rate of adaptation in asexual populations. *Proceedings of the National Academy of Sciences of the United States of America* **109**, 4950–4955, DOI: [10.1073/pnas.1119910109](https://doi.org/10.1073/pnas.1119910109) (2012).
- [52] Orr, H. A. The distribution of fitness effects among beneficial mutations. *Genetics* **163**, 1519 (2003).
- [53] Desai, M. M. & Fisher, D. S. Beneficial mutation selection balance and the effect of linkage on positive selection. *Genetics* **176**, 1759–98, DOI: [10.1534/genetics.106.067678](https://doi.org/10.1534/genetics.106.067678) (2007).
- [54] Hallatschek, O. Selection-Like Biases Emerge in Population Models with Recurrent Jackpot Events. *Genetics* **210**, 1053–1073, DOI: [10.1534/genetics.118.301516](https://doi.org/10.1534/genetics.118.301516) (2018).
- [55] Okada, T. & Hallatschek, O. Dynamic sampling bias and overdispersion induced by skewed offspring distributions. *Genetics* **219**, iyab135, DOI: [10.1093/genetics/iyab135](https://doi.org/10.1093/genetics/iyab135) (2021).
- [56] Hallatschek, O. & Fisher, D. S. Acceleration of evolutionary spread by long-range dispersal. *Proceedings of the National Academy of Sciences of the United States of America* **111**, 4911–9, DOI: [10.1073/pnas.1404663111](https://doi.org/10.1073/pnas.1404663111) (2014).

Acknowledgements

We thank Adam Arkin, Benjamin Good, Jonas Denk, Kelly Wetmore, QinQin Yu, and all members of the Hallatschek lab (past and present) for helpful comments and advice on the project. We thank Richard Lenski for sending us the LTEE-derived strains and populations, along with experimental advice and feedback. We thank Tim Cooper for sending us the REL606 $\Delta pykF$ mutant. Research reported in this publication was supported by a National Science Foundation CAREER Award (1555330). This work was supported by the National Institute of General Medical Sciences of the NIH under award R01GM115851 and by a Humboldt Professorship of the Alexander von Humboldt Foundation. JAA acknowledges support from an NSF graduate research fellowship, a Berkeley fellowship (from UC Berkeley), and Lloyd and Brodie scholarships (from UC Berkeley Dept of Bioengineering). We thank Mary West of the Cell and Tissue Analysis Facility (CTAF) at UC Berkeley. This work was performed in part in the QB3 CTAF, that provided the ThermoFisher Attune Flow Cytometer (2017 model).

Competing Interests Statement

The authors declare no competing interests.

Chapter 5: Conclusions

The evolutionary stories of *Escherichia coli* strains that we unraveled through this thesis offers far more than just a glimpse into the life of a single microorganism. It provides a powerful, albeit imperfect, lens through which the complexity and dynamism of evolution itself can be understood.

The story begins at the microscopic level, with genetic variations acting as the initial brush strokes in the broader picture of evolution. These genetic variations, though minute, set the stage for the diverse evolutionary paths observed in *E. coli*. As we zoom out, the ecological interactions come into focus, adding complexity and depth to this evolutionary canvas. The interplay between *E. coli* and its environment, highlighted in the research, underscores the adaptive dance between organism and habitat. This dance is not a simple two-step but a complex ballet, choreographed by evolutionary pressures, survival strategies, and non-adaptive processes. The journey of *E. coli*, therefore, becomes a metaphor for the evolutionary journey of life itself—a journey marked by constant adaptation, resilience, and transformation.

The implications of this thesis extend beyond the confines of microbial evolution. It challenges us to think about evolution not just as a series of genetic mutations or ecological responses, but as a complex process shaped by a myriad of interconnected factors. It invites us to ponder the adaptability of life in the face of environmental changes and the ongoing evolution of species on our planet.

While this thesis was focused on a few humble strains of *E. coli*—hardly wholly representative of life on this planet—it still allows us to celebrate the complexity and beauty of evolution as a whole. It serves as a reminder of the intricate interplay between genetics and ecology—a reminder that the evolution of life is a tapestry woven from countless threads, each significant in its own right.